Identification of novel inhibitors of the Co-Chaperone HOP in the context of KSHV infection

Frederick John Weaver

Submitted in accordance with the requirements for the degree of

Doctor of Philosophy

The University of Leeds

Faculty of Biological Sciences

School of Molecular and Cellular Biology

Date

December 2023

I confirm that the work submitted is my own and that appropriate credit has been given where reference has been made to the work of others.

This copy has been supplied on the understanding that it is copyright material and that no quotation from the thesis may be published without proper acknowledgement.

The thesis was proof-read before submission by a third-party proof-reader. The PGR confirms that the third-party proof-reading undertaken was in accordance with the Postgraduate Researcher Proof-reading Policy.

Acknowledgements

Abstract

Molecular chaperones are an evolutionarily conserved family of proteins found across the five kingdoms of life. Molecular chaperone function is essential for maintenance of the proteome, ensuring proteins and protein complexes adopt the correct folding and conformational states. Kaposi's sarcoma-associated herpesvirus (KSHV), like many other viruses, utilise host cell molecular chaperones, in particular the heat shock protein (HSP) machinery, enhancing both its latent and lytic replication cycles. Therefore, targeting HSPs may be an attractive antiviral therapeutic strategy. This is supported by findings that show HSP70 and HSP90 specific ATPase inhibitors result in effective inhibition of the KSHV lytic replication cycle. However, utilisation of these HSP inhibitors is not a clinically viable approach, due to redundancy in the HSP network and toxic side effects. Thus, alternative approaches to modulating the HSP70 and HSP90 system is an active area of research for pharmaceutical development.

This thesis describes an alternative approach to inhibiting the host cell HSP machinery, by targeting the molecular co-chaperone HOP, which facilitates the transfer of client proteins from HSP70 to HSP90. The first aim was to determine whether HOP was essential for KSHV lytic replication and a viable therapeutic target. Results in chapter 3 show that HOP is redistributed to the nucleus during KSHV lytic replication with a proportion of HOP localising to KSHV replication and transcription complexes (vRTCs). Moreover, depletion studies show HOP is essential for efficient viral protein expression and infectious virion production. The second aim was to develop and validate a high-throughput fluorescent polarisation assay to screen potential inhibitors of HOP-HSP PPIs. Whilst no positive hit compounds were detected, assay efficacy and effectiveness were demonstrated. Therefore, in chapter 5 alternative approaches to develop HOP-HSP70 PPI inhibitors were investigated, including selective functional group and fragment screening, as well as peptide SAR development. Results provided some interesting findings to be taken forward in the development of early SAR relating to carboxylic acids. Moreover, peptide SAR identified a tryptophan containing peptide with enhanced activity.

In conclusion, this work demonstrated that HOP is intrinsically involved in KSHV lytic replication and may provide future pharmaceutical opportunities. However, targeting HOP-HSP interactions is a challenging medicinal chemistry problem.

Contents

List of Figures

11

15

List of tables

Abbreviations

ACN	Acetonitrile
AI	Artificial intelligence
AIDS	Acquired autoimmune deficiency syndrome
ADP	Adenosine diphosphate
ADMET	Absorption, distribution, metabolism, excretion and toxicity
ATP	Adenosine triphosphate
Cdc-37	cell division cycle 37 protein
CHIP	C-terminus of Hsc70-interacting protein
csHSP90	Cell surface heat shock protein 90
CTD	C-terminus domain
DCM	Dichloromethane
DMF	Dimethylformamide
DNA	Deoxyribose nucleic acid
dsDNA	Double stranded deoxyribose nucleic acid
DTT	Dithiothreitol
EBV	Epstein-Barr virus
ER	Endoplasmic reticulum
FP	Fluorescent polarisation
HAART	highly active antiretroviral therapy
HCMV	Human cytomegalovirus
HHV	Human herpes virus
HIV	Human immunodeficiency Virus
HOP	Hsp70/Hsp90 organising protein
HPLC	High pressure liquid chromatorgraphy
HSF	Heat shock factors
HSE	Heat shock elements
HSP	Heat shock protein
HSP 70	Heat shock protein 70
HSP 90	Heat shock protein 90
HSPG	Heparan sulfate proteoglycans
HTS	High throughput screening
IL	Interleukin
kb	Kilo bases
kd	Knock down
Kd	equilibrium dissociation constant

KICS	KSHV inflammatory cytokine syndrome
KS	Kaposi's sarcoma
KSHV	Kaposi's sarcoma associated herpes virus
LANA	Latency associated nuclear antigen
LB	Lysogeny broth
LC-MS	Liquid chromatography coupled mass spectrometry
MCD	Multicentric Castleman Disease
MD	Middle domain
MS	Mass spectrometry
MSM	Men who have sex with men
NBD	Nucleotide binding domain
NEF	Nucleotide exchange factor
NTD	N-terminus domain
ORF	Open reading frame
PEL	Primary effusion lymphoma
PAINs	Pan assay interference
PPI	Protein protein interaction
qPCR	Quantitive polymerase chain reaction
RNA	Ribose nucleic acid
RRE	RTA response element
RTA	Replication and transcription activator
RT-qPCR	Reverse transcription quantitive polymerase chain reaction
SAR	Structure activity relationship
SBD	Substrate binding domain
shRNA	Short hairpin RNA
SILAC	Stable isotope labeling by amino acids in cell culture
siRNA	Silencing RNA
SMI	Small molecule inhibitor
SPR	Surface plasmon resonance
STIP1	Stress induced phosphoprotein-1
TPR	Tetratricopeptide repeat
TR	Terminal repeating
TPA	12-O-Tetradecanoylphorbol-13-acetate
vRTC	Viral replication and transcription centres
VZV	Varicella zoster virus
UV	Ultraviolet light

Table 1: Scientific units prefixes utilised during report.

Symbol	Meaning	Factor
K	Kilo	10^3
m	Milli	10^{-3}
µ	Micro	10^{-6}
n	Nanao	10^{-9}

Table 2: DNA base prefixes

Base	Prefix
Adenine	A
Cytosine	C
Guanine	G
Thymine	T

Table 3: Amino acid prefixes

Amino acid	three letter code	Single letter cod
Alanine	Ala	A
Arginine	Arg	R
Asparagine	Asn	N
Aspartate	Asp	D
Cysteine	Cys	C
Glutamate	Glu	E
Glutamine	Gln	Q
Glycine	Gly	G
Histidine	His	H
Isoleucine	Ile	I
Leucine	Leu	L
Lysine	Lys	K
Methionine	Met	M
Phenylalanine	Phe	F
Proline	Pro	P
Serine	Ser	S
Threonine	Thr	T
Tryptophan	Trp	W
Tyrosine	Tyr	Y
Valine	Val	V

Chapter 1

~

Introduction

1   Introduction

1.1   *Herpesvirales*

Herpesvirales are an order of dsDNA viruses included in the Baltimore group I classification of viruses which only affect animal hosts. Classification of the taxonomy of *Herpesvirales* by the International Committee on Taxonomy of Viruses dictates three distinct families, which was updated from the initial single family, *Herpesviridae*. The updated families still include *Herpesviridae*, which is the largest and whose primary hosts are avian, reptilian or mammal species; but now also includes *Alloherpesviridae* whose primary hosts are amphibian or fish and *Malacoherpesviridae* whose primary hosts are Bivalve molluscs. Classification was initially based upon phenotypic properties of the virus, however more modern methods have utilised genetic sequencing to align appropriate taxonomy. *Herpesvirales* are characterised by both a large genome and virion size, an icosahedral capsid which is enveloped by a tegument layer and lipid layer (Davison et al., 2009).

1.1.1   *Herpesviridae*

The family of *Herpesviridae* is known to have at least 135 members and is further divided into three distinct sub families comprising *Alphaherpesvirinae, Betaherpesvirinae* and *Gammaherpesvirinae,* with *Alphaherpsvirinae* being the most genetically divergent of the three. They all encode a set of approximately 40 common genes and are believed to have evolutionarily diverged around 400 million years ago (McGeoch and Gatherer, 2005; Davison et al., 2009; Owen et al., 2015). Across all three subfamilies a total of eight routinely affect humans as a primary host. Like all members of the *Herpesviridae* family, these eight human infecting viruses have a common characteristic of establishing a lifelong persistent infection, with a biphasic replication cycle of either a dormant latent phase or an active lytic replication phase (Arvin A et al., 2007; Sharma et al., 2016). Of the eight human herpesviruses, notably two *Gammaherpesvirinae* are oncogenic: Kaposi's sarcoma-associated herpesvirus (KSHV) and Epstein-Barr virus (EBV) (Figure 1).
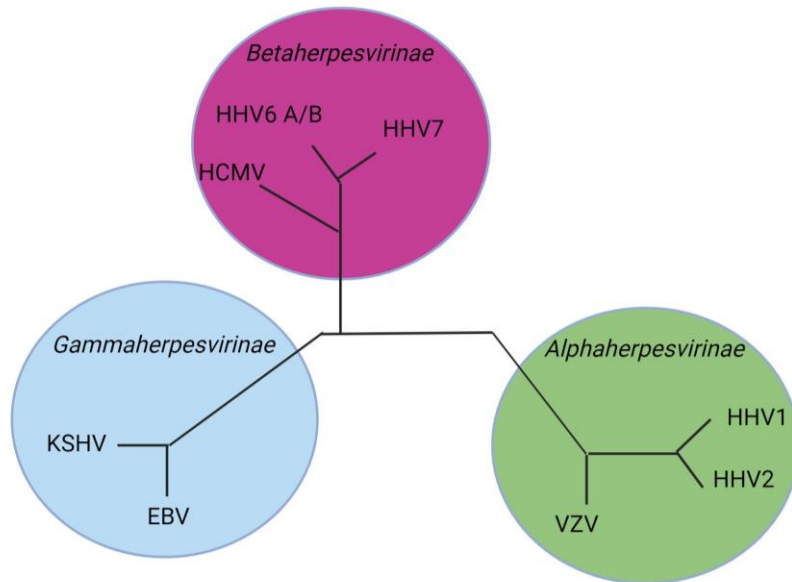
Figure 1: Classification of the eight human Herpesviridae members and their respective sub families as a non scaled simplified phylogenetic tree. Created with BioRender.com

1.1.1.1 *Alphaherpesvirinae*

This subfamily contains three herpesviruses that can infect human hosts and is the least host specific of the subfamilies. These include herpes simplex virus types 1 and 2 (HHV1 and HHV2), and varicella-zoster virus (VZV) (Owen et al., 2015). VZV primary infection is the causative agent of chickenpox (varicella), with reactivation from latent dormancy occurring in approximately 25% of patients resulting in shingles (herpes zoster) (Pinchinat et al., 2013). Whereas HHV1 and HHV2 infection can result in lifelong recurrence of sporadic acute mucocutaneous lesions of oral and genital areas (Whitley R J, 1996). These three viruses reside in a dormant latent phase most frequently in sensory ganglia neurons, whereas lytic replication occurs mainly in epithelial cells, although productive replication can occur less commonly in a wide variety of cell types. The lytic replication cycle is characterised by a short time span and cell death of replicating cells by lysis (Engel et al., 2015; Owen et al., 2015).

1.1.1.2 *Betaherpesvirinae*

This subfamily contains four herpesviruses that can infect human hosts. These include human cytomegalovirus (HCMV), human herpesvirus 6 (HHV-6A and HHV-6B), and human herpesvirus 7 (HHV-7) (Sausen et al., 2021) . *Betaherpesviruses* are characterised by having a slow replication cycle, forming large cytomegaly in infected cells and have a higher degree of host specificity than *Alphaherpesviruses*. HHV6 and HHV7 only infect lymphocytes, whilst HMCV can infect a wide range of cell types such as epithelial, endothelial cells, fibroblasts,

and myeloid cells. HCMV infection is a leading cause of birth defects and is linked to degradation of the host immune system with ageing. HHV6 and HHV7 both cause Roseola in infants with suggested links to development of Alzheimer's disease, although this remains an area of controversy (Whitley R J, 1996; Itzhaki et al., 2020).

1.1.1.3 *Gammaherpesvirinae*

This subfamily contains two human herpesviruses, Epstein-Barr virus (EBV) and Kaposi's Sarcoma-associated herpes virus (KSHV) with oncogenic potential. *Gammaherpesvirinae* are characterised by being the most specific for host and cell type. Both EBV and KSHV establish a stable latent state in B cell lymphocytes, but can infect other cell types such endothelial and epithelial cells upon reactivation (Whitley R J, 1996; Arvin A et al., 2007). EBV is the etiological agent of mononucleosis, alongside driving oncogenesis associated with Burkitt's lymphoma, post-transplant B cell lymphomas, Hodgkin's disease and nasopharyngeal carcinoma. Furthermore, EBV has recently been found to be implicated in the development of Multiple sclerosis (Soldan and Lieberman, 2023). KSHV is the etiological agent of Kaposi's sarcoma (KS), KSHV inflammatory cytokine system (KICS) and primary effusion lymphoma (PEL), it is also associated with the formation of multicentric Castleman's disease (MCD). In both EBV and KSHV infection, the latent and lytic life cycles are implicated in oncogenesis (Manners et al., 2018). This thesis focuses on KSHV and a deeper explanation of the biology of this gammaherpesvirus is outlined below.

1.1.2 KSHV

KSHV was first identified in 1994 by Professors Chang and Moore, isolated from Kaposi's sarcoma samples from AIDS (acquired autoimmune deficiency syndrome) patients (Chang et al., 1994). It has been classified to be one of the twelve members of the gammaherpesviruses of the Genus *rhadinovirus*. Due to it being the etiological agent of KS, PEL and MCD, it is classified as one of the seven proven human oncoviruses. Based on this, it is classed as a category one carcinogen by the International Agency for Research on Cancer (Bouvard et al., 2009).

1.1.2.1 Structure of KSHV virion

The structure of KSHV virion is consistent with other Herpesviruses. Working inwards, the virion is comprised of an outer lipid envelope studded with multiple glycoproteins, a tegument layer, followed by an icosahedral capsid containing the viral genome (Figure 2). The *Herpesviridae* genome consists of linear dsDNA located within the core of the virus particle,

with the KSHV genome comprising approximately 165 kb in length (Trus et al., 2001; Zhu et al., 2005; Arias et al., 2014).
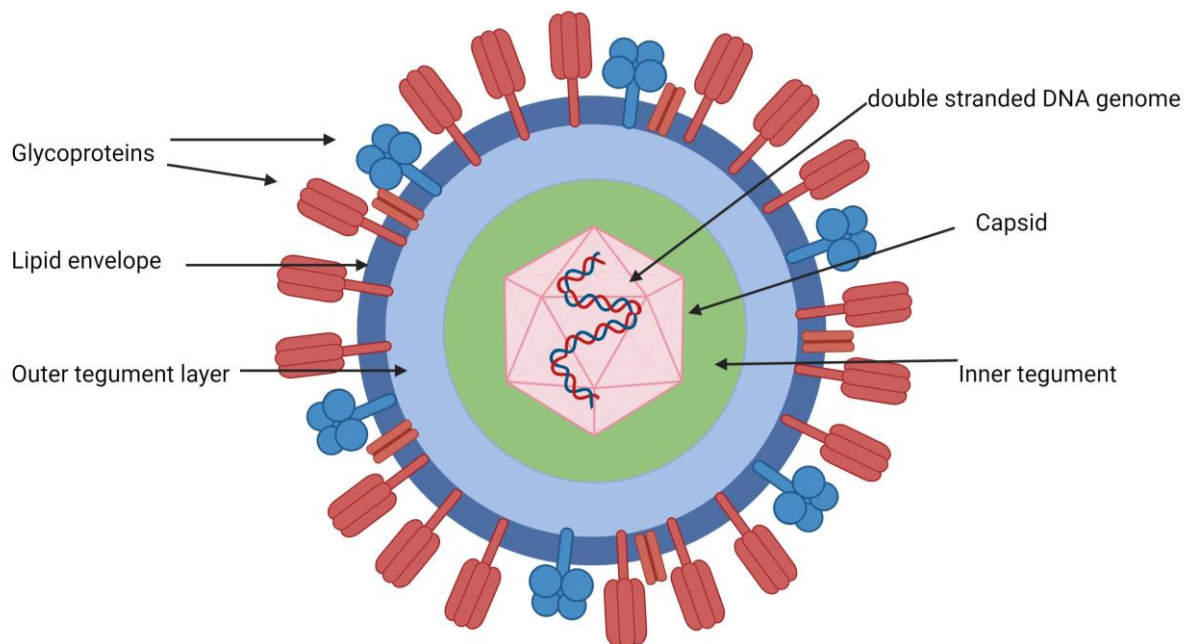
Figure 2: Structure of the KSHV virion, comprised of a lipid envelope with associated glycoproteins, a two layer tegument with an inner and outer layer, an icosahedral capsid and finally the KSHV genome within the capsid. Created with BioRender.com

1.1.2.1.1 Lipid envelope

The KSHV virion lipid envelope is formed from the host lipid bilayer within the Golgi apparatus during budding into golgi-derived vesicles (Wang Xin and Zhu, 2015). Within the lipid envelope of the KSHV virion, a total of nine glycoproteins are present which protrude out of the envelope. Of these glycoproteins K8.1A, ORF4, ORF28, ORF45, and ORF68 are specific to KSHV, with glycoproteins gB, gH/gL, gM, and gN having homologs in other herpesviruses. These glycoproteins are key for binding to the host cell and triggering viral entry however, the specific roles of all nine glycoproteins have not been fully elucidated (Dollery, 2019).

1.1.2.1.2 Tegument

The tegument of KSHV has the largest number of protein species within the virion and is loosely structured by a variety of protein-protein interactions (PPIs). These PPIs form two generalised layers; the inner which interacts with the capsid, and the outer which interacts with the lipid envelope and its associated glycoproteins. Alongside KSHV-encoded proteins, a number of host proteins have been detected in the tegument, including the molecular

chaperones HSP70 and HSP90, although why they are contained into the tegument has not been defined (Zhu et al., 2005). Unsurprisingly, given the number of proteins in the tegument it has an array of roles relating to both virion formation and *de novo* infection of host cells. With respect to virion formation, the KSHV tegument protein ORF45 is involved in translocation of the capsid tegument complex to the golgi for lipid envelopment via the host microtubule network, while other proteins such as KSHV ORF64, act as a scaffold protein to enable binding of the tegument to the capsid (Rozen et al., 2008; Sathish et al., 2009). During *de novo* infection ORF45 and ORF63 proteins have also been shown to inhibit host innate immune and inflammation responses, allowing KSHV to effectively infect new cells (Sathish et al., 2011; Gregory et al., 2011).

1.1.2.1.3 Capsid

The KSHV capsid is composed of 162 protein subunits: 150 hexon capsomers forming the faces of the capsid, 11 capsid vertices, and 1 DNA portal. Initial capsid formation nucleates from the portal protein, with this protein being essential for loading and release of the KSHV genome. The final capsid has an icosahedral capsid structure and a t = 16 symmetry with an overall size of approximately 130 nanometer (Trus et al., 2001; Dai et al., 2018; Gong et al., 2019; Naniima et al., 2021).

1.1.2.1.4 Genome

The KSHV genome is comprised of double stranded DNA and is approximately 165 kb in length. The genome can be divided into two components; a terminal repeating (TR) region of 30 kb and 130 kb unique region. The terminal repeating region contains a high guanidine and cytosine content with a repeating unit of 801 bases. This repeating region aids in circularisation of the genome to form KSHV episomes required for latency (Russo et al., 1996; Arias et al., 2014). Within the unique region, KSHV encodes for an assortment of microRNAs, circRNAs and lncRNAs alongside over 80 gene products. These genes are classified by their timepoint of initial expression, namely latent, early lytic (0-8hrs), delayed early lytic (8-24hrs) and late lytic (24hrs onwards). Multiple KSHV open reading frames (ORFs) modulate the host immune response, with many of these being homologs of proteins that have been captured from the host genome via a process referred to as molecular piracy (Arias et al., 2014; Purushothaman et al., 2016; Abere et al., 2020).

1.1.2.2 KSHV infection and replication cycles

As previously stated, KSHV like all herpesviruses, has a biphasic life cycle consisting of a latent and a lytic replicative phase. During latency, relatively few genes are expressed and a circularised form of the KSHV genome referred to as an episome is tethered to host

chromosomes. During lytic replication, a controlled temporal cascade of the vast majority of KSHV genes occurs, resulting in production of infectious virions. In this section a more in-depth exploration of these distinct but crucial phases will be described, alongside the initial infection of a host cell (*de novo* infection). This biphasic life cycle is critical to both KSHV survival and results in its oncogenic phenotype. The control of the biphasic life cycle revolves around two KSHV-encoded proteins, namely LANA (latency associated nuclear antigen) and RTA (replication and transcription activator) which promote latency and lytic replication cycles, respectively (Yan et al., 2019; Broussard and Damania, 2020).

1.1.2.2.1 *De novo* infection of a cell

Multiple KSHV glycoproteins are involved in initial binding to the host cell surface. Multiple glycoproteins allow for a wider cellular tropism, with numerous cell types susceptible to infection including endothelial cells, B cells, epithelial cells, dendrites/dendritic cells and fibroblasts (Chandran, 2010). Initial binding occurs in a non-cell type specific manner to cell surface proteoglycans. A particularly well studied interaction is the binding of three virion glycoproteins gB, gHgL and K8.1A to heparan sulphate proteoglycans (HSPG). Interestingly these three glycoproteins redundantly interact in HSPG binding, so each glycoprotein is not essential but greatly enhances KSHV infection (Dollery, 2019). In contrast, infection of B cells, the latent reservoir of KSHV, specifically requires the presence of K8.1A, however this appears to be independent of HSPG (Dollery et al., 2019).

Once initial attachment to the cell surface has occurred, the interaction between viral glycoproteins and cell surface signalling receptors occurs. It has been documented that gB interacts with cell surface integrins, whilst gHgL interact with ephrin receptors, and it is postulated that more KSHV glycoproteins are active in this signalling receptor binding phase (van der Meulen et al., 2021). The activation of numerous defined and undefined signalling receptors correspondingly activates a wide variety of signalling pathways including FAK, Src, PI3-K, Rho-GTPase and ROS. These in turn result in endocytosis of the virion, through various mechanisms including micropinocytosis, clarithin and caveolin-mediated and is cell type dependant (Chandran, 2010; Kumar and Chandran, 2016).

During the process of endocytosis, the binding of the KSHV envelope to vesicle membrane is triggered by a lowering of internal vesicle pH, resulting in fusion and release of the capsid into the cytoplasm. The formal trigger for this process is currently not understood. However, following entry, the next defined stage of infection is the translocation of the capsid to the nucleus. This is mediated via Rho-GTPase activation of the microtubule network and powered by dynein motor proteins, resulting in delivery of the capsid to the nucleus. At the

nucleus, the capsid binds the nuclear pore thus triggering the translocation of the KSHV genome in its linear form into the nucleus (Chandran, 2010; Kumar and Chandran, 2016).

Once released into the nucleus, the KSHV linear genome undergoes circularisation and is tethered to host DNA and histones. The exact process by which this occurs is not fully understood. However deliberate triggering of a number of host pathways, in particular the DNA damage repair pathway is critical, with inhibition of this pathway resulting in 80% reduction in KSHV gene expression in tissue culture models (Singh et al., 2014). Circularisation of the KSHV genome is critical as it enables the tethering of genome to host histones by the major latency-associated protein, LANA. Tethering of the episome is essential as it, as it establishes and maintains a latent infection in the dividing B cell population (Lieberman, 2013; Kumar and Chandran, 2016).
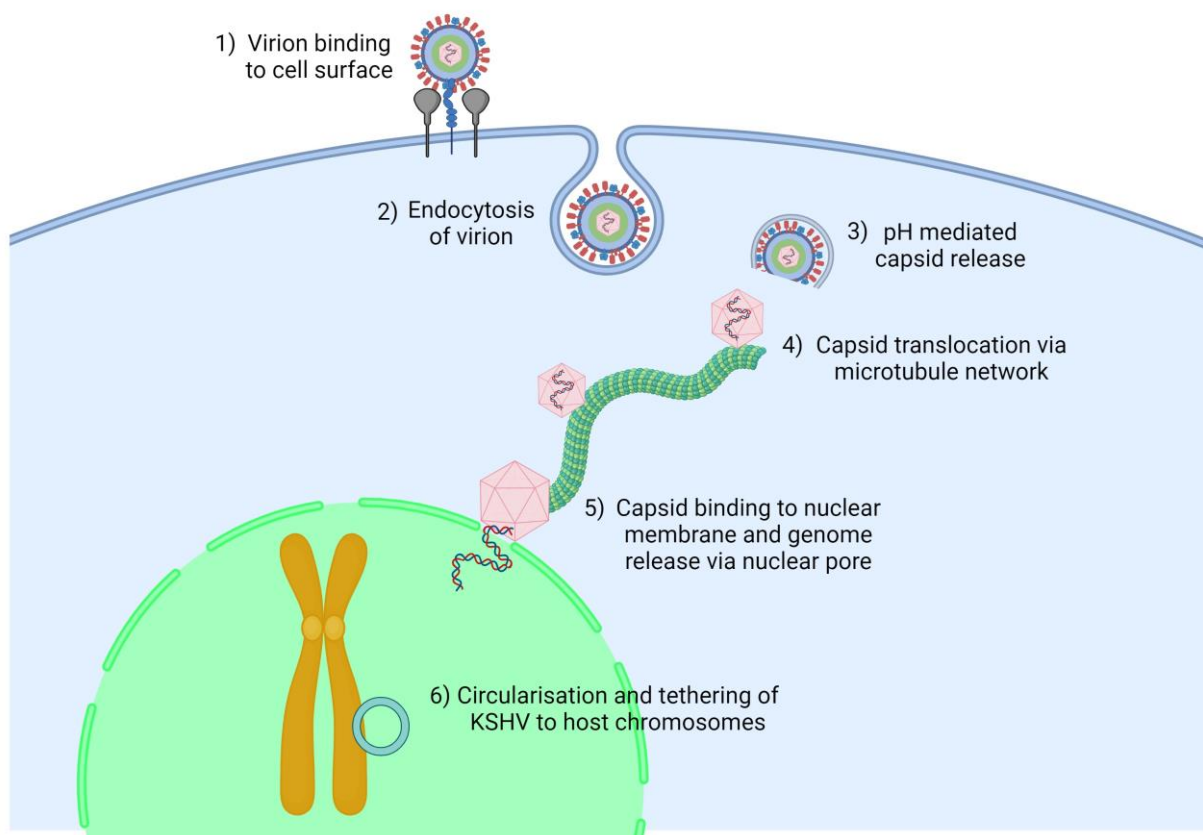
Figure 3: Schematic of *de novo* infection of a generalised cell by KSHV (1) Cell surface attachment to cell surface proteoglycans and resultant activation of cell surface signal receptors. (2) Endocytosis of virion into cell. (3) Lowering of pH triggers release of capsid into cytoplasm. (4) Translocation of capsid via microtubule network to nucleus. (5) Binding of capsid to nuclear membrane and release of linear KSHV genome into nucleus. (6) Circularisation and tethering of KSHV to host chromosomes.

1.1.2.2.2 Latency

The role of latency is crucial to KSHV success, the latent state allows the KSHV episome to persist in the host in a comparatively immunologically silent state, avoiding both innate and adaptive systems while promoting infected cell survival and reproducing the genome during cell division. It should be noted that a purely latent state is not sustainable, and no cell type has been documented to have this phenotype, with spontaneous lytic reactivation a feature of KSHV infection (Grundhoff and Ganem, 2004). During latency, episome replication occurs during the S phase of the cell cycle and maintains a stable number of episomes (approximately 50-100 episomes in PEL samples) bound to host chromatin. During latency comparatively few KSHV-encoded genes are expressed, with LANA being the key protein in maintenance of latency. A specific latency associated locus within the KSHV genome exists and encodes for the expression of LANA alongside other proteins v-Cyclin, v-FLIP, K12/Kaposin A, B and C in addition to 25 mature microRNAs. Moreover, leaky expression of the lytic viral genes ORF74, K14, vIL-6 and ORF59 during latency has been observed and it is believed that the cumulative expression of all these factors is required for effective latency (Uppal et al., 2014; Qin et al., 2017; Broussard and Damania, 2020).

LANA has a multifunctional role during latency via interactions with both proteins and DNA. LANA binds to the TR region of the episome and host histones allowing the episome to be tethered to host chromatin. Moreover, LANA recruits host DNA replication machinery, such as factors that induce double stranded DNA breaks, to enable linearization and replication of the episome. Furthermore, LANA interacts with numerous host factors, such as p53 and pRb to prevent apoptosis and promote cell proliferation. Finally, LANA is the key regulator of the lytic switch protein, RTA, by acting as a transcriptional repressor of the RTA promoter (Uppal et al., 2014; Yan et al., 2019; Broussard and Damania, 2020).

1.1.2.2.3 Lytic Replication

The KSHV lytic replication cycle results in the production of infectious virions which is key for persistence within the host, transmission to new hosts and ultimately KSHV-mediated oncogenesis. Expression of lytic genes occur in a temporal cascade, which is classified into three timepoints of gene expression: early (0-8hrs), delayed early (8-24hrs) and late (24hrs onwards) with viral DNA replication occurring between delayed early and late phases, followed by virion assembly (Yan et al., 2019). Triggers for reactivation from the latent state and initiation of lytic replication are varied, however all result in the transcription of the KSHV RTA protein, which acts as a master switch for lytic reactivation (Guito and Lukac, 2012).

RTA and LANA thus have a key antagonistic interplay promoting their respective replicative states of the KSHV life cycle.

Triggers for reactivation from the latent state include hypoxia, oxidative stress, co-infection, immunosuppression and inflammatory cytokines. In cell culture models, utilisation of specific chemical reagents such as TPA (12-O-Tetradecanoylphorbol-13-acetate) and sodium butyrate can induce reactivation (Aneja and Yuan, 2017). These result in changes to the epigenetic environment of and surrounding the episome, in particular histone acetylation and episome methylation. Acetylation specifically prevents transcription from the RTA promoter, with deacetylation in turn allowing the expression of RTA from the KSHV episome resulting the initiation of the temporal cascade of lytic gene expression and production of infectious virions (Hopcraft et al., 2018; Yan et al., 2019). Furthermore, as LANA acts as a transcriptional repressor of RTA and immediate early gene expression, post-translational modifications occur on LANA preventing it from functioning as an RTA repressor (Uppal et al., 2014).

Once translated, RTA has multiple roles in driving lytic reactivation. RTA functions as a transcription factor, binding to several KSHV gene promoters that contain an RTA response element (RRE) resulting in their expression, including autoregulating its own promoter. Furthermore, it functions to recruit other cellular transcription factors, such as Oct-1 and RBP-Jκ. RTA binds to these transcription factors and results in activation of numerous KSHV gene promoters controlled by Oct-1 and RBP-Jκ proteins. LANA also binds RBP-Jκ and must be outcompeted by RTA levels, with this interplay acting as another level of control of the two replication cycles. RTA also possess E3 ubiquitin ligase activity, which allows it to target specific host and viral proteins for proteasomal degradation such as LANA and vFLIP, which both contribute to the maintenance of latency. Interestingly, abortive lytic reactivation can occur in which induction of RTA is initiated, but production of infectious virion and full lytic cascade fails to occur, which is thought to enhance tumorigenesis although how this is achieved is not fully understood (Aneja and Yuan, 2017; Hopcraft et al., 2018; Yan et al., 2019; Broussard and Damania, 2020).

1.1.2.3 KSHV seroprevalence and associated pathologies

Similar to many pathologies, the likelihood of KSHV infection is linked to numerous risk factors. Globally, KSHV infection and prevalence correlates strongly with geographic area. Higher rates of infection are reported in sub-Saharan Africa with 30-80% of the population being sero-positive, compared to 1-5% in the US and 10-20% in the Mediterranean. In addition, the rate of KSHV infection is 2-3 times higher in men. KSHV infection rates also

strongly correlates with MSM (men who have sex with men) and HIV positivity status, with increased infection rates of 3-20% and 30-35%, respectively (Cesarman et al., 2019). Notably, KSHV infectious virions have been identified in bodily fluids such as saliva, blood, semen and cervical-vaginal secretions. However, infection in endemic regions of sub-Saharan Africa is primarily believed to occur via saliva in childhood, while infections in other regions are believed to be via sexual transmission during adulthood. Furthermore, increased rates are seen in solid organ transplants with iatrogenic KS discussed below (Rohner et al., 2014).

1.1.2.3.1 Kaposi's sarcoma (KS)

Despite Kaposi's Sarcoma (KS) being first described by Moritz Kaposi in 1872, it only achieved infamy as an AIDS defining malignancy during the 1980s and 1990s (Cesarman et al., 2019). However, the link between the etiological agent of KS and the virus was not made until KSHV was discovered in KS biopsies in 1994 (Chang et al., 1994). KS is a spindle cell tumour of endothelial origin, characterised by a heterogenous, multicentric and angioproliferative nature. These tumours can be present on skin, mucous membranes, and internal organs. KS has been characterised into four well defined subtypes: classic, endemic, iatrogenic and epidemic. In all subtypes, infection with KSHV is essential but requires further compounding factors to result in tumorigenesis, such as immunosuppression (Schneider and Dittmer, 2017; Cesarman et al., 2019; Esser et al., 2022). Unlike EBV, both KSHV latent and lytic replication cycles are needed for oncogenesis to occur (Manners et al., 2018).

Classic KS is defined as occurring most frequently in old age, particularly in men of Mediterranean and Ashkenazi Jewish descent. It is often indolent, affecting the skin of lower limbs, however it can be aggressive. HIV/AIDS-associated KS is driven by immune suppression caused by HIV infection, particularly present in MSM and is highly prevalent in sub-Saharan Africa. This form of KS is heavily linked with poor control of HIV and low CD4 counts, however patients with a viral load of HIV below the limit of detection can still be affected (Schneider and Dittmer, 2017; Cesarman et al., 2019). Endemic KS is found in a subtype of patients who are from sub-Saharan Africa but are HIV negative, it affects both children and adults with noted aggression of disease amongst children, particularly affecting internal organs and is also associated with swelling of lymph nodes. Iatrogenic KS is defined as a result of medical treatment most frequently post-transplant. Transplant patients are given immunosuppressive drugs to prevent rejection of the transplanted organ, however this can result in KS development. It is usually localised, however can involve internal organs (Schneider and Dittmer, 2017; Esser et al., 2022).

1.1.2.3.2 Primary effusion lymphoma (PEL)

PEL is a rare type of B cell lymphoma and is associated with KSHV and other risk factors, including coinfection with EBV (60-90% of cases) and immune suppression (frequently HIV/AIDS-mediated). These malignant B cells most frequently form inside the cavities of the body causing accumulation of fluid, however solid tumours occur in a third of patients normally afflicting multiple organs. Prognosis is poor with a life expectancy of 6-9 months post diagnosis (Narkhede et al., 2018; Gathers et al., 2022).

1.1.2.3.3 Multicentric Castleman disease (MCD)

KSHV-associated multicentric Castleman disease is a polyclonal lymphoproliferative disorder originating in B cells. Its presentation varies with a generalised swelling/growth of lymph nodes seen as an initial symptom. This variation is on a spectrum with either angiogenesis and increasing vascularisation of the lymph nodes or accumulation of KSHV infected B cells, with the majority of cases presenting with both to some degree. Immune suppression, normally HIV driven, is a major risk factor for development of KSHV-associated MCD. Lytic reactivation within B cells leads to expression of viral interleukin 6 (vIL-6) and upregulation of human interleukin 6 (IL-6) and interleukin 10 (IL-10) expression, with these cytokines activating angiogenesis/proliferation pathways (Carbone et al., 2015; Ramaswami et al., 2021).

1.1.2.3.4 KSHV inflammatory cytokine syndrome (KICS)

KSHV inflammatory cytokine syndrome affects patients who are positive for both KSHV and HIV, typically in patients with KS presenting with sepsis type symptoms. KICS is associated with high levels of lytic reactivation resulting in high viral load, and increased expression of the cytokines vIL-6, IL-6, and IL-10 which drive the inflammation and sepsis type symptoms. Approaches to treatment seek to trade off tempering the immune response to combat KICS vs boosting immune response to target KS and/or prevent lytic reactivation (Karass et al., 2017; El-Mallawany et al., 2019).

1.1.2.3.5 Treatment for KSHV and associated pathologies

The development of an effective treatment for KSHV and its associated pathologies has been an active area of research for many years, but currently no targeted strategies exist to specifically inhibit KSHV infection and its replication phases. Treatment of KSHV targeting both its lytic and latent phases have been trialled, due both phases being required for pathologies to progress, although no KSHV specific targeting therapies have been clinically licenced

(Manners et al., 2018; Naimo et al., 2021). The biphasic life cycle has however, led to many potential viral and host targets.

Currently treatments for KSHV pathologies are dependent on patient clinical presentation. In cases of immunosuppression linked KS or MCD, treatment plans to boost the immune system is often the most effective approach. In iatrogenic cases where patients are being treated with immune suppressants post-transplant reduction of immune suppressing drugs can be beneficial, however this can lead to transplant rejection (Schneider and Dittmer, 2017; Cesarman et al., 2019). In HIV patients, HAART (highly active antiretroviral therapy) is used to target HIV-mediated immune degradation. Although, a complication defined as KS-IRIS (Immune Reconstitution Inflammatory Syndrome Associated Kaposi Sarcoma) has been associated with HAART treatment which results in existing or new KS tumours appearing in a highly aggressive manner, despite improved CD4 count (Cheng and Hsu, 2017; Poizot-Martin et al., 2022). KS-IRIS is now a major contributor to KS-related, here patients experience a worsening disease after starting ART in up to 39% of cases, depending on KS severity, degree of immunosuppression and treatment availability (Poizot-Martin et al., 2022). It should also be noted that in PEL patients, restoration of the immune system does not result in remission of the disease (Narkhede et al., 2018; Gathers et al., 2022). For the treatment of classic or epidemic KS, where immunosuppression is not a major factor, treatments involve a combination of surgery, radiotherapy, chemotherapy, and nucleoside analogue antiviral approaches. However, life expectancy is highly dependent upon specific disease type and treatment is not always efficacious (Naimo et al., 2021; Esser et al., 2022). KS and MCD the 5-year life expectancy has improved and is now at 72% and 65%, however PEL life expectancy is still very poor, with a 6-9 month survival rate from diagnosis. (Ramaswami et al., 2021; Koren et al., 2021; American Cancer Society, 2023).

A large body of work has focussed on the utilisation of currently available and clinically licensed herpesviral DNA polymerase inhibitors such as foscarnet, cidofovir, valganciclovir and ganciclovir (Figure 4), as direct treatments for KSHV. These nucleoside analogues are delivered as pro-drugs and activated by virally-encoded kinases, once phosphorylated they are incorporated in newly synthesised DNA by the viral polymerase, resulting in chain elongation termination and resulting death of the infected cell (Naimo et al., 2021). However, efficacy of these inhibitors varies between herpesvirus subfamilies. Trials of various nucleoside analogues tend to show greater activity in preventing lytic replication of the alphaherpesvirus subfamily compared to gammaherpesviruses. As such, treatment with these nucleoside analogues showed slight reduction of KSHV viral loads in saliva of patients (Casper et al., 2008; Cattamanchi et al., 2011). However, efficacy in KSHV-associated pathologies is limited,

with multiple other patient trials showing no efficacy in reducing KSHV load and resulting KS lesions (Simonart et al., 1998; Krown et al., 2011; Plachouri et al., 2020). In a KSHV context, poor activity of these drugs is due to a combination of factors, firstly the two KSHV-encoded kinases ORF36 (Serine/Threonine kinase) and ORF21 (thymidine kinase) poorly phosphorylate the pro-drug leading to its active form (Arias et al., 2014; Naimo et al., 2021), and secondly most cells within a KS tumour harbour the virus in a latent state, with low levels of lytic reactivation occurring to maintain infection and drive disease progression. It is hypothesised that this low level of lytic reactivation is an additional factor for the lack of efficacy, as there is little activation of the prodrug, whilst biologically preactivated forms lack the desired specificity. Together this means lytic reactivation cannot be halted sufficiently to act as an effective treatment (Manners et al., 2018; Naimo et al., 2021). Thus, the development of alternative drug targets and drugs is required.
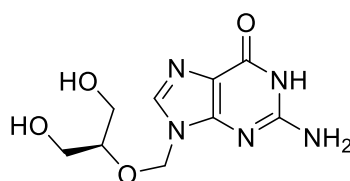
Ganciclovir

Figure 4: Structure of nucleoside analogue ganciclovir which was found to have some activity in tissue culture settings against KSHV.

Novel therapeutic strategies have also been developed to prevent the establishment of a latent state in KSHV-infected cells. For example, identifying small molecule inhibitors which can prevent the interaction between LANA and viral DNA, which is key for the persistence of KSHV episome. Utilising an FP assay to screen 670 compounds, results found three distinct scaffolds which demonstrated competition (Figure 5). However, this work is in preliminary stages since inhibition is in the micromolar range of hit identification (Kirsch et al., 2020). Other approaches validated in tissue culture, have been viral capsid formation inhibitors with analogous approaches achieving success in other herpesviruses (Acker et al., 2017). However, currently no viral targeting inhibitors have entered clinical trials for the treatment of KSHV-associated diseases.
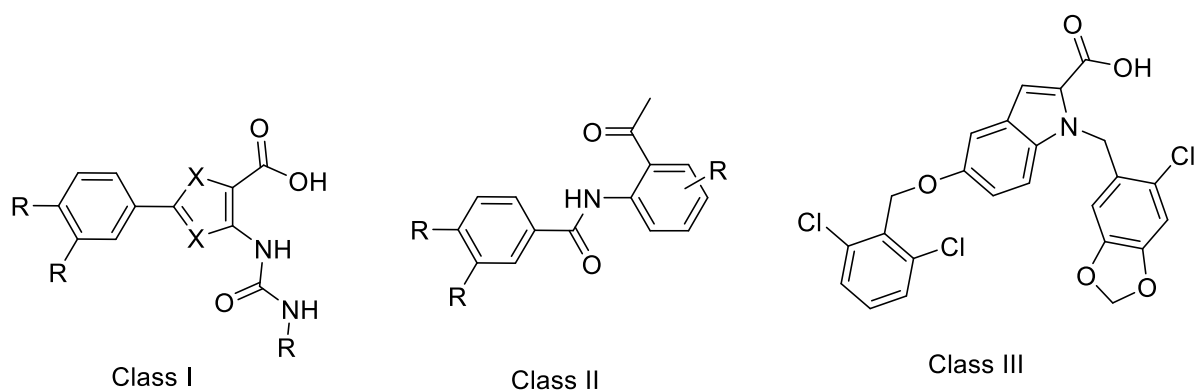
Figure 5: Three hit scaffolds described by Kirsh *et al.* as demonstrating inhibition of LANA-DNA interaction.

1.2 Molecular Chaperones

Molecular chaperones are an evolutionarily conserved protein class which are ubiquitous across all five kingdoms of life. These chaperones are involved in ensuring biological macromolecules such as proteins and protein complexes maintain the correct folding and conformational structures, as such they act as cellular housekeepers of the proteome (Whitley et al., 1999). The correct folding of proteins is essential for protein functionality, thus maintenance of cellular homeostasis and survival (Pearl, 2016; Rosenzweig et al., 2019). This fundamental importance is further reinforced by the diversity and range of chaperones that exist, with many distinct families, subtypes and isoforms (Macario, 1995; Saibil, 2013; Pearl, 2016).

The targets of molecular chaperones are referred to as clients. Chaperone clients are diverse and so is the scenario for chaperone involvement. From stabilisation of the *de novo* polypeptide chain during translation, control of protein activity and refolding of misfolded or aggregated proteins to name but a few (Rosenzweig et al., 2019). However, given the omnipresent and key role of molecular chaperones in the cell, a wide array of diseases are associated with their dysregulation. Unsurprisingly given their role in protein folding, chaperones have been implicated in numerous protein misfolding diseases, where conformational and aggregation control of protein homeostasis has been lost. Examples of these conditions include alzheimers, huntingdons disease and parkinsons disease (Tittelmeier et al., 2020). In addition, molecular chaperones have been heavily implicated during the development of cancer. In malignant cells, rapid and uncontrolled cell division results in the production of vast amounts of cellular proteins, placing a high demand on the cell to ensure correct folding. As such the upregulation of many molecular chaperones has been reported in multiple types of cancer. This is further compounded by the role of chaperones in numerous

signalling pathways which are key for cancer survival, such as preventing apoptosis (Sherman and Gabai, 2015; Calderwood and Gong, 2016; Wu et al., 2017).

Another key role that molecular chaperones has been implicated is in viral infection. It has long been known that viruses utilise the host machinery to effectively complete their replication cycle, and the host molecular chaperone system is involved during numerous phases of the viral replication cycle from initial infection to the endpoint of viral egress (Field et al., 2003; Wen and Damania, 2010; Qin et al., 2010; Zhu et al., 2012; Aviner and Frydman, 2020; Wang et al., 2020). During infection, large quantities of viral proteins are rapidly produced in a choreographed sequence which require chaperoning. In addition, due to the comparatively small genome size of viruses many of these proteins are multifunctional and structurally complex, making them even more reliant upon chaperones. However, very few viruses encode their own chaperone-like protein, instead relying heavily on the host chaperone system to produce correctly folded functional viral proteins. Alongside viral proteins being chaperone clients, viruses also modulate the chaperone system. Given the key role of chaperones in maintenance of the cellular environment, molecular chaperones also have a role in altering the cellular environment to benefit viral replication through a variety of pathways such as, antiapoptotic signalling and facilitating nuclear import (Aviner and Frydman, 2020; Wang et al., 2020).

1.2.1 Heat shock Proteins (HSP)

A major group of molecular chaperones are the heat shock proteins (HSP). This is itself a diverse family that vary in size, structure and clients, with many acting in concert together. The name is derived from the discovery that they are upregulated in cells exposed to heat (Ashburner and Bonnert, 1979; Whitley et al., 1999). Within this group exists two families: HSP70 and HSP90, named by their respective molecular weights in KDa (kilodaltons). Both function to maintain the proteome, through non-covalent interactions with their client proteins and are assisted by a range of co-chaperones, alongside multiple protein folding and proofing pathways (Mayer and Bukau, 2005; Clerico et al., 2015; Pearl, 2016).

Due to many of the HSP family interacting with clients in a 1:1 stoichiometric ratio, the quantity of HSP proteins within a cell can be adjusted quickly to increasing levels of proteome stress, such as during heat shock. The induction of the heat shock 70/90 family of proteins is controlled by a group of transcription factors, known as heat shock factors (HSF). These DNA binding proteins, once activated, bind to promoter regions on HSP genes referred to as heat shock elements (HSE), resulting in the upregulation of HSP gene expression. The major HSF required for the upregulation of HSP70 and HSP90 is HSF1. In an unstressed cell, HSF1 remains bound to HSP90, as a cytoplasmic inactive monomer, however upon cell stress HSF1

is released from HSP90 and forms a homotrimer complex that activates HSP transcription (Prodromou, 2016; Gomez-Pastor et al., 2018).

1.2.1.1 HSP70

HSP70 comprises a family of proteins that are evolutionary conserved across all kingdoms of life, playing a crucial role in maintenance of the proteome and are involved in all phases of protein maturation in the cell. The diverse roles of HSP70 proteins include operating under normal cellular conditions in a housekeeping role, but also as part of a stress response to protect and repair the proteome. In humans up to 13 isoforms have been documented, these isoforms are made up of specific variants relating to organelle location and their inducible versus constitutively expressed nature. Table 4 highlights some of the many roles of HSP70 proteins during stressed and unstressed cellular conditions. HSP70 inducible isoforms can be triggered by a wide variety of cell stressors, such as canonical heat shock, UV radiation, viral infection and heavy metals exposure. These factors result in increased demand for chaperoning activity due to proteotoxic stresses and damage that they induce on host proteins. Substrate or client recognition occurs through short polypeptide recognition motifs that are loosely defined, however tend to contain hydrophobic and positive residues (Clerico et al., 2015; Rosenzweig et al., 2019).

Table 4: Roles of HSP70 within the cell during normal and stressed conditions.

HSP70 Roles
Stabilisation of the *de novo* polypeptide chain as it exits ribosome
Translocation of proteins across membranes
Regulation of protein activity
Assembly and disassembly of protein complexes
Transfer of clients to other folding and quality control mechanisms for further refolding, disaggregation, and degradation
Prevention of protein aggregation
Protein refolding
Protecting proteins from proteolysis

HSP70 isoform structures vary, however all contain an ATPase site within the nucleotide binding domain (NBD), a flexible linker connecting domain linked to a substrate binding domain (SBD) with an associated lid structure. The HSP70 ATPase cycle results in allosteric remodelling of the SBD domain linker and lid. It is this allosteric ATP driven remodelling that allows HSP70 to load clients and chaperone them. The cycle is aided by a suite of co-

chaperones, with the client protein either processed to a correct confirmation or handed off to alternative pathways for further processing (Mayer and Bukau, 2005; Genest et al., 2019). A major family of co-chaperones which interact with HSP70 are the TPR (Tetratricopeptide repeat) co-chaperones which include HOP (HSP70/HSP90 organising protein). The TPR co-chaperones are named due to them all containing TPR domains. Some of these TPR domains interact with the C-terminus region of HSP70 containing the EEVD amino acid motif, with specific HSP90 isoforms also having a conserved EEVD amino acid motif in its C-terminus. Interactions with co-chaperones are key for HSP70 many roles in maintenance of the proteome. Only certain HSP70 isoforms contain this have this EEVD containing disordered region including the inducible and constitutively expressed cytoplasmic forms (Assimon et al., 2015).
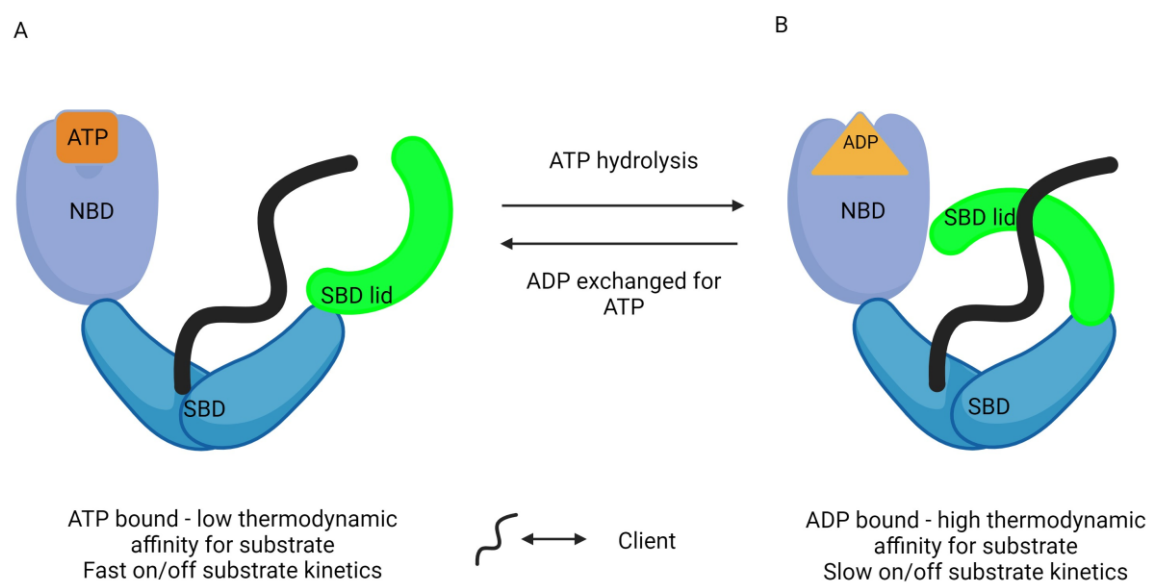
Figure 6: Schematic of HSP70 protein structure comprised of its individual domains interacting with a representative client protein. (A) During ATP bound state (B) during ADP bound state. ATP bound results in an open structure with low thermodynamic affinity for client and fast on off kinetics. ADP bound results in closed structure with high thermodynamic affinity and slow on off kinetics of clients. Created with BioRender.com
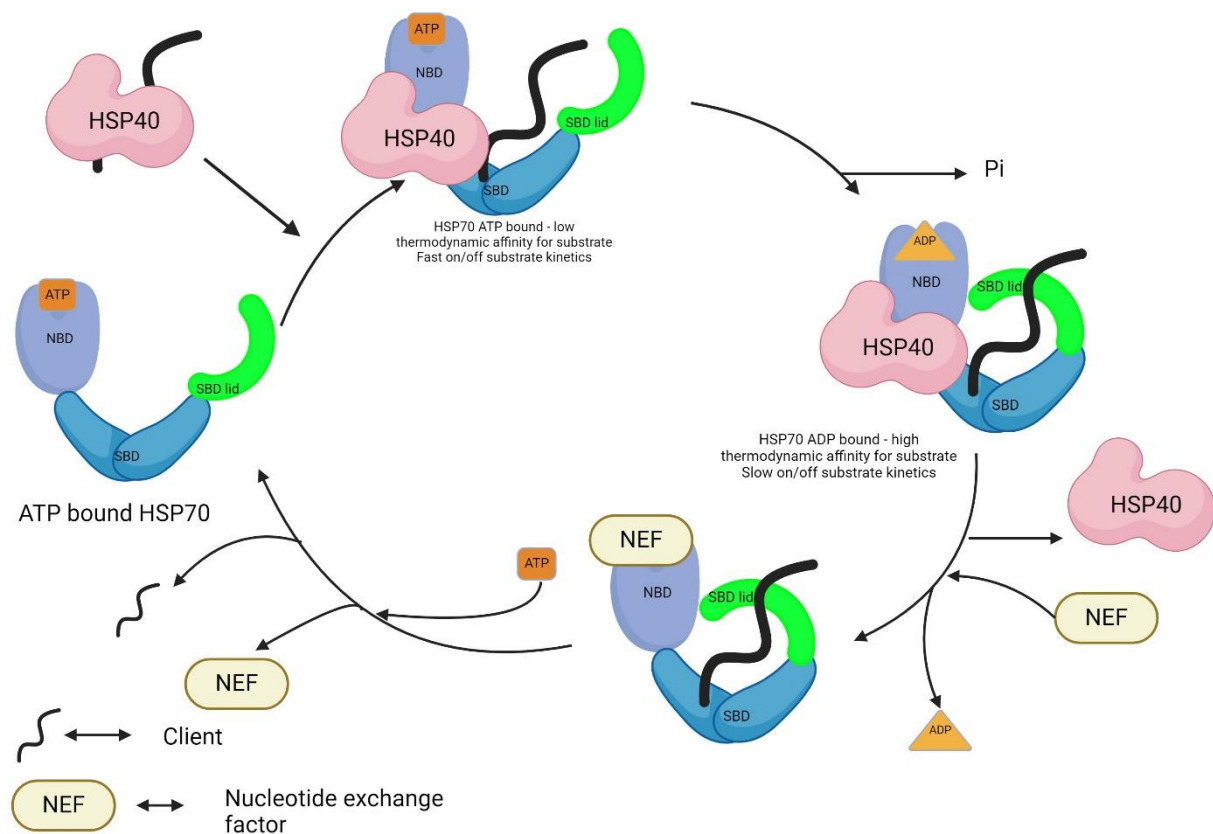
Figure 7: Simplified depiction of a generalised HSP70 ATPase cycle and chaperone functioning. ATP binds to HSP70 resulting in the open structure. HSP40 binds to HSP70 and transfers a client to HSP70. Binding of HSP40 promotes HSP70 ATPase activity alongside substrate binding. ATP is hydrolysed resulting in closed structure. HPS70 chaperoning function of client occurs in closed confirmation client undergoes restructuring and conformational changes towards biologically desired structure. Nucleotide exchange factors (NEF) bind resulting in release of ADP. ATP then displaces NEF resulting in open structure and client release. Created with BioRender.com

Figure 6 shows a simplified schematic of HSP70 structures with ATP or ADP bound. In the ATP bound state of HSP70, its substrate binding domain site and its lid are in an open conformation. In this open state, clients have a low thermodynamic affinity for binding but have fast on/off kinetics due to the open state. Figure 7 gives a simplified depiction of HSP70 ATPase cycle and client binding. Here, HSP40 presents clients to the HSP70 SBD and stimulates HSP70 ATPase activity (Kampinga and Craig, 2010). Successful client binding to the SBD stimulates the ATPase activity of the NBD resulting in conversion of ATP to ADP. In the ADP state, the lid of the SBD domain closes resulting in a high thermodynamic affinity state of HSP70 for clients and slow kinetics. Stimulation of HSP70 by a nucleotide exchange factor results in ADP being displaced for ATP resulting in the release of the client (Rosenzweig et al., 2019).

Three alternative pathways have been hypothesised for clients during this cycle. Acting as a holdase and kinetic partitioner is the simplest, in which clients prone to aggregation are repeatedly bound and unbound until the desired native conformational state of the protein is achieved. This results in free cellular concentration of aggregation prone confirmations to be kept below a critical threshold, thus inhibiting aggregation overall. An alternative model is HSP70 acting as an unfoldase, in which it specifically unfolds parts of the client protein during binding to allow refolding into the correct active native conformation, which can take place over multiple rounds of binding. The final alternative is that client proteins can be passed onto alternative pathways for additional processing leading to a variety of fates (Mayer and Bukau, 2005; Clerico et al., 2015).

HSP70 has been implicated in numerous pathologies from viral infections to cancer. In particular, it is frequently seen upregulated in multiple cancers leading to an increased activation of cell signalling pathways involved in driving cancer progression (Sherman and Gabai, 2015; Aviner and Frydman, 2020; Wang et al., 2020). Based upon the observation for a role of HSP70 in numerous pathologies, many attempts have been made to develop specific HSP70 inhibitors. Targeting of both the SBD and NBD with small molecule inhibitors has given rise to several successful compounds, however none of these have passed beyond phase II clinical trials due to an issue with side effects. HSP70 inhibition has been shown to lead to a redundant mechanism of HSP90 upregulation and cellular toxicity being particularly noted due to the large number of key clients that HSP70 is involved in chaperoning (Trepel et al., 2010; Hendriks and Dingemans, 2017; Nitzsche et al., 2023). However, developing more selective small molecular modulators of HSP70 is still of interest as results targeting HSP70 ATPase activity, using inhibitors such as VER-155008 (Figure 8), have shown a significant reduction in KSHV protein expression and infectious virion production (Baquero-Pérez and Whitehouse, 2015).
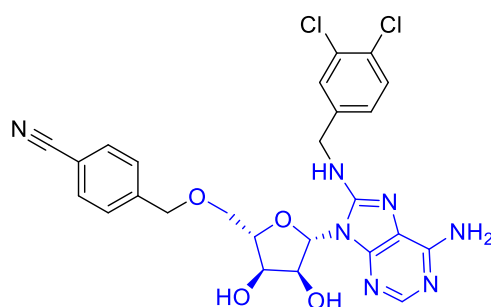
VER-155008

Figure 8: Structure of the HSP70 ATPase inhibitor VER-155008 which showed activity against KSHV lytic replication. Adenosine motif highlighted in blue.

1.2.1.2 HSP90

HSP90 is family of ATPase containing molecular chaperones with a molecular weight of 90 kDa. In mammals, similar to HSP70, five isoforms exist including constitutive and inducible forms with cellular organelle variants found in the cytoplasm, endoplasmic reticulum and mitochondria. HSP90 proteins are expressed in all kingdoms of life except archaea (Hoter et al., 2018). Under normal cellular conditions HSP90 accounts for 1-2% of proteins present in the cell, rising further under stress. This emphasises how important HSP90 proteins are for cellular function. The inducible cytoplasmic variant has a high sequence homology to the constitutive form and performs many of the same functions, with both cytoplasmic isoforms also being found in the nucleus in smaller amounts (Gasc et al., 1990). Like other chaperones, HSP90 functions by binding to unfolded proteins or disordered proteins, with specificity towards later stages of protein folding nearing their active conformational state. General cellular roles of HSP90 are further outlined in Table 5 (Pearl, 2016; Hoter et al., 2018; Genest et al., 2019).

Table 5: Roles of HSP90 within the cell during normal and stressed conditions

HSP90 roles
Transfer of clients to other folding and quality control mechanisms for further refolding, disaggregation, and degradation
Aiding in antigen presentation to cell surface
Protein aggregate prevention and disassembly
De novo protein folding
Protein folding and refolding
Regulation of protein activity
Arrangement and protection of cytoskeleton
Cell cycle
Cellular differentiation
Assembly and disassembly of protein complexes

HSP90 structure is comprised of monomers containing a C-terminus domain (CTD), a middle domain (MD) and an N-terminus domain (NTD). The CTD allows for the dimerization of the two monomeric species forming the active dimer (Hoter et al., 2018). The cytoplasmic isoforms of HSP90 CTD also contains the EEVD domain, responsible for binding to a variety of TPR containing chaperones (Genest et al., 2019). The NTD and MD contain the ATPase binding site with a flexible linker present in cytoplasmic and endoplasmic reticulum isoforms and is believed to allow binding to a wider array of clients. All three domains are involved in client

binding, with the MD being responsible for high affinity binding, which is enhanced by the NTD and CTD regions. Analogous to HSP70, HSP90 cycles though an open and closed state via ATP binding and hydrolysis, Figure 9 shows a representation of the open and closed state of cytoplasmic HSP90 isoforms, where ATP binding results in dimerization of NTD (Pearl, 2016; Hoter et al., 2018; Genest et al., 2019).
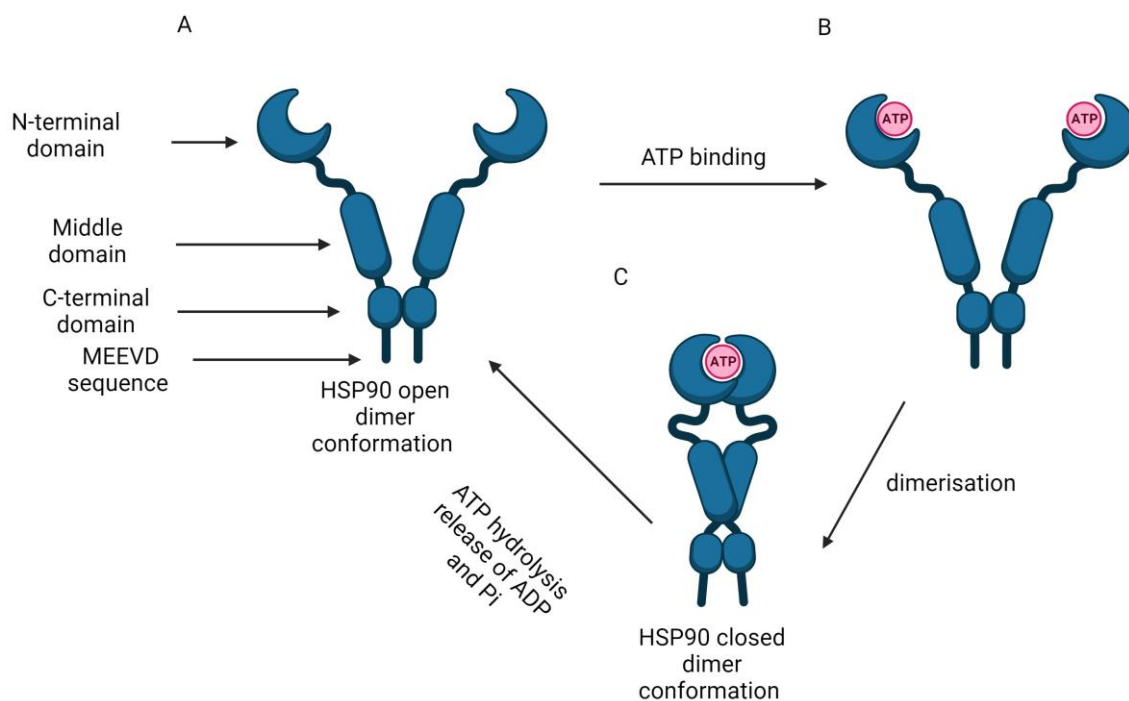
Figure 9: Representative structure of HSP90 dimer in (A) open state without ATP bound (B) Open state with ATP bound (C) closed state post dimerization and ATP hydrolysis possible. Created with BioRender.com

The recognition of clients by HSP90, unlike many chaperones, does not appear to be sequence specific but rather relates to the inherent thermodynamic stability of a protein's particular confirmation, alongside loading of clients via co-chaperones and other chaperones. This thermodynamic specificity tends to involve proteins in a metastable state at a higher energy state. An example of this metastable state is carbon atoms in diamonds. They are in a thermodynamically higher energy state than graphite, however they are kinetically locked from rapidly degrading to the lower energy graphite. In a structural sense, this means HSP90 clients tend to have protein surfaces containing an over representation of amino acids that have charged and/or hydrophobic properties (Li et al., 2012; Taipale et al., 2012; Karagöz and Rüdiger, 2015; Genest et al., 2019).

The ATPase cycle of HSP90 is critical to its ability to function as a molecular chaperone. This conformational cycling is controlled by a suite of co-chaperones which bind at different stages, stabilising certain conformations and client-HSP90 interactions, or alternatively allowing initial client loading. The initial loading of many HSP90 clients occur from HSP70-bound clients, scaffolded by the HOP co-chaperone. Other clients, in particular kinases, may require additional assistance for loading by other co-chaperones, such as Cdc37 (Lang et al., 2021). A simplified schematic of HOP-mediated HSP90 client loading, and conformational cycling is outlined in Figure 10.
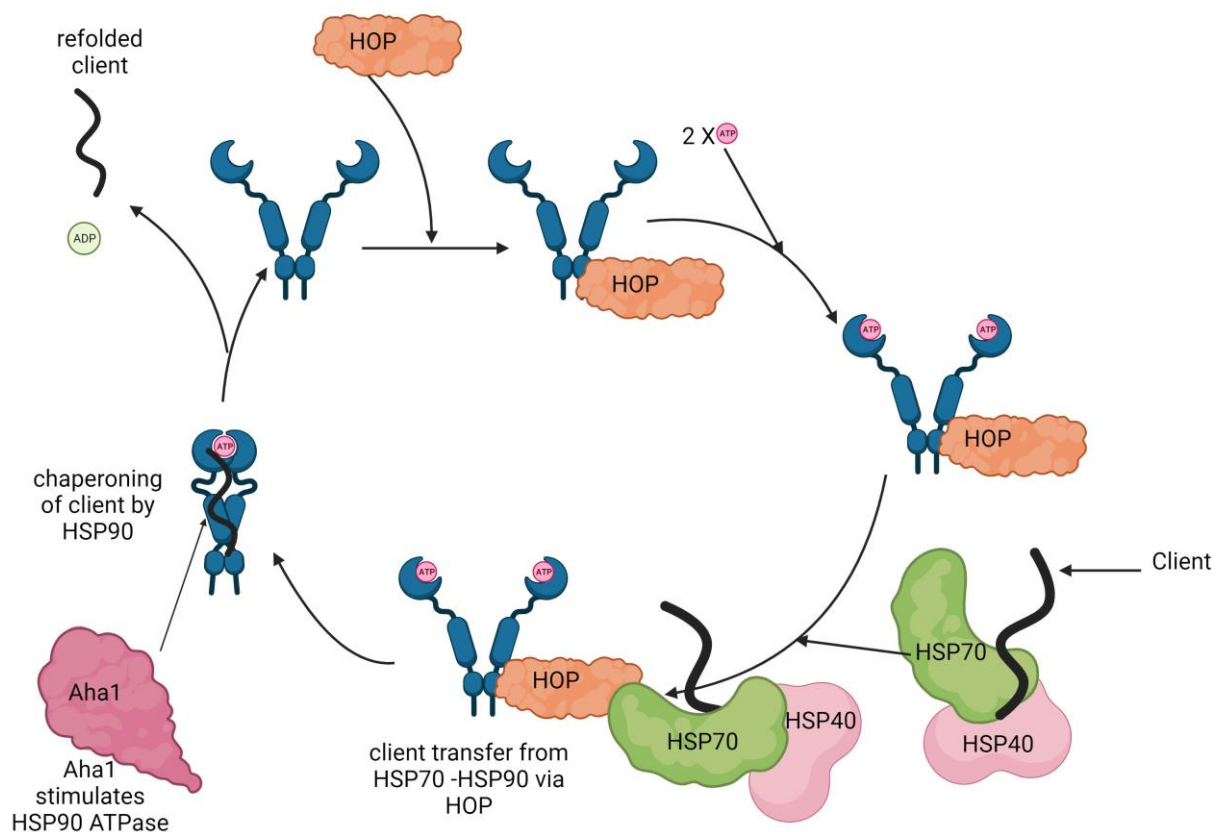
Figure 10: A simplified schematic of the HSP90 client loading and ATPase cycle via HOP. Beginning in the open dimer conformation of HSP90, HOP binds to HSP90 MEEVD peptide motif in HSP90 CTD. ATP then binds to HSP90 dimer. HOP then recruits HSP40-HSP70-client complex via interaction with TPR1 domain of HOP with HSP70 EEVD CTD motif. Client transfer occurs from HSP70 to HSP90 and HOP dissociates from HSP90. HOP dissociation allows dimerization of NTD domains to occur resulting in closed structure. Chaperoning of client occurs during this closed dimer state of HSP90. Aha1 stimulates ATPase activity of HSP90. Dissociation of ADP and refolded clients occurs with HSP90 returning to an open dimer conformation. Created with BioRender.com

Unsurprisingly, HSP90 has been an active pharmaceutical target for many years due to its involvement in a swathe of conditions, particularly in cancer. HSP90 upregulation is observed in multiple cancers and has been shown to play a key role in the inhibition of apoptosis and in pathways driving malignant transformation processes (Trepel et al., 2010; Calderwood and Gong, 2016). As such, attempts to inhibit or modulate HSP90 function via small molecules has been investigated as a potential pharmaceutically relevant target in a cancer context. Several specific inhibitors have been developed, with most success in targeting the ATPase site in the NTD. Many of these compounds have entered clinical trials. In addition, some CTD targeting compounds have also been identified, although none have progressed to the clinical trial phase (Zuehlke et al., 2018).

Two natural product compounds geldanamycin and radicicol (Figure 11) were found to target and inhibit the ATPase activity of HSP90, preventing cycling with slightly different binding poses. Notably, both showed activity in disrupting HSP90 conformational cycling and selectivity for HSP90, however they were both metabolically unstable and too toxic in *in-vitro* studies. As such, geldanamycin SAR development was undertaken, with a suite of compounds entering clinical trials. However, many of these compounds failed due to a lack of clinical efficacy in cancer trials coupled with severe side effects. Only one compound, IPI-504, progressed to phase III clinical trials in a cancer context but its development was discontinued due to a lack of clincial efficacy, with no further geldanamycin derivative compounds in trials to date (Zuehlke et al., 2018).

geldanamycin   radiciciol
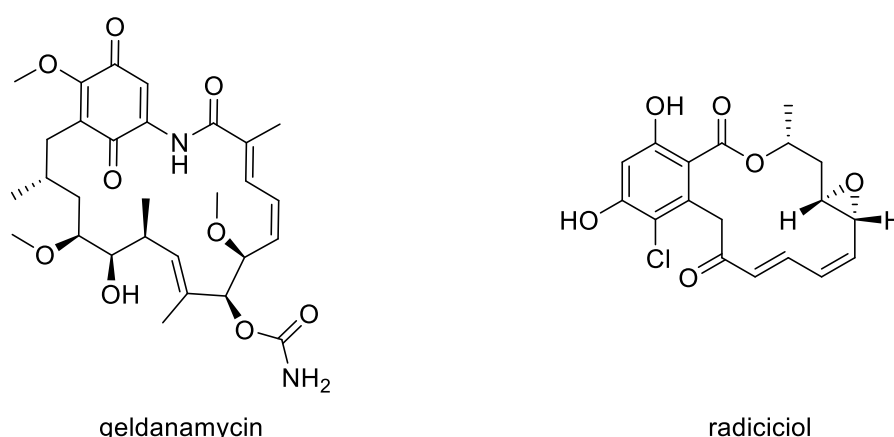
Figure 11: Chemical structures of the natural products geldanamycin and radicicol which were found to inhibit the ATPase site of HSP90 and were investigated as potential anticancer treatments.

A number of radicicol analogues have also entered clinical trials for cancer treatments with KW-2478 and AT13387 currently in phase I and phase II trials, respectively. Unfortunately, across the spectrum of HSP90 ATPase inhibitors low clinical efficacy has been prevalent, with

redundancy of the chaperone system apparent, particularly by HSP70 upregulation. Interestingly, focus has shifted from direct utilisation of these HSP90 ATPase inhibitors as treatments, but instead as drug conjugates to confer tumour specificity due to HSP90 upregulation in cancerous cells. An example of this approach is STA-8666, a HSP90 ATPase inhibitor conjugated to irinotecan, which has entered phase I clinical trials. Irinotecan is a topoisomerase 1 inhibitor that is used in the treatment of colon and lung cancer. The rationale for this approach is that the HSP90 inhibitor would lead to be a more targeted delivery of irinotecan in malignant cells, due to frequent upregulation of HSP90 in malignant cells (Heske et al., 2016; Zuehlke et al., 2018).

1.2.1.3 The potential role of HSP70 and HSP90 in KSHV infection

The role of HSP70 and HSP90 has been documented across a number of pathologies. Notably, multiple specific interactions between these heat shock proteins and various stages of the KSHV replication cycle, both in the latent and lytic phases have been documented (Field et al., 2003; Wen and Damania, 2010; Qin et al., 2010; Baquero-Pérez and Whitehouse, 2015; Aviner and Frydman, 2020)..

1.2.1.3.1 HSP70 and replication transcription centres

Work by Baquero-Pérez *et al.* found that HSP70 isoforms are redistributed and colocalise to KSHV replication and transcription centres (vRTCs) within the nucleus (Baquero-Pérez and Whitehouse, 2015). HSP70 was also demonstrated to be critical for the binding of RNA polymerase II to viral DNA promoters and the formation of vRTCs (Baquero-Pérez and Whitehouse, 2015). Importantly, vRTC formation is essential for KSHV replication as they are the sites of viral transcription, DNA synthesis and capsid assembly (Schmid et al., 2014). A SILAC-based quantitative proteomic screen, showed increased levels of constitutively expressed and induced HSP70 isoforms within nuclear envelope associated with vRTCs during KSHV lytic replication compared to the latent state, suggesting HSP70 had a potential role in the KSHV lytic replication cycle.
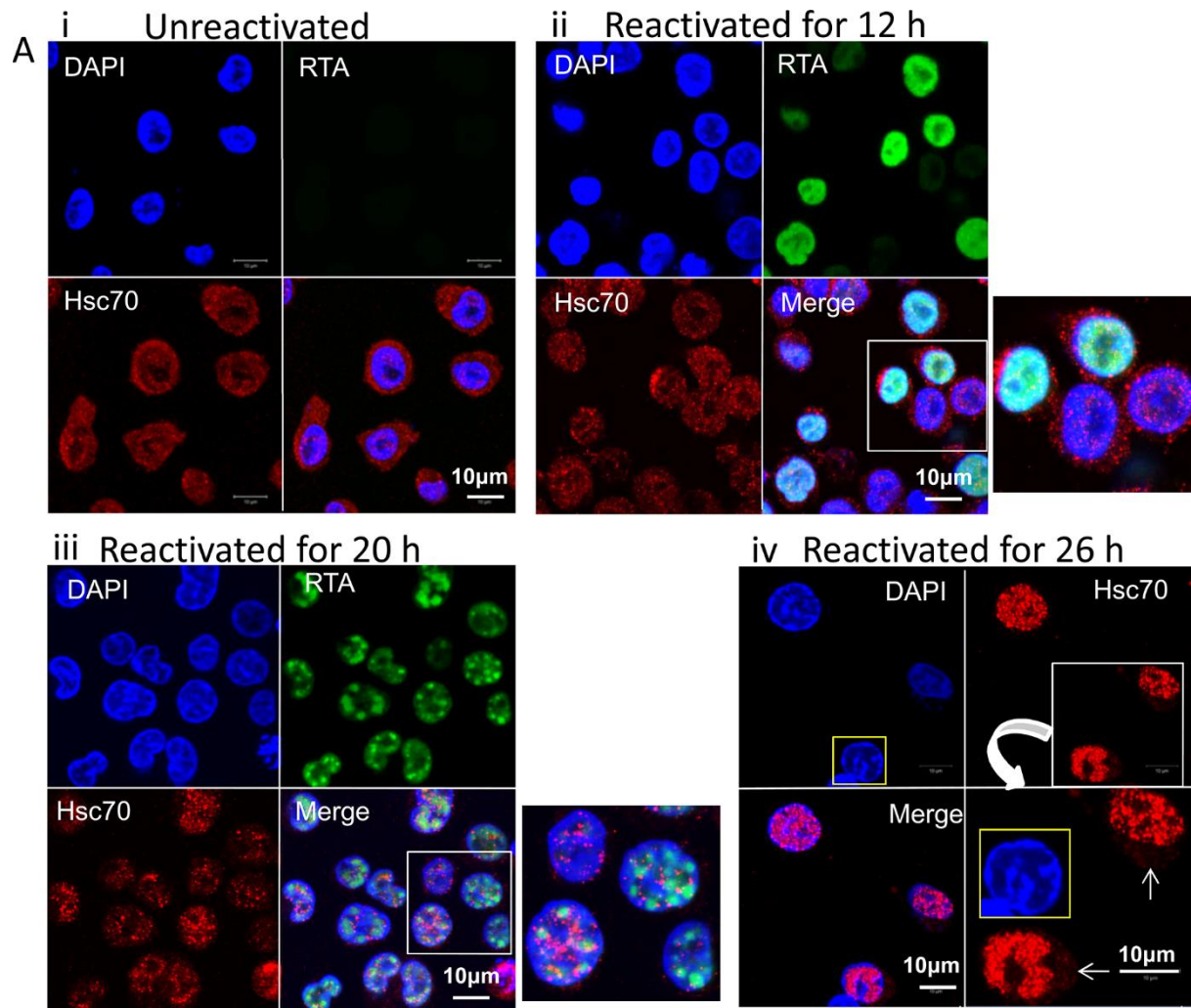
Figure 12: Immunofluorescent images showing constitutively expressed HSP70 at different time points of reactivation and its relocalisation to vRTCs. (Taken from (Baquero-Pérez and Whitehouse, 2015)

HSP70 relocalisation into vRTCs was confirmed by immunofluorescence studies and showed cells undergoing KSHV lytic reactivation alongside redistribution of distinct HSP70 isoforms. Both cytosolic HSP70 proteins were found to be redistributed and colocalised with RTA in vRTCs in the nucleus (Figure 12). A specific HSP70 inhibitor, VER-155008, employed at non-cytotoxic concentrations lead to a reduction of KSHV infectious particles due to decreasing DNA replication and levels of virally-encoded proteins (Wen et al., 2014). Further investigation showed that HSP70 inhibition prevented vRTC formation and RNAPol II from binding to viral promoters. These results suggest targeting HSP70 is a viable option for inhibiting KSHV lytic replication.

KSHV 12 hours into lytic replication cycle

KSHV 20 hours into lytic replication cycle

KSHV 26 hours into lytic replication cycle

△ HSP70

○ RTA

● Replication transcription centres
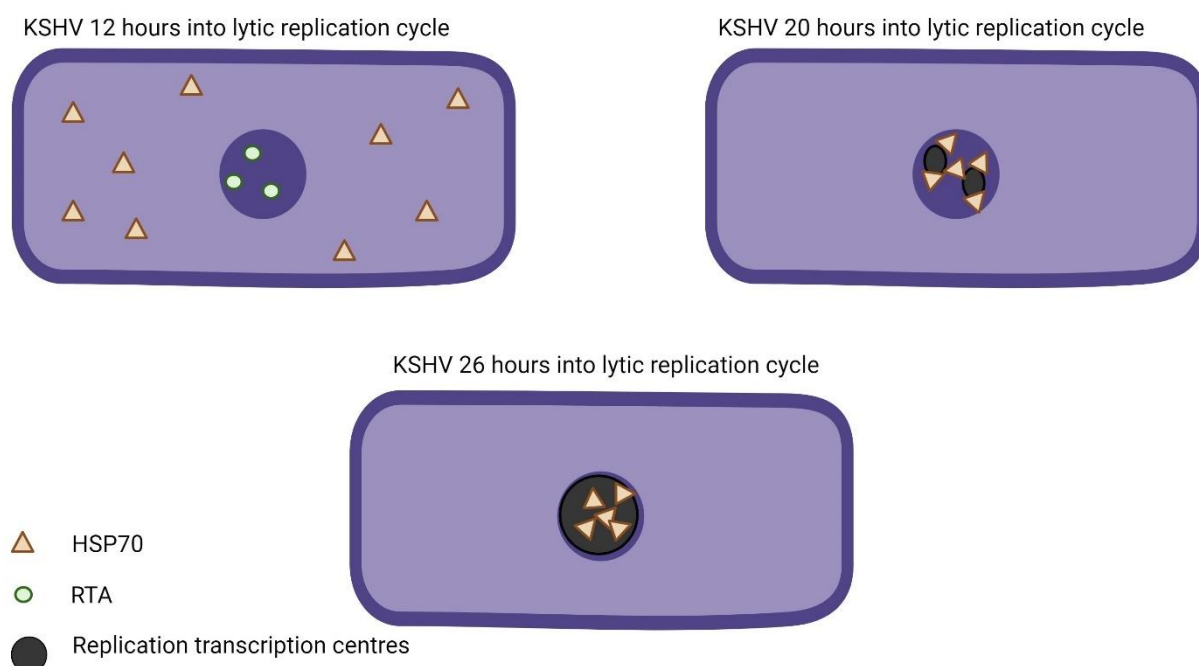
Figure 13. HSP70 proteins role during the KSHV lytic cycle. Early in the lytic cycle (12 hours post reactivation (P.A.)), RTA localises to the nucleus and HSP70 is found in the cytoplasm. At 20 hours P.A., the formation of individual replication centres (RTCs) occurs and HSP70 re-localises to the periphery of RTCs in the nucleus. As the lytic cycle reaches 26 hours P.A., RTCs amalgamate into one central RTC and HSP70 re-localises into the RTC. Created with BioRender.com

1.2.1.3.2 Fak activation and cell surface HSP90

An alternative HSP target has also been investigated in the context of KSHV infection, namely cell surface associated HSP90. Inhibition of this HSP90 variant was assessed to determine if its inhibition could prevent infection of new cells (Qin et al., 2010). This built on previous work which suggested HSP90 acted as a receptor for a number of viruses during entry (Reyes-del Valle et al., 2005). Firstly, KSHV susceptible cell lines, HeLa (cervical cancer cells) and DMVEC (endothelial cells) underwent a combination of flow cytometry and immunofluorescence studies to confirm the presence of cell surface HSP90. Following these results, a non-cell permeable HSP90 inhibitor based upon geldanamycin, DMAG-N-oxide (DNo), was used to elucidate the role of csHSP90 in KSHV infection. Using latently infected DMVEC cells, quantitative reverse transcription (qRT-PCR) and immunofluorescence studies were then carried out with cells treated with DNo. Surprisingly, results showed a reduction in latent gene expression, however, this effect was cell type specific, only occurring in DMVEC cells. Interestingly, addition of DNo did not affect the ability of KSHV to infect cells, as levels

of latent gene expression were equally reduced in both KSHV-infected cells treated with DNo and DNo treated cells infected with KSHV. This suggested that the role of csHSP90 is distinct from viral entry and highlights a novel role in KSHV infection.

To gain entry into cells, KSHV virions bind to cell surface receptors, including α3β1 integrins, which results in Fak activation. In turn, Fak regulates multiple pathways, primarily the P-13K anti-apoptotic pathway and the MAPK pro-survival pathway. Therefore, the interaction between KSHV and α3β1 is now thought to be essential for viral entry and establishing an intracellular environment conducive to KSHV infection (Sharma-Walia et al., 2004; Krishnan et al., 2006). It has therefore been postulated that csHSP90 could have a role in the α3β1 signalling pathway, as the ratio of phosphorylated to unphosphorylated kinases, including MEK and ERK, were altered when cells were exposed to DNo. Levels of phosphorylated MEK and ERK were reduced significantly, which inhibited the MAPK pathway. This aligns with previous work showing that phosphorylated MEK and ERK are essential for the expression of KSHV genes and establishment of infection (Sharma-Walia et al., 2005). Thus, treatment of cells with DNo, inhibits csHSP90 during naive KSHV infection, and prevents KSHV-induced phosphorylation and activation of ERK and MEK proteins. To confirm these results, MEK and ERK overexpression vectors were transfected into cells treated with DNo, to determine if overexpression of these kinases could rescue KSHV gene expression. Results showed approximately 50-80% of control levels of LANA, while cells treated with a MAPK inhibitor showed minimal LANA expression. Together, these results suggest that KSHV targets the cell surface HSP90 to regulate the MAPK signalling pathway, suggesting modulation of HSP90 could be a potential pharmaceutical target.

1.2.1.3.3 KSHV glycoprotein K1 and HSPs

KSHV encodes the transmembrane glycoprotein K1, which resembles a B-cell receptor and has been linked to the activation of PI3K, Akt and mTOR kinases. This suggests that KSHV may affect multiple cell growth, proliferation, survival, motility and apoptosis pathways. Furthermore, K1 prevents Fas-mediated apoptosis in endothelial cells and promotes release of angiogenic agents. Thus, it is believed that K1 has key roles in tumorigenesis (Ganem, 2010; Wen and Damania, 2010). Further studies to identify interactions between K1 and host proteins used tandem affinity purification of a K1-flag construct coupled with quantitative proteomic analysis. Results showed K1 associates with constitutively expressed HSP90 and ER HSP40 (Wen and Damania, 2010). Furthermore, the implication of this interaction were investigated using an apyrase enzyme that depletes ATP and ADP in cells, and results showed that the interaction between constitutive HSP90 and K1 was ATP-dependent. This was further supported by the use of the HSP90 ATPase inhibitor geldanamycin, which dramatically

reduced the levels of K1, leading to lower levels of phosphorylated Akt. Similar results were also observed using siRNAs targeting HSP90 and ER HSP40, which again resulted in higher rates of apoptosis. Interestingly, maximum levels of apoptosis were observed upon knockdown of both heat shock proteins. This indicates that both heat shock proteins are necessary for K1-mediated cell survival during Fas stimulation.

1.2.1.3.4 HSP90 and NF-kB activation

Another essential KSHV-encoded protein related to the anti-apoptotic effect observed in KSHV infection is vFLIP. vFLIP is a KSHV-latently expressed protein and alongside HSP90, is involved in mediating NF-kB activation (Field et al., 2003). NF-kB is a protein complex that acts as a transcription factor during times of cell stress, such as inflammation and infection. Activation of NF-kB results in its translocation to the nucleus, allowing expression of over 150 genes, which regulate cytokine production and anti-apoptosis pathways. The IKK complex is responsible for the retention of NF-kB in the cytoplasm, by masking its nuclear localisation signal and thus inhibiting its function as a transcription factor (Hinz and Scheidereit, 2014). In KSHV infected PEL cells, the NF-kB pathway is constantly active, thereby inhibiting apoptosis. vFLIP binds IKK, resulting in the downstream release of NF-kB into the nucleus, leading to expression of anti-apoptotic genes. This activation of the NF-kB pathway demonstrates both the essential role vFLIP during infection, but also its importance in KSHV-associated pathologies. Further research demonstrated that vFLIP affected the kinase activity of IKK, which regulates NF-kB release. Interestingly the use of the HSP90 inhibitor geldanamycin significantly reduced kinase activity, showing that activation of IKK by vFLIP was HSP90 dependant. Geldanamycin treatment in KSHV-infected PEL cell lines resulted in 40% more cell death than a DMSO control, due to a reduction in NF-kB nuclear localisation and a lack of anti-apoptosis gene expression (Field et al., 2003).

These results suggest that the cell death observed in KSHV-positive PEL cells was due to an inhibition of vFLIP-mediated IKK kinase suppression which prevented NF-kB nuclear localisation. In contrast however, the aforementioned work by Wen *et al.* also showed HSP90 ATPase inhibition of KSHV-positive PEL cells resulted in cell cycle arrest and cell death, due to reduced K1 expression and reduced MAPK activation (Wen and Damania, 2010). Both studies present evidence of HSP90 interacting with two different KSHV viral proteins, and HSP90 ATPase inhibition causing a dramatic effect on virus-mediated control over cell signalling pathways. This demonstrates the challenge of determining the exact method of action of an inhibitor even if binding partner is known. This is especially relevant in the case of a protein like HSP90, as it is involved in multiple cellular pathways in normal and abnormal cells.

1.2.1.4 Co-chaperones of HSP70 and HSP90

The above sections detail the involvement of HSP70 and HSP90 proteins across a range of pathologies, with specific examples relating to their critical role in the KSHV replication cycle. However direct small molecule inhibition of these HSPs has proven ineffective. Therefore, to modulate the activity of HSP-related pathways and function, a potential alternative route is by targeting the activity of their co-chaperones that facilitate effective chaperoning of clients to HSPs. To modulate and aid in the specific roles of the vitally important HSP70 and HSP90 proteins, a variety of co-chaperones help to maintain proteostasis via their interactions with each HSP. The role of these co-chaperones are varied from client recognition to stimulating HSP ATPase activity. As this thesis focuses on the co-chaperone HOP and its TPR domains, further insight is given below into the TPR-containing co-chaperones.

1.2.1.4.1 TPR containing Co-chaperones

The tetratricopeptide repeat (TPR)-containing family of co-chaperones interact with HSP70 and HSP90 through the C terminus EEVD and MEEVD domains within HSP70 and HSP90, respectively. The TPR domain itself is present across a wide variety of organisms, including prokaryotes and eukaryotes, and has been found in over 200 human proteins. Although many of these lack co-chaperone activity or interact with HSP proteins (Haslbeck et al., 2013). TPR co-chaperones are key to the regulation and function of the molecular chaperone machinery and play a vital role in deciding the fate of many of HSP70 and HSP90 client proteins. Notably, the TPR interacting HSP70/90 conserved EEVD and MEEVD amino acid sequences are only present in cytosolic HSP70 and HSP90 constitutive and inducible expressing forms. The TPR domain is defined as 3-16 repeating unit, composed of 34 amino acids which form amphipathic, antiparallel α-helix hairpins (D'Andrea and Regan, 2003). Table 6 outlines some of the TPR domain-containing co-chaperones which interact with HSP70/90. The TPR co-chaperones interact in a 1:1 ratio with respective EEVD and MEEVD amino acid sequences, however, the HSP90 dimeric nature allows for two TPR binding events to occur simultaneously.

Table 6: Co-chaperones containing a TPR domain which interact with HSP90 and/or HSP70

Protein name	Generalised role
HOP	Transfer of clients from HSP70 to HSP90
CHIP	E3 ligase that binds with HSP90 and HSP70 resulting in client proteasomal degradation
FKBP51/2	Co-chaperone of HSP90 in activating hormone signalling
DnaJC7	HSP40 isoform acting as a chaperone in client recruitment to HSP70

1.2.1.4.1.1 HOP

The stress induced phosphoprotein 1 (STIP1) gene encodes for the 63 kDa HOP protein. HOP contains three TPR domains, TPR1, TPR2A and TPR2B with two DP (aspartate and proline rich) domains, and a flexible linker connecting DP1 to TPR2A (Figure 14). TPR1 interacts with HSP70, whilst TPR2A interacts with HSP90. TPR2B can interact with both HSP70 and HSP90 but with a weaker affinity. These interactions occur between the TPR domains and the disordered C-termini containing EEVD and MEEVD motifs of HSP70 and HSP90, respectively (Röhl et al., 2015). HOP appears to have ATPase functionality, however an exact defined binding site has not been elucidated (Yamamoto et al., 2014). In addition, HOP does not possess any chaperoning functionality itself (Bose et al., 1996). Despite the domains of HOP being well characterised and some of these domains have been structural determined by X-ray crystallography, the full length structure is still undetermined.

Figure 14: Schematic structure of HOP protein. Three TPR domains which interact with HSP70 and HSP90 coupled with DP domains. A flexible linker region is present between DP1 and TPR2A. Created with BioRender.com

HOP is found across eukaryotes and has been identified in a diverse array of species but is not present in prokaryotes. Like its gene name suggests it is stress inducible, however it can also be expressed constitutively in certain cells. HOP is mostly found in the cytoplasm, although it has been observed in the nucleus, golgi and in extracellular environments (Bhattacharya and Picard, 2021). HOP knockout studies display vastly different phenotypes, for example in lower organisms milder phenotypes are displayed, whilst in mice knockdown is embryonically lethal Bhattacharya et al., 2020). This suggests that cell type, cell state alongside which particular organism all play a role in the degree of phenotypic response (Nicolet and Craig, 1989; Song et al., 2009; Beraldo et al., 2013).

The major characterised role of HOP is facilitating the transfer of clients from cytosolic isoforms of HSP70 to cytosolic isoforms of HSP90. It primarily achieves this function by acting as a scaffold between the two HSPs. Alongside this, HOP binding to HSP90 results in allosteric inhibition of ATP hydrolysis, but not the binding of ATP. The binding of both TPR2A and TPR2B is required for this allosteric inhibition. As such, HOP control of HSP90 ATPase

activity results in an open ATP bound state ready for client loading, but also primes HSP90 dimerization with ATP, upon HOP dissociating post client binding (Schmid et al., 2012). Work has investigated the HSP70-HOP-HSP90 client transfer network (Alvira et al., 2014) and summarised in Figure 15. Their hypothesised mechanism shows HSP70 binds a client with aid of HSP40, during this time HSP90 is in an open state with no ATP present, which allows binding to the HOP TPR2A and TPR2B domains. ATP then binds to the HSP90 NTD but is prevented from dimerizing to the other HSP90 NTD domains. This results in an open HSP90 ATPase bound dimer that is prevented from NTD dimerization and ATP hydrolysis by TPR2A and TPR2B. The HSP90-HOP complex then recruits the HSP70 client bound complex via TPR1, with HOP in an open conformation, HOP then rearranges to a closed conformation allowing the transfer of the HSP70 client to HSP90. HOP then dissociates from HSP90 allowing HSP90 to dimerise around the client protein and perform its chaperone activity.
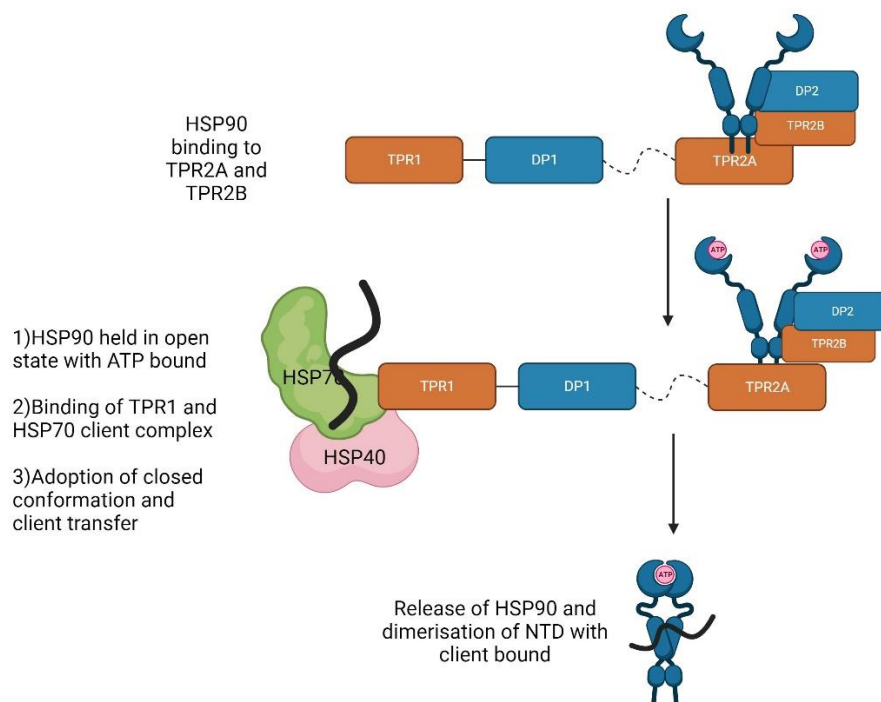
Figure 15: A simplified schematic of HOP protein interaction with HSP90 & HSP70 during the transfer of client protein. Created with BioRender.com

Further analysis of HOP knockout cell lines has shown that HSP70 and HSP90 can return to a prokaryotic folding network, in which HSP70 and HSP90 interact and transfer clients without HOP (Bhattacharya et al., 2020). This prokaryote-like HSP pathway fascinatingly resulted in an increase in client folding and a reduction in degradation via the proteosome, Notably, these knockout cells were frequently more resistant to induced stress upon the proteome. The work suggested that HOP acts as an inhibitor of the HSP90 ATPase cycle,

resulting in a faster chaperoning in the prokaryote state. In addition, knockout cells failed to properly chaperone the proteasome complex. However, this work emphasises the lack of understanding of the role of HOP in higher organisms. Interestingly, HOP knockdown in multiple cancer cell lines reduces cancer phenotypes involved in invasion and metastasis (Bhattacharya and Picard, 2021). Conversely, upregulation of HOP is seen in many cancers, in both the intra and extracellular environment. Similarly, treatment with TPR2A mimic peptides that blocked HSP90-HOP interactions showed promising anticancer activity (Horibe et al., 2011).

1.2.1.4.1.1.1 Drug development of HOP

Development of HOP inhibitors has focused on the TPR2A domains PPI with HSP90. Yi and Regan utilised an alpha screen approach to conduct a HTS and identified a potential PPI inhibitor, 3-methyl toxoflavin (Yi and Regan, 2008). Similarly, further work claimed inhibition of the PPI with a methyl and ethyl substituted analogue of 3-methyl toxoflavin (Pimienta et al., 2011) (Figure 16). Unfortunately, this family of toxoflavin compounds are known PAINS (pan-assay interference compounds) due to their ability to undergo redox cycling and produce hydrogen peroxide. Moreover, both approaches only utilised assays that demonstrated competition via assays that can suffer from colorimetric interference, another known property of toxoflavins (dos Santos, 2015; Baell and Nissink, 2018).

3-methyl toxoflavin   Pimienta *et al*. derivative
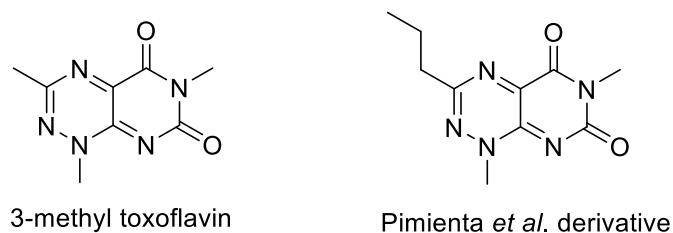
Figure 16: Structure of toxoflavin based proposed inhibitors of HOP's TPR2A domain and HSP90 C-terminus.

The TPR2A HSP90 PPI can also be disrupted using a large hybrid peptide analogous to a section of the TPR2A domain combined with a cell membrane penetrating tag (Horibe et al., 2011). This peptide was shown to be active in various cancer cell lines at non-cytotoxic concentrations. In addition, extended experiments in mouse models using pancreatic cancer cell xenografts, showed that peptide treatment caused a reduction in tumour size with no observable damage to mouse organs. Concurrent work developed analogues of the natural product peptide sansalvamide A (Figure 17). These analogues bound to the NTD and CTD of the HSP90 dimer (Ardi et al., 2011). This sansalvamide derivative allosterically inhibited the C-terminus containing HSP90 MEEVD binding domain, preventing the binding of HOP.

However, this approach was found to be non-specific and resulted in inhibition of three other co-chaperones protein which had the ability to bind to the HSP90 CTD.

Sansalvamide A   Sansalvamide A derivative
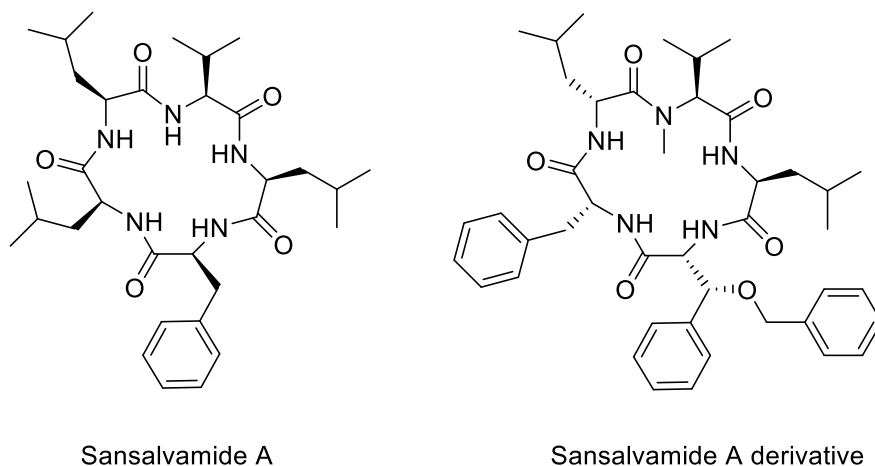
Figure 17: Sansalvamide A and its derivative which act as an allosteric inhibitor of HSP90 C-terminus binding.

Recently, a multifaceted approach by Darby *et al.* identified the activity of dicarboxylic acids in inhibiting the interaction of TPR2A with a HSP90 CTD peptide fragment (Darby et al., 2020). They further developed this fragment work into a carboxylic acid compound with a tryptoline motif, that again demonstrated competition with the HSP90 peptide, but showed no evidence of specifically disrupting the HOP/TPR2A HSP90 PPI. Notably, they discuss the challenges of targeting TPR domains, due to shallow nature and positive charge of the motif. Similar work by Vaalytn *et al.* utilised a bio-isostere approach of a tetrazole replacement for the carboxylic acid (Vaaltyn et al., 2022). The MEEVD HSP90 TPR recognition peptide motif contains three carboxylic acid side chains with two glutamic acid and aspartic acid residues. An initial fragment screen identified tetrazole activity and replacement of the second glutamic acid with a semi-synthetic amino acid containing a tetrazole side chain further improved inhibition. Notably, repurposing of several approved tetrazole containing drugs showed competition of full length HSP90 and TPR2A, however only at mM ranges.

Taken together the challenge of targeting the TPR domains is clear, with all approaches targeting only the TPR2A domain. Furthermore, to date no work has presented a selective small molecule-based inhibitor of the TPR2A HSP90 interaction with a small enough IC_{50} for potential pharmaceutical development. Large peptides do show activity however challenges relating to utilising these *in-vivo* limit the utility of these compounds.

1.2.1.4.1.2 CHIP

Another crucial TPR containing co-chaperone is CHIP (carboxy terminus HSP-70 interacting protein). The major role of CHIP relates to protein degradation via the ubiquitin–proteasome system. Structurally it is comprised of three domains; an N-terminus containing three TPR regions which allow CHIP to interact with both HSP70 and HSP90. A central charged domain which aids in TPR region functionality, and a final U-box domain that contains E3 ligase activity enabling ubiquitination of proteins for onward degradation. Thus a major role of CHIP is thought to be in the ubiquitination of client proteins that the HSP systems cannot conformationally correct (Mcdonough and Patterson, 2003; Quintana-Gallardo et al., 2019). Interestingly CHIP has been found to ubiquitinate proteins without the presence of either HSP binding partner, but currently an understanding of why certain clients show HSP mediated versus independent ubiquitination is not documented. Not surprisingly therefore, CHIP is involved in numerous pathologies, such as cancer, protein aggregation disorders and cardiovascular disease. Its role in cancer is multifaceted with reported roles in both tumour suppression and oncogenesis, with some indication this may be cell type specific (Kumar et al., 2022).

1.3 Drug Development

The development of new and effective pharmaceutical treatments is vital for a variety of reasons; treatment of untreatable conditions, disease resistance to previous treatment methods, improvement of patient prognosis and quality of life and responding to a globally aging population. Drug discovery and development in the modern age is a costly, failure prone and time-consuming endeavour. This is highlighted by the following statistics which don't account for failed attempts. Worryingly there is an approximately 90% failure rate occurring from phase I to phase III (Sun et al., 2022). The average timespan from hit identification to the development of a novel therapeutic for first in class drugs is believed to be around 20-25 years (Eder et al., 2014). A 2020 analysis placed the cost of bringing a new drug to market is in the region of $1.33 billion, with a 2016 analysis estimating a yearly increasing cost of 8.5% above inflation (DiMasi et al., 2016; Wouters et al., 2020).

Approaches to small molecule drug discovery can fall broadly into three categories defined by phenotypic, chemocentric and target-based approaches (Eder et al., 2014). Phenotypic approaches utilise large scale screening of a diverse library of compounds into an assay, with hits generating a desired phenotype. Hits from this assay are then examined for mechanism of action and then further SAR optimised. Chemocentric approaches begin with an identified compound, such as a natural product, which is then analysed for phenotypic effects and mode of action.

Target-based approaches assess inhibition or activation of a known biological target, such as an enzyme active site or PPI via screening of compounds. Several different approaches can be used within the target-based approach, after an appropriate target has been selected and validated for small molecule inhibition. Utilisation of *in-silico* docking of compounds into target sites in both a random and targeted manner is frequently employed. This can be a useful methodology in streamlining HTS screening and can also be further utilised downstream to aid in the development of SAR if a hit has been identified. This classical approach of *in-silico* prediction utilises discrete categorised values for interactions and builds assumption from this data (Stokes et al., 2020).

A key step to drug development is assay selection, generation, optimisation, and validation. With decisions surrounding assay suitability such as desired HTS screening size, pharmacological relevance, reproducibility, and cost being key factors. Once an appropriate and validated assay has been developed, screening approaches can vary greatly from HTS of full-sized drug like molecules, fragment screening and rational structural based design. Parameters for defining a hit should be set and any compound that is identified as a positive hit should then proceed onto further validation by generating binding/competition data that fulfils appropriate potency aims and tested with orthogonal assays. In addition, analysis of hits, should follow general guidelines such as Lipinski rule of 5 (Table 7), which can be useful in streamlining compounds for future suitability for orally active compounds. It should however be noted that such rules may not always be appropriate and that further optimisation of a hit compound for pharmacokinetics and pharmacodynamics is always employed. For example, in a fragment screen, the Lipinski rule of 5 would not be appropriate initially.

Table 7: Lipinski rule of 5 that have been utilised for assessing if a compound can be orally bioavailable pharmaceutical.

Lipinski rule of 5
Mw less than 500 daltons
No more than 5 hydrogen bond donors
No more than 10 hydrogen bond acceptors
Octanol–water partition coefficient log P not greater than 5

Development of SAR (structure activity and relationship) through iterative rounds of chemical modifications should then be undertaken to improve pharmacodynamics. Determining *in-vitro*

activity as a proof of concept is incredibly valuable at this stage. Alongside this, key considerations into the pharmacokinetics of the compounds with ADMET (absorption, distribution, metabolism, excretions and toxicity) properties being a useful guide. Considerations of solubility, cellular therapeutic window, CYP450 inhibition and hERG inhibition to name but a few should be adopted in compound development. Once an appropriate lead molecule has been identified, *in-vivo* studies can then be undertaken and assessed before progressing with a final compound into the clinical trial stage (Hughes et al., 2011).

In recent years, the use of artificial intelligence (AI) deep learning approaches has begun to be employed in drug discovery, with a 34% increase in publications year on year related to AI approaches. A 2023 report by the Wellcome Trust detailed its perceived major uses for AI in drug discovery; including target identification, small molecule design and optimisation, mRNA vaccine design, antibody design and ADMET prediction models (Loynachan et al., 2023). A major benefit of utilising artificial intelligence systems for *in-silico* compound screening over traditional models is based upon the continuous rather than discrete preassigned calculations of a molecule's properties. This continuous variable of a molecules fingerprint can allow for a more accurate depiction of interactions during screening (Stokes et al., 2020). Recent work demonstrated the efficacy of deep learning approaches in the discovery of a novel antibiotic, Halicin, which has a unique mode of action and identified by virtual screening of over a billion molecules (Stokes et al., 2020). The utilisation of AI approaches combined with appropriate training libraries and empirical investigation has great potential going forward in the development of novel pharmaceuticals.

1.4   Thesis Objectives

The crucial role of HSP70 and HSP90 across a range of pathologies is clear, including multiple roles in infection. Therefore, targeting HSP70 and HSP90 directly with SM inhibitors is a promising pharmaceutical target. Development of specific inhibitors of the ATPase site has been achieved, however issues such as redundancy across the HSP network and toxic side effects has prevented the progression of these inhibitors into clinical trials.

The co-chaperone network is critical to the correct functioning of the chaperone network. Thus, these may be potential pharmaceutical targets, offering a more finessed approach to modulate the HSP machinery to ameliorate some of the issues with direct ATPase inhibition. The role of HOP in client transfer from HSP70 to HSP90 makes it an intrinsically interesting target, as clients are transferred from one chaperone network to the next. Based upon structural and biological data we believe the key to HOP inhibition is targeting the PPI interactions with HSP70 and HSP90. Within the literature several attempts have been made to develop a successful small molecule inhibitor, disrupting the interaction between the HOP TPR2A domain and HSP90, however they all possess limitations of efficacy, selectivity or large peptide nature.

Hence this thesis aimed to probe the role of co-chaperone HOP in the specific context of KSHV infection and validate its potential as an antiviral candidate. In addition, we also wished to develop a novel inhibitor targeting the HOP-HSP interaction. In chapter 3, results demonstrated that HOP is upregulated during KSHV lytic replication, redistributed to vRTCs and is critical for efficient KSHV lytic replication. In chapter 4, two HTS assays were developed, validated and optimised to efficiently interrogate and identify potential inhibitors of the HSP70-TPR1 (HOP) and HSP90-TPR2A (HOP) interactions. Finally in Chapter 5, two alternative approaches, fragment screening and inhibitory peptides, were utilised to begin exploring potential SAR of the TPR1-HSP70 interaction. Together, this demonstrates the critical role of HOP in the KSHV lytic replication cycle, however, targeting TPR-HSP interactions is a challenging medicinal chemistry problem.

Chapter 2

~

Materials and Methods

2 Materials and Methods

2.1 Materials

2.1.1 Antibodies

2.1.1.1 KSHV antibodies

Table 8: List of KSHV antibodies utilised including supplier, species, dilution and product code

Antibody	Supplier	Species	Dilution	Product code
ORF57	Santa Cruz	Mouse	1 in 5,000	sc-135746
ORF59	Gift from Prof. Britt Glaunsinger, University of California Berkeley	Rabbit	1 in 1,000	-
ORF65	Cambridge bioscience	Rabbit	1 in 500	crb2005224d

2.1.1.2 Non-viral antibodies

Table 9: List of non-viral antibodies utilised including supplier, species, dilution and product code.

Antibody	Supplier	Species	Dilution	Product code
GAPDH	Proteintech	Mouse	1 in 5,000	60004-1-Ig
HOP	Abcam	Rabbit	1 in 2,000	EPR6605
Anti-mouse horseradish peroxidase	Agilent Technologies	Goat	1 in 5,000	P044701-2
Anti-rabbit horseradish peroxidase	Agilent Technolgoies	Goat	1 in 5,000	P044801-2

2.1.2 Cell lines

Table 10: List of cell lines utilised and the source of these cell lines.

Cell line	Source
BCBL-1 TREx-Rta	Gift from J. U. Jung (UCLA)
HEK-293T cells	ATCC
rKSHV .219	Gift from Dr Jeffery Vieira University of Washington Seattle
LEMO21	New England Biolabs
Dh5α	New England Biolabs

2.1.3 Chemicals and reagents

Table 11: List of chemicals and reagents used including supplier and associated product code.

Chemical/Reagent	Supplier	Product code
Acetic Acid 99.5%	Fisher Scientific	LC101003
Acrylamide/Bis-acrylamide 30% 37.5:1	BioServ	BS-4329E
Agarose	Sigma-Aldrich	A9539-500G
Agar	Sigma-Aldrich	A1296-100G
Ammonium persulfate	Sigma-Aldrich	215589-100G
Bis-tris	Fisher Scientific	10041463
Bovine serum albumin	Sigma-Aldrich	A7906-100G
Bromophenol blue	Sigma-Aldrich	B5525
B-mercaptoethanol	Sigma-Aldrich	M6250-100ML
Chloramphenicol	Sigma-Aldrich	85 744-0
Coomassie blue R-250	ThermoFisher Scientific	20278
DMSO	Sigma-Aldrich	D5879-100ML
DTT	Fisher Scientific	BP172-5
Ethanol	Sigma-Aldrich	32221-2.5L
ECL Western Blotting Substrate	Promega	W1008
Formaldehyde	Sigma-Aldrich	F8775-25
Glycerol	Sigma-Aldrich	G5516
Glycine	Fisher Scientific	10467963
HCl	Fisher Scientific	H/1100/PB17
Imidazole	Sigma-Aldrich	I2399-500G
IPTG	Sigma-Aldrich	I6758-5G
Isopropanol	Sigma-Aldrich	34863-2.5L
LB broth base	Invitrogen	12795027
Methanol	Fisher Scientific	M/4056/17
NaCl	Sigma-Aldrich	S9888-2.5KG
Nitrocellulose membrane	Cytiva	10600002
NP-40 surfact-amps™ detergent solution	Fisher Scientific	13434269
Nuclease free water	Promega	P119E
Protease inhibitor cocktail	Roche	58698000
Protease inhibitor cocktail	Expedeon	FISEX44201
Phosphate buffered saline	Lonza	BE17-516F

Protein Ladder	Bio-Rad	1610374
SDS	Sigma-Aldrich	L5750-1KG
Skimmed milk powder	Sigma-Aldrich	102540027
SYBR safe	Invitrogen	S33102
Tetramethylethylenediamine (TEMED)	Sigma-Adrich	T9281-100ML
Tris Base	Santacruz	Sc-3715B
Tris-Borate-EDTA 10 X stock	Invitrogen	AM9863
Transfer pads	Bio-Rad	1703966
Tween 20	Fisher Scientific	BP337-500
VECTASHIELD® Antifade Mounting Medium with DAPI	Vector Laboratories	H-1200-10

2.1.4   Cell culture reagents and materials

Table 12: Cell culture reagents and materials alongside supplier and product code.

Reagent	Source	Code
Doxycycline hyclate	Sigma-Aldrich	D9891-1G
Dulbecco's Modified Eagle Medium (DMEM)	Gibco	41965-039
Foetal bovin serum (FBS)	Gibco	10270106
Hygromycin B	Invitrogen	10687010
Lipofectamine® 2000	Invitrogen	11668027
Opti-Mem®	Gibco	31985062
Penicillin/streptomycin	Gibco	11548876
Puromycin	Gibco	10296974
Roswell Park Memorial Institute (RPMI1640)	Gibco	21875-034
Sodium butyrate	Sigma-Aldrich	B5887-1G
TPA	Sigma-Aldrich	524400-10MG

2.1.5 Peptide synthesis reagents

Table 13: List of reagents utilised during peptide synthesis experiment with associated supplier and product code.

Chemical/Reagent	Supplier	Product code
Acetonitrile	Sigma-Aldrich	34851-2.5L
H-ASP(OTBU)-2-Chlorotritylresin	Merck Life Science Limited	8560650005
Fmoc-Ala-OH	Fluoro chem	M03347
Fmoc-Asp(OtBu)-OH	Fluoro chem	M03404
Fmoc-Gln(Trt)-OH	Fluoro chem	M03356
Fmoc-Glu(OtBu)-OH	Sigma-Aldrich	47625-100
Fmoc-Gly-OH	Sigma-Aldrich	47627-250G
Fmoc-Ile-OH	Fluoro chem	M03362
Fmoc-Leu-OH	Fluoro chem	M03365
Fmoc-Lys(Boc)-OH	Fluoro chem	M03419
Fmoc-Pro-OH	Fluoro chem	M03372
Fmoc-Thr(tBu)-OH	Fluoro chem	M03389
Fmoc-Trp(Boc)-OH	Fluoro chem	M03376
Fmoc-Tyr(tBu)-OH	Fluoro chem	M03428
Fmoc-Ser(tBu)-OH	Fluoro chem	M03382
Fmoc-Val-OH	Fluoro chem	M03378
M,N-Diisopropylcarbodiimide	Fluoro chem	132050
Oxyma base	Sigma-Aldrich	8510860100
Piperidine	Sigma-Aldrich	104094-1L
Dichloromethane	Sigma-Aldrich	270997-2.5L
Diethyl ether	Sigma-Aldrich	673811-2.5L
Dimethylformamide	Fisher Scientific	10206460
Triisopropyl silane	Sigma-Aldrich	233781-250G
Trifluoro acetic acid	Sigma-Aldrich	T6508-100ML

2.1.6 Kits

Table 14: List of kits utilised with the associated supplier and product code.

Kit	Supplier	Product code
Plasmid Miniprep kit	New England Biolabs	T1010S
2X Q5 master mix	New England Biolabs	M0492S
2X Gibson master mix	New England Biolabs	E2611S
Total RNA Miniprep kit	New England Biolabs	T2010S
Quick Start Bradford 1 X Dye Reagent	Bio-Rad	5000205
LunaScript® RT SuperMix Kit	New England Biolabs	E3010L
MagneHis kit	Promega	V8500
GoTaq® qPCR Master Mix	Promega	A6002
CellTiter 96® Aqueous One Solution Cell Proliferation Assay	Promega	G3580
Monarch DNA Gel extraction kit	New England Biolabs	T1020S
DNeasy® Blood & Tissue Kit	Qiagen	69504

2.1.7 Plasmids

Table 15: List of plasmids utilised with associated source.

Plasmid	Source
pVSV.G	Edwin Chen (University of Westminster)
psPAX2	Edwin Chen (University of Westminster)
pOPINF	University of Leeds PIXC facility
pOPINS	University of Leeds PIXC facility
pOPINJ	University of Leeds PIXC facility
pOPINM	University of Leeds PIXC facility
GIBZ scr shRNA	Professor Adrienne Edkins (Rhodes University)
GIBZ shRNA STIP1	Professor Adrienne Edkins (Rhodes University)
pCA528-SUMO-HOP	Professor Adrienne Edkins (Rhodes University)

2.1.8 Primers

2.1.8.1 Viral primers

Table 16: List of viral primers utilised and associated sequence.

Primer	Sequence (5'-3')
ORF57 fwd	GCCATAATCAAGCGTACTGG
ORF57 rvs	GCAGACAAATATTGCGGTG
ORF65 fwd	AAGGTGAGAGACCCCGTGAT
ORF65 rvs	TCCAGGGTATTCATGCGAGC

2.1.8.2 Non-viral primers

Table 17 List of non-viral primers utilised and associated sequence.

Primer	Sequence (5'-3')
STIP1 fwd	GCCAAGCGAACCTATGAGGAG
STIP1 rvs	GGATCACTGAGTAGTGTCCTTGT
GAPDH fwd	TGTGGTCATGAGTCCTTCCACGAT
GAPDH rvs	AGGGTCATCATCTCTGCCCCCTC

2.1.8.3 Protein production primers

Table 18: List of primers utilised in protein production methodology and associated sequence

Primer	Sequence (5'-3')
TPR1 fwd	AAGTTCTGTTTCAGGGTCCCATGGAGCAGGTCAATG
TPR1 rvs	CTGGTCTAGAAAGCTTTTACCTGGCCTCCATATTC
TPR2A fwd	AAGTTCTGTTTCAGGGTCCC AGCGGT GAGAATCTATACTTCCAGGGC GAGAATAAGAAGCAGG
TPR2A rvs	CTGGTCTAGAAAGCTT TTA CAGCCGCTCTTGCTCC

2.2 Methods

2.2.1 Cell culture

2.2.1.1 Cell lines maintenance, passage and counting.

To ensure appropriate maintenance of cells the following procedures were followed. BCBL-1 TREx-Rta cell lines are a B-cell lymphoma cell containing KSHV in a latent state. These cells were grown in RPMI 1640 growth medium with glutamine and the media additives: 10% FBS (v/v), hygromycin (100 µg/mL), and penicillin/streptomycin (100 µg/mL). If puromycin selection was required, puromycin was utilised at 2 µg/mL.

HEK-293T cell lines are an embryonic kidney derived cell line. These cells were grown in DMEM growth media with the following additives: 10% (v/v) FBS, and penicillin/streptomycin (100 µg/mL). rKSHV .219 cell lines are a HEK-293T cell line that contains KSHV.219 a recombinant form of KSHV genome. These cells were cultured as HEK-293T however with addition of puromycin (2 µg/mL) selection for the KSHV genome.

All cell lines were passaged every 3-4 days unless recovering from lentiviral transduction or freeze down. Confluency of adherent HEK-293T (also rKSHV .219) cells were allowed to reach a maximum 90% confluency before kinetic resuspension and 1 in 10 dilution with media. Suspension BCBL-1 TREx-Rta cells were split upon confluency of 1.2×10^6 to

confluency of approximately 1.0×10^5. In cases of lentiviral transduction or freeze down recovery, cells were pellet by centrifugation at 500 $x\,g$ for 5 mins and old media replaced with fresh.

Cell counting was only utilised for BCBL-1 TREx-Rta with approximated confluency utilised for HEK-293T cell lines. BCBL-1 TREx-Rta were resuspended, and an aliquot removed. From aliquot 10 µL of sample mixed with 10 µL of trypan blue (0.4%) and 8 µL loaded onto a hemocytometer and live cells counted.

2.2.1.2 Cell harvesting

Cells were resuspended, transferred into a 1.5 mL Eppendorf and centrifuged at 500 $x\,g$ for 5 mins at 4 °C. Supernatant was removed and cells were washed with sterile PBS, centrifuged at 500 x g for 5 mins at 4 °C, and remaining PBS was removed. The cell pellet was either used immediately, or stored at -20 °C.

2.2.1.3 Cell freezing

For longer term storage and safeguarding of cell lines, cell freezing was undertaken. To generate freeze downs 2×10^6 cells were counted and centrifuged at 500 $x\,g$ for 5 mins at 4 °C. Supernatant was removed and pellets were then resuspended in drug free RPMI or DMEM freezing media (doped 10% (v/v) DMSO) for either BCBL-1 TREx-Rta and HEK 293T's respectively. Resuspended cells were then transferred onto ice before storage at either –80 °C or in liquid nitrogen.

2.2.1.4 Lentiviral system

Using a lentiviral system, two plasmids containing either a HOP shRNA or scramble sequence were utilised in this project to transduce BCBL-1 TREx-Rta cells. HEK 293T's were plated at 80% confluency in a 6 well dish in 2 mL of media. For each condition, the following were combined in 100 µL of OPTI-MEM: 0.65 µg of psPAX2, 0.65 µg of pVSV.G and 1.2 µg of the shRNA targeting plasmid of interest with gentle mixing. Separately per condition 100 µL of OPTI-MEM was combined with 4 µL of lipofectamine 2000 with gentle mixing. These were incubated at room temperature for 10 minutes separately before combining and a further 10 minutes of incubation at room temperature. The solution was added dropwise to individual wells of HEK 293T cells. Cells were incubated for 8 hours at 37 °C, replaced with fresh DMEM media then further incubated at 37 °C for 40 hours. The contents of the wells were collected, spun down at 500 $x\,g$ for 5 minutes and supernatant was filtered through a 0.45 µM filter. 1 mL of the filtered supernatant was added to 5×10^5 BCBL-1 TREx-Rta cells in 1 mL of media with polybrene (8 µg/mL). After 8 hours, BCBL-1 TREx-Rta cells were pelleted

again, and transduction media was removed and replaced with drug free RPMI. Cells were incubated for a further 48 hours at 37 °C before drug free RPMI removed and replaced with puromycin (2 µg/mL) containing RPMI.

2.2.1.5 Transformations

To an Eppendorf of 50 µL of competent *E.Coli* cells, 1 µL (1 µg/µL) of purified plasmid DNA was added and mixed by flicking. Cells were incubated for 30 mins at 4 °C, heat shocked for 45 seconds at 42 °C then immediately returned to ice for 2 mins. Cells were then supplemented with 250 µL of LB broth and incubated at 37 °C with shaking for 1 hr. 150 µL and 20 µL of cultures were then spread onto selective LB agar plates and incubated at 37 °C overnight.

2.2.2 Cell assays

2.2.2.1 Non-viral assays

2.2.2.1.1 Cell growth assays

BCBL1 TREx-Rta cells expressing STIP1 KD shRNAs or scr shRNAs were seeded into a 6-well plate at 2.0×10^5 /mL confluency. After 24 and 48 hours, the cells were counted as per section 2.2.1.1 in triplicate and averaged.

2.2.2.2 MTS assay

An MTS assay was employed to ascertain appropriate concentration of small molecule inhibitors to trial utilsing CellTiter 96 AQueous reagent (Promega) kit. BCBL-1 TREx-Rta 1.0×10^4 cell were plated into 96-well plates in 100 µL of media, a cell free media only well was also plated. A separate serial dilution of compounds in DMSO was undertaken. 2 µL of each of these dilution series were added to wells in duplicate alongside 20% DMSO and untreated controls wells. Cells incubated for 48 hours before addition of 20 µL of MTS reagent. The plate was incubated for 1 hour at 37 °C with no light exposure before reading at 490 nM on Infinite F50 Robotic microplate reader (Tecan).

2.2.2.3 Viral assays

2.2.2.3.1 Induction of KSHV lytic replication cycle

To induce model lytic reactivation of BCBL1 TREx-Rta, media was treated with doxycycline hyclate at 2 µg/mL final concentration. Similarly, KSHV.219 contains a recombinant form of KSHV genome. To induce lytic reactivation cells were treated with sodium butyrate (4 mM) and TPA (20 ng/mL). Timepoints were then collected relative to induction.

2.2.2.3.2 Drug assays

To investigate the effect of compounds on KSHV lytic reactivation the following procedure was utilised. Compounds were screened at non-cytotoxic concentrations on BCBL-1 TREx-Rta cells determined from MTS assay 2.2.2.2. BCBL-1 TREx-Rta cells were counted and 2.0 X 10^6 were plated per well of 6 well plate in 3 mL of media. Compounds were added at respective concentration dissolved in DMSO and BCBL-1 TREx-Rta cells reactivated via doxycycline system as outlined in 2.2.2.3.1. Cells were collected at 0 hr, 24 hr and 48 hr and analysed via western blot and qPCR (outlined in 2.2.3 and 2.2.4.4 respectively).

2.2.2.3.3 KD vs SCR reactivation

To investigate the effect on production of marker RNAs and Proteins during KSHV lytic reactivation with and without presence of HOP BCBL-1 TREx-Rta cells expressing HOP KD shRNAs or Scr shRNAs were used. These cells were counted and 2 X 10^6 plated into a 6-well plate in 2 mL of media. Cells were reactivated via doxycycline system outlined in 2.2.2.3.1 and incubated for 24 hr and 48 hr with a non-reactivated control.

2.2.2.3.4 KSHV reinfection and viral load assays

To investigate production of viral DNA and infectious virion production, reinfection and viral load assays were employed. BCBL-1 TREx-Rta cells expressing HOP KD shRNAs or Scr shRNAs were counted 7.5 X 10^5 and plated into a 6-well plate in 2 mL of puromycin free media. Cells were reactivated via doxycycline system outlined in 2.2.2.3.1 and incubated for 72 hr with a non-reactivated control. Cells were collected and the pellet underwent processing for viral DNA production 2.2.4.3. 1 mL of supernatent was removed and added to a 6-well plate containing 80% confluent HEK 293Ts in 1 mL of DMEM media. These samples were incubated for a further 48 hr before collecting and the pellet underwent processing for viral RNA production 2.2.4.1.

2.2.2.4 Transfection of peptides via lipofectamine

Glass coverslips were washed in 100% ethanol and allowed to dry before adding to a 24 well dish. To a coverslip, 1 mL of 40% confluent HEK293Ts were seeded and allowed to adhere overnight to 80% confluency. For each condition to be tested, two Eppendorf were made up. One contained 250 µL of OPTI-MEM and 4 µL lipofectamine-2000, the other 250 µL OPTI-MEM and the desired volume of peptide stock, with both gently mixed. These were incubated for 10 minutes before combining for a further 10-minute incubation. Resultant solution was added dropwise to cells with gentle swirling. Cells were incubated for variable lengths of time before processing as outlined in 2.2.2.5.

2.2.2.5 Immunofluorescence staining

For BCBL1 TREx-Rta cells glass coverslips washed in 100% ethanol and allowed to dry in a 24 well dish. Coverslips were coated with 200 µL of poly-L-lysine and incubated for 5 minutes before removal. Coverslips were washed in 1 mL PBS before 1 mL of 2.0 X 10^5 BCBL1-TREx-Rta cells added and incubated for 8 hours at 37 °C to allow the cells to adhere to the coverslip. Cells were reactivated with doxycycline and incubated for desired timepoint (see 2.2.2.3.1 for reactivation details). Coverslips containing cells from methodology above or 2.2.2.4 were then processed in the following manner. Media was removed and cells washed 3 X in 1 mL of PBS before fixing in 1 mL PBS containing 4% formaldehyde (v/v) for 15 minutes at room temperature. The 4% formaldehyde was removed, and cells were washed gently again with 3 X 1 mL of PBS. Cells were permeabilised in 1 mL of PBS with 1% titron-X100 (v/v) for 15 minutes at room temperature. Cells were again washed with 3 X 1 mL of PBS. If no antibodies were required, then coverslips were mounted onto a slide using Vectashield containing DAPI. If antibodies were required, then coverslips were transferred to humidity chambers and cells were blocked for 1 hour with 200 µL of 1 % BSA in PBS (w/v) at 37 °C. The blocking solution was aspirated and 100 µL of fresh blocking solution containing primary antibody diluted to 1 in 10 of western blotting concentration were added to the coverslip and incubated for 1 hour at 37 °C. The solution was aspirated and washed 5 X 1 mL PBS. Secondary antibody made up to a 1/500 dilution in 100 µL blocking solution was added to the coverslip and incubated for 1 hour at 37 °C. There was a final 5 X 1 mL PBS wash step before mounting with Vectashield containing DAPI as above. Slides were stored at 4 °C in darkness before use.

2.2.3 Protein analysis via western blotting

2.2.3.1 Lysate extraction

Cell pellets were lysed on ice for 30 mins in 37.5 µL of RIPA buffer (150 mM NaCl, 25 mM Tris/HCl, 1% (v/v) NP-40 1 x Roche protease inhibitor cocktail pH 7.6) per one million cells. Mixture was separated into a clear supernatant and pellet via centrifuge (16,000 *x g*, 10 mins, 4 °C). The supernatant was then combined with a volume equal to initial RIPA buffer of loading dye (100 mM Tris/HCl 20% (v/v) glycerol 4% (w/v) SDS 0.02% (w/v) bromophenol blue pH 6.8) and boiled at 95 °C for 5 mins. Samples were stored at –20 °C.

2.2.3.2 Sodium dodecyl sulphate – polyacrylamide gel electrophoresis (SDS-PAGE)

Utilising Biorad Mini-Protean gel electrophoresis kit, polyacrylamide gels were cast with 10 or 15 wells. The concentration of polyacrylamide within gels varied from a 5% stacking region to

8% - 15% in resolving regions, depending on molecular weight. Composition and volumes of these are outlined in Table 19: Volumes of individual components to make one polyacrylamide gel at different percentages of acrylamide. Gels were added to electrophoresis tank containing running buffer (192 mM Glycine, 25 mM Tris, and 0.1% (w/v) SDS). Combs were removed and samples were added to wells with a biorad dual colour ladder employed as a standard. Electrophoresis was undertaken at 180 V for approximately 45 mins.

Table 19: Volumes of individual components to make one polyacrylamide gel at different percentages of acrylamide.

Component (mL)	Gel percentage				
	8	10	12	15	Stacking
1.5M Tris/HCl pH 8.8	2.5	2.5	2.5	2.5	-
dH$_2$O	4.6	4	3.3	2.3	1.495
30% (v/v) acrylamide	2.7	3.3	4	5	0.33
10% (w/v) SDS	0.1	0.1	0.1	0.1	0.02
10% (w/v) APS	0.1	0.1	0.1	0.1	0.02
TEMED	0.16	0.16	0.16	0.16	0.01
1M Tris/HCl pH 6.8	-	-	-	-	0.125

2.2.3.3 Transfer of SDS-PAGE gel onto nitrocellulose membrane

To allow for immunoblotting analysis of resolved proteins on SDS-PAGE gel, a transfer to 0.45 µM nitrocellulose was employed. Semi-dry transfer was utilised via Biorad, Trans-Blot Turbo Transfer system. The resolved gel was washed in transfer buffer (192 mM glycine 25 mM Tris and 20% (v/v) methanol) and blotting paper and nitrocellulose membrane also thoroughly wetted. Components were then loaded into the Turbo Transfer system in a stack in the following order from cathode: blotting paper, nitrocellulose membrane, polyacrylamide gel then blotting paper. Transfer utilised the preloaded biorad protocol of 30 mins at 25 V and 0.1 A.

2.2.3.4 Immunoblotting

Nitrocellulose blots were processed in varying solutions all made up of TBST stock (150 mM NaCl, 50 mM Tris/HCl, 1% (v/v) Tween-20, pH 7.6) with constant motion by a rocker. To improve signal to noise ratio and reduce non-specific binding blots were initially blocked for 1 hr in TBST containing 5% skimmed milk at room temperature. Blots were then placed into a TBST 5% milk solution containing primary antibodies complementary to the protein of

interest at concentrations outlined in 2.1.1 and incubated overnight at 4 °C. Blots were then washed three times in TBST for 5 mins at room temperature. Blots were then transferred into IgG secondary antibody containing horseradish peroxidase at 1/5000 dilution in 5% skimmed milk TBST for 1 hr at room temperature. Wash steps were repeated. Blots were imaged using digital G:Box Chemi XX9 imager (Alpha Metrix). If necessary, blots were reprobed with analogous washing step, then repeating of primary antibody step onwards.

2.2.4 Nucleic acid purification and analysis

2.2.4.1 RNA purification from mammalian cell pellet

To purify RNA from cell samples the Monarch® Total RNA Miniprep Kit was used. Cell pellet was lysed in 300 µL of RNA lysis buffer for 1 min at room temperature. Lysate was then transferred to a gDNA removal column and spun for 30 seconds at 16,000 x g. The gDNA column was disposed of and flow through collected, with an equal volume of 100% ethanol added and mixed via pipetting. Mixture was then transferred to an RNA purification column and spun for 30 seconds at 16,000 x g and flow through discarded. To the column 500 µL of RNA wash buffer was added and spun for 30 seconds at 16,000 x g. A separately mixed solution containing 75 µL of DNase I reaction buffer and 5 µL of Dnase was then added to column and allowed to incubate for 15 mins at room temperature. To the RNA purification column 500 µL of RNA priming buffer was added at spun for 30 seconds at 16,000 x g with flow through discarded. RNA purification column was washed with 500 µL of RNA wash buffer and spun for 30 seconds at 16,000 x g then a further wash with 500 µL of RNA wash buffer and spun for 2 mins at 16,000 x g. To the RNA purification column 50 µL of nuclease free water was added allowed to incubate for 30 seconds and spun for 30 seconds at 16,000 x g giving purified RNA. RNA was then stored on ice and concentration determined via UV-VIS (NANODROP 2000 Spectrophotometer Thermo Scientific). Longer term storage occurred at –80 °C.

2.2.4.2 Reverse transcription of RNA samples

To allow for (RT-qPCR) analysis of relative levels of mRNA, reverse transcription to cDNA of purified RNA was required. To achieve this LunaScript® RT SuperMix Kits was used following manufacturers instructions. A total reaction volume of 20 µL was made up of 4 µL of the 5X LunaScript® RT SuperMix, 1 µg of purified RNA with remaining volume made up with nucleases free H$_2$O. Utilising the QIAamlifier 96 (Qiagen) thermocycler the RT reaction was carried out as outlined in Table 20. Longer term storage occurred at –20 °C.

Table 20: Thermocycler RT conditions utilised for conversion of RNA to cDNA

Order	Time (mins)	Temperature (°C)	Operation
1	2	25	Primer annealing
2	10	55	cDNA synthesis
3	1	95	Heat inactivation

2.2.4.3 DNA purification from mammalian cell pellet

To purify DNA from mammalian cell pellets a Qiagen Dneasy® Blood & Tissue Kit was used. Cell pellet was resuspended in 200 µL of PBS and 20 µL proteinase K. To this mixture, 200 µL of Buffer AL was added and mixed via vortexing. To this, 200 µL of 100% ethanol was added and mixed via vortexing. Mixture was transferred to a Dneasy mini spin column and centrifuged at 6,000 $x\,g$ for 1 min with flow through discarded. To Dneasy mini spin column 500 µL of buffer AW1 was added and centrifuged at 6,000 $x\,g$ for 1 min with flow through discarded. To Dneasy mini spin column 500 µL of buffer AW2 was added and centrifuged at 16,000 $x\,g$ for 3 mins with flow through discarded. Elution of DNA was achieved by adding 200 µL of nuclease free water to Dneasy mini spin column and incubating for 1 minute before being centrifuged at 6,000 $x\,g$ for 1 min. DNA concentration was then determined via UV-VIS (NANODROP 2000 Spectrophotometer Thermo Scientific).

2.2.4.4 Quantitative polymerase chain reaction qPCR

Primers sets were designed for each gene of interest and a primer master mix of 10 µM forward and reverse made up. All primer sets underwent a primer efficiency check via a 5 dilution series test before utilisation, falling in ranges between 90%-110% efficiency. cDNA from LunaScript RT was diluted 1 in 10. A Rotor-Gene Q platform (QIAGEN, 9001550) was employed for all qPCRs. Total reaction volume of 20 µL per reaction was loaded into 0.1 mL Rotor gene style strip tubes (Star lab). Loading compromised of 19 µL of a master mix outlined in Table 21 and 1 µL DNA/cDNA. Master mix was made to up n + 1 (n = number of samples in duplicate) to account for pipetting errors. Experiment conditions began with initial activation at 95 °C for 10 minutes. Then 40 repeats of a three step cycle of denaturing for 15 seconds at 95 °C, annealing for 30 seconds at 60 °C and elongation for 20 seconds at 72 °C.

Table 21: Components of qPCR master mix per single tube.

Component	Volume (µL)
2X GoTaq	10
Nuclease free water	8
10 µM Primer master mix	1

2.2.4.5 DNA purification of plasmids

Purification of DNA plasmids from E.*coli* LB broth cultures was achieved using Monarch®
Plasmid Miniprep Kit was used. LB broth culture 5 mL were pelleted via centrifugation at
16,000 *x g* for 30 seconds and supernatant removed. *E.coli* cell pellet was resuspended in
200 µL of plasmid resuspension buffer B1 via pipetting and vortexing. To this mixture 200 µL
of plasmid lysis buffer B2 was added, and the mixture was inverted 5 times then incubated
for 1 min at room temperature with a colour change to dark pink seen. To this mixture, 400
µL of plasmid neutralization buffer B3 was added with mixture inverted for 2 mins at room
temperature or until uniform yellow colour and precipitate seen. Mixture was then centrifuged
at 16,000 *x g* for 5 mins. Supernatant was then transferred to a spin column and centrifuged
at 16,000 *x g* for 1 min with flow through discarded. To column 400 µL of plasmid wash
buffer 1 was added and column centrifuged at 16,000 *x g* for 1 min with flow through discard
process then repeated with 400 µL of wash buffer 2. To column 50 µL of nuclease free water
was added and incubated for 1 min then centrifuged at 16,000 *x g* for 1 min. DNA
concentration was then determined via UV-VIS (NANODROP 2000 Spectrophotometer
Thermo Scientific).

2.2.4.6 Agarose gel analysis of DNA

To analyse and separate DNA products from PCR agarose gel electrophoresis was used. A
2% (m/v) agarose gel was produced in TBE buffer (90mM Boric acid 90 mM Tris 2 mM EDTA
pH 8.3) via heating. Once cool to touch, 1 in 10,000 of SYBRSafe was added and solution
was poured into a Bio-Rad Mini-Sub® Cell GT cassette alongside comb. Once the gel had
fully set, DNA samples were loaded alongside ladder. Electrophoresis was undertaken at 90
V until dye front reached gel end. Gels were analysed via UV light.

2.2.4.7 Gel extraction

Should excision of a DNA product from an agarose gel be required the following approach
was utilised. DNA bands were exercised and the Monarch DNA gel extraction kit was then

used to isolate the DNA from gel. The excised gel was weighed and quadruple volume of gel dissolving buffer added and incubated at 50 °C for 10 minutes. Dissolved sample was loaded onto a column and centrifuged at 16,000 *x g* for 1 minute. The supernatant was disposed of and the column was washed with 200 µL of DNA wash buffer and centrifuged at 16,000 *x g* for 1 minute two times. The column was placed into a fresh Eppendorf and 6 µL of elution buffer added, incubated for 1 minute then centrifuged at 16,000 *x g* for 1 minute. DNA concentration was then determined via UV-VIS (NANODROP 2000 Spectrophotometer Thermo Scientific).

2.2.5   *E.coli* expression and purified protein production

2.2.5.1   TPR2A and TPR1

2.2.5.1.1 Plasmid production

The NEB Gibson assembly approach was utilised to generate pOPIN plasmids with desired TPR1 or TPR2A domain. Work began by designing primers via NEBuilder website for desired TPR1 and TPR2A DNA fragments. These fragments were amplified via PCR from pCA528-SUMO-HOP plasmid kindly provided by Professor Adrienne Edkins (Rhodes University). This amplification reaction had a total volume of 25 µL (components outlined in Table 22). The reaction cycle consisted of 98 °C for 30 seconds, 35 cycles of: 98 °C for 10 seconds, primer tm melt for 30 seconds, 72 °C for 30 seconds, with a final 72 °C extension for 2 minutes.

Table 22: Components of PCR reactions used to generate TPR1 and TPR2A fragments

Component	Volume (µL)
pCA528-SUMO-HOP plasmid	1.25
2X Q5 master mix	12.5
10 µM fwd & rvs primer mix	1.25
Nuclease free water	10

Resultant solution underwent agarose gel analysis as outlined in 2.2.4.6 and the correct sized band excised and underwent a gel extraction outlined in 2.2.4.7. PCR product was then combined into a Gibson assembly reaction with total volume of 20 µL. This reaction mixture was made up of 50 ng of linearised plasmid with approximately 150 ng of insert, 10 µL of 2X Gibson Master mix with remaining volume made up in nuclease free water. This solution was incubated at 50 °C for 15 minutes before freezing for use in transformations once correct sequence was confirmed present via sequencing.

Table 23: PCR amplification mixture components and volumes.

Reagent	Volume (µL)
10 µM primer master mix	2.5
2X Q5 Master mix	25
1 ng of plasmid	X
Nuclease free water	=50-(27.5+X)

2.2.5.1.2 Transformation

Transformation performed as outlined in section 2.2.1.5.

2.2.5.1.3 Small scale expression screening TPR1 & TPR2A

To determine optimum conditions for expression of TPR2A, small scale expression screens were carried out. This process investigated different tags, *E.coli* strains and temperatures. Small scale expression testing was performed using automated liquid handling. 1mL cultures were inoculated with individual colonies, grown in 2.2mL 96 well deep well plates to OD600 of 0.4-0.6 and induced with 0.4mM IPTG. Overnight growth at varying temperatures was followed by centrifugation at 4,000 *x g*. Soluble protein was purified from cell pellets on a Hamilton Microlab Star Automated Liquid Handling Platform utilising the Promega MagneHis kit and a custom liquid handling method. Soluble protein was analysed by SDS-PAGE stained with Coomasie.

2.2.5.1.4 Large scale growth, induction and harvesting of TPR1 and TPR2A

Individual colonies of transformed LEMO 21 *E.coli* were picked into 10 mL of selective LB broth (Ampicillin 100 µg/mL and Chloramphenicol 34µg/mL). These starter cultures were grown for 8 hrs with shaking at 37 °C before placing into 200 mL of selective LB broth (Ampicillin 100 µg/mL and Chloramphenicol 34 µg/mL) and grown overnight with shaking at 37 °C. These intermediate cultures were then used 1:50 into 1L of selective LB broth (Ampicillin 100 µg/mL and Chloramphenicol 34 µg/mL). These cultures were grown at 37 °C with shaking till an OD600 of 0.4–0.6 was achieved. Protein expression was triggered using 0.4 mM isopropyl-β-D-thio-galactoside (IPTG) and incubated at 22 °C with shaking overnight. Cultures spun down at 4,000 *x g* for 30 mins at 4 °C resolving a pellet.

2.2.5.1.5 Purification of TPR2A

For 1L of culture, cell pellets were resuspended in 20 mL of Ni^{2+} affinity purification low salt buffer (300 mM NaCl, 50 mM Tris/HCl, 20 mM imidazole, 5% (v/v) glycerol, 0.075% (v/v) β-

mercaptoethanol pH 7.6) with freshly added protease inhibitor (Expedeon Proteoloc Protease Inhibitor cocktail, used at 1 X according to manufacturer's instructions) at 4 °C. Homogenised sample were then lysed using Avestin cell disruptor at 1500 PSI at 4 °C. Lysis was repeated till genomic DNA was degraded as seen by a loss of sample viscosity. Lysate was centrifuged at 30,000 $x\,g$ for 45 mins at 4 °C generating a clear lysate and pellet. Lysate then underwent Ni^{2+} chromatography on ÄKTA pure™ chromatography system with a nickel affinity column (HisTrap^{TM} FF 5 mL column) using the following buffers Ni^{2+} affinity purification low salt buffer (300 mM NaCl, 50 mM Tris/HCl, 20 mM imidazole, 5% (v/v) glycerol, 0.075% (v/v) β-mercaptoethanol pH 7.6), Ni^{+2} affinity purification high salt buffer (500 mM NaCl, 50 mM Tris/HCl, 20 mM imidazole, 5% (v/v) glycerol, 0.075% (v/v) β-mercaptoethanol pH 7.6) and Ni^{2+} affinity elution buffer (3000 mM NaCl, 50 mM Tris/HCl, 500 mM imidazole, 5% (v/v) glycerol, 0.075% (v/v) β-mercaptoethanol pH 7.6). Fractions were eluted in 1 mL increments into 96 well plates and analysed using SDS-PAGE (2.2.3.2) and Coomassie staining (2.2.5.1.7). Fractions containing protein were collected. Dialysis was carried out in 4 L of low salt ion exchange buffer (20 mM Bis-Tris/HCl, 10 mM NaCl pH 6.5) at 4 °C in 3,500 MW cut off dialysis cassettes (Thermo Scientific Slide-A-Lyzer® Dialysis Cassette) overnight. Dialysed sample then underwent Ion exchange chromatography using HiTrap™ SP columns with low salt ion exchange buffer (20 mM Bis-Tris/HCl, 10 mM NaCl pH 6.5) and high salt ion exchange buffer (1 M NaCl, 20 mM Bis-Tris/HCl pH 6.5). Fractions were eluted in 1 mL increments in 96 well plates and analysed using SDS-PAGE (2.2.3.2) and Coomassie staining(2.2.5.1.7). Fractions containing protein were collected and concentrated to 1 mL using concentrators (Pierce^{TM} Concentrators, PES) with 3,000 MW cutoff. The sample was loaded onto ÄKTA pure™ chromatography system and underwent gel filtration using a HiLoad™ 16-600 Superdex 75 pg column into buffer (50 mM NaCl, 20 mM Tris/HCl, 1 mM DTT pH 8). Fractions were eluted in 1 mL increments in 96 well plates and analysed using SDS-PAGE (2.2.3.2) and Coomassie staining (2.2.5.1.7). Fractions containing protein were collected and concentrated using concentrators with 3000 MW (Pierce^{TM} Concentrators, PES) cutoff until a concentration of approximately 80 μM was achieved. To determine protein concentration a Bradford assay was carried out using Bio-Rad Quick Start^{TM} Bradford Protein Assay kit (2.2.5.1.8). A final SDS-PAGE and Coomassie staining was carried out to check purity of final protein. Longer term storage occurred at –80 °C.

2.2.5.1.6 Purification of TPR1

For 1 L of culture, cell pellets were resuspended in 20 mL Ni^{2+} affinity purification low salt buffer (300 mM NaCl, 50 mM Tris/HCl, 20 mM imidazole, 5% (v/v) glycerol, 0.075% (v/v) β-mercaptoethanol pH 7.6) with freshly added protease inhibitor (Expedeon Proteoloc Protease

Inhibitor cocktail, used at 1 X according to manufacturer's instructions) at 4 °C. Homogenised samples were then lysed using Avestin cell disruptor at 1500 PSI at 4 °C. Lysis was repeated until genomic DNA was degraded as seen by a loss of sample viscosity. Lysate was spun down at 30,000 $x\,g$ for 45 mins at 4˚C generating a clear lysate and pellet. Lysate then underwent Ni^{2+} chromatography on ÄKTA pure™ chromatography system with a nickel affinity column (HisTrap™ FF 5 mL column) using following buffers, Ni^{2+} affinity purification low salt buffer (300 mM NaCl, 50 mM Tris/HCl, 20 mM imidazole, 5% (v/v) glycerol, 0.075% (v/v) β-mercaptoethanol pH 7.6), buffers Ni^{2+} affinity purification high salt buffer (500 mM NaCl, 50 mM Tris/HCl, 20 mM imidazole, 5% (v/v) glycerol, 0.075% (v/v) β-mercaptoethanol pH 7.6) and Ni^{2+} affinity elution buffer (3000 mM NaCl, 50 mM Tris/HCl, 500 mM imidazole, 5% (v/v) glycerol, 0.075% (v/v) β-mercaptoethanol pH 7.6). Fractions were eluted in 1 mL increments in 96 well plates and analysed using SDS-PAGE (2.2.3.2) and Coomassie staining (2.2.5.1.7). Fractions containing protein were collected. Dialysis was carried out using 4 L of low salt ion exchange buffer (20 mM Tris/HCl, 10 mM NaCl pH 8) at 4 ˚C in 3,500 MW cut off dialysis cassettes (Thermo Scientific Slide-A-Lyzer® Dialysis Cassette) overnight. Dialysed sample then underwent Ion exchange chromatography using HiTrap™ Q columns with low salt ion exchange buffer (20 mM Tris/HCl, 10 mM NaCl pH 8) and high salt ion exchange buffer (1 M NaCl, 20 mM Tris/HCl pH 8). Fractions were eluted in 1 mL increments in 96 well plates and analysed using SDS-PAGE (2.2.3.2) and Coomassie staining (2.2.5.1.7). Fractions containing protein were collected and concentrated to 1 mL using concentrators 3,000 MW (Pierce™ Concentrators, PES) till a concentration of approximately 80 uM was achieved. To determine protein concentration a Bradford assay was carried out using Bio-Rad Quick Start™ Bradford Protein Assay kit (2.2.5.1.8). A final SDS-PAGE and Coomassie staining was carried out to check purity of final protein. Longer term storage occurred at –80 °C.

2.2.5.1.7 Coomassie staining.

To visulise expressed TPR1 and TPR2A protein Coomasie staining was utilised. SDS-Page resolved Polyacrylamide gels (as outlined in 2.2.3.2) containing fractions or final product of purification and were analysed using Coomassie staining. Gels were washed in dH_2O three times before addition of 20 mL of Coomassie stain (50% (v/v) methanol, 10% (v/v) acetic acid 0.1% (v/v) Coomassie Blue R-250) and incubated for 4 hr at room temperature. Stained gels were then washed three times in dH_2O and then placed into Coomassie destain solution (50% (v/v) methanol, 10% (v/v) acetic acid 0.1%) for 4 hr at room temperature and wash steps repeated again. Gels were then imaged using digital G:Box Chemi XX9 imager (Alpha Metrix) or digital camera.

2.2.5.1.8 Bradford assay to determine protein concentration

A Bradford assay was employed to calculate protein concentration of expressed TPR1 and TPR2A domains. Following Bio-Rad Quick Start™ Bradford Protein Assay instructions a series of dilutions of BSA were made and utilised to compare to TPR2A domain. Dilutions of TPR2A were undertaken if initial concentration of protein resulted in absorbances over 1.

2.2.6 Fluorescent polarisation assay

Fluorescent polarisations assays were used to conduct HTS screening of MCCB compounds for PPI inhibitors of TPR1/2A and their respective HSP partners. In all assays corning black non-binding 384-well (3820) plates were used and read at room temperature utilising Perkin Elmer EnVision™ 2103 MultiLabel plate reader. Measurements used an excitation at 480 nM and emission at 535 nM (30 nM bandwiths). All peptide tracers were labelled with Fluorescein (5/6-FAM) at 99% purity from ThermoFischer Scientific. All data for direct titration and competition studies was plotted using OriginPro 2020.

5-Carboxyfluorescein   6-Carboxyfluorescein
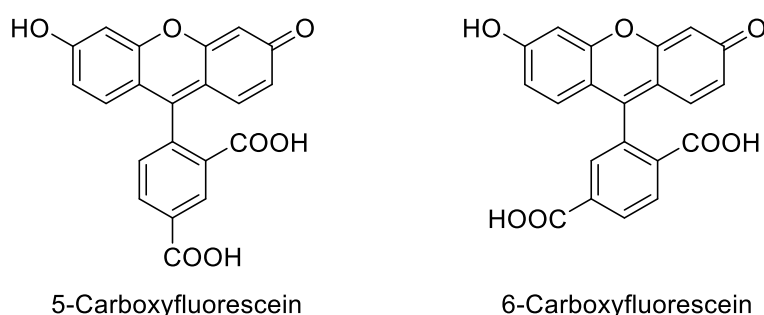
Figure 18 Fluorescein dyes structures attached as isomeric mix to peptides

2.2.6.1 Compound picking

From University of Leeds MCCB library DMSO solutions (4 μL 10 mM) were picked and placed into 16 μL of DMSO on corning NBS plates (3544). The colour of solutions and presence of precipitates was noted with plate sealed and stored at 4 ˚C for shortest duration possible till screening.

2.2.6.2 TPR2A fluorescent polarisation assay

A fluorescent polarisation assay consisting of the TPR2A domain of HOP and fluorescein labelled HSP90 peptide. All components were dissolved in FP buffer 90 (50 mM NaCl, 20 mM Tris/HCl, 1mM DTT, pH 8).

Table 24: TPR2A Fluorescent polarisation tracers with associated names and sequences and unlabelled form

Tracer	Sequence
Unlinked	(5/6-FAM)DDTSRMEEVD
PEG2 linked	(5/6-FAM)(PEG2)DDTSRMEEVD
Unlabelled HSP90	DDTSRMEEVD

2.2.6.2.1 Direct binding assay

A binding assay to show interaction between the TPR2A domain of HOP and fluorescein labelled HSP90 peptide. To corning black non-binding 384-well plates (3820) 20 µL of TPR2A FP buffer was added to wells A1-F1 through to A20-F20. To wells A1-F1 20 µL of 60 µM TPR2A protein was added and serially diluted down to A20-F20 with final dilution discarded. To this 20 µL of 40 nM tracer made up in TPR2A FP buffer was added to all A-C wells with mixing via pipette. Wells D-F 20 µL TPR2A FP buffer was added. Plates were incubated for 4 hours at room temp before reading.

2.2.6.2.2 DMSO testing

To examine the impact of DMSO to TPR2A-HSP90 direct binding assay 10% DMSO was added and kD calculated. To corning black non-binding 384-well plates (3820) 20 µL of TPR2A FP buffer was added to wells A1-F1 through to A20-F20. To wells A1-F1 20 µL of 60 µM TPR2A protein was added and serially diluted down to A20-F20 with final dilution discarded. To this 16 µL of 50 nM tracer made up in TPR2A FP buffer was added to all A-C wells with mixing via pipette. Wells D-F 16 µL TPR2A FP buffer added as control. Finally, 4 µL of DMSO added to all wells. Rows G-L filled as section 2.2.6.2.1 as a no DMSO control direct titration. Plates were incubated for 4 hours at room temp before reading.

2.2.6.2.3 Competition assay

To demonstrate the potential for a small molecule inhibitor to out compete fluorescein labelled HSP90 peptide from TPR2A, an increasing concentration of unlabelled HSP90 peptide was used as a positive control. This methodology was also used to test potential HTS hit compounds in which the unlabelled peptide was replaced with compond of interest. To corning black non binding 384-well plates (3820) 20 µL of TPR2A FP buffer was added to wells A2-F2 through to A20-F20. To wells A1-F1 and A2-F2 20 µL of 1 mM unlabelled HSP90 peptide was added and serially diluted down wells A2-F2 to A20-F20 with final dilution discarded. To this 20 µL of protein tracer solution added (2.7 µM of TPR2A, 40 nM tracer, TPR2A FP buffer) to wells A-C with mixing. Rows D-F filled with 20 µL of protein only

solution (2.7 μM TPR2A domain, TPR2A FP buffer) with mixing. Plates were incubated for 4 hours at room temp before reading.

2.2.6.2.4 Z'

A Z' assay was carried out to investigate the efficacy of TPR2A-HSP90 FP assay for HTS screening. This is a statistical measure of assay window, variability and the potential of false positives and negative results Two master mixes were made up in TPR2A FP buffer: negative control containing 1.35 μM TPR2A and 20 nM unlinked tracer and positive control containing only 20 nM unlinked tracer. These solutions were placed in alternating wells filling the plate completely. Plates incubated for 4 hours at room temperature before reading.

2.2.6.2.5 High throughput screening

This method was used to screen of MCCB library compound in triplicate as potential SM inhibitors of TPR2A-HSP90 PPI. Three sets of control wells were randomly selected in blocks of 10 and these wells covered with foil blockers. Wells A1-A20 down to N1-N20 excluding control wells were filled with 38 μL of HTS master mix (1.42 μM TPR2A, 21.1 nM unlinked Tracer in TPR2A FP buffer) to these wells 2 μL of 2 mM MCCB compounds were added with mixing in repeating triplicate sets of compounds. Compound identity was logged per each well. DMSO was added to HTS master mix wells without compounds as DMSO control wells. Control wells had 30 μL of master mix added (1.8 μM TPR2A, 26.6 nm Tracer in TPR2A buffer) to this 10 μL 1mM unlabelled HSP90 peptide or TPR2A buffer added with mixing. Plates incubated for 4 hours at room temperature before reading.

2.2.6.3 TPR1 fluorescent polarisation assay

A fluorescent polarisation assay consisting of the TPR1 domain of HOP and fluorescein labelled HSP70 peptide. Components were dissolved in FP buffer 70 (20 mM NaCl, 10 mM Tris/HCl, 1 mM DTT, pH 8) including dicarboxylic acid fragments, however small molecule compounds from MCCB and tetrazole screening dissolved in DMSO.

Table 25: TPR1 fluorescent polarisation tracers with associated names and sequences and unlabelled form

Tracer	Sequence
Long unlinked	(5/6-FAM)GSGPTIEEVD
Short unlinked	(5/6-FAM)PTIEEVD
Short PEG2 linked	(5/6-FAM)[PEG2]PTIEEVD
HSP70 unlabelled peptide	GSGPTIEEVD

2.2.6.3.1 Direct binding Assay

A binding assay to show interaction between the TPR1 domain of HOP and fluorescein labelled HSP70 peptide. To corning black non-binding 384-well plates (3820) 20 µL of FP buffer 70 was added to wells A1-F1 through to A16-F16. To wells A1-F1 20 µL of 400 µM TPR2A protein was added and serially diluted down to A16-F16 with final dilution discarded. To this 20 µL of 40 nM tracer made up in FP buffer 70 was added to all A-C wells with mixing via pipette. Wells D-F 20 µL FP buffer 70 added. Plates incubated for 4 hours at room temperature before reading unless otherwise stated.

2.2.6.3.2 DMSO tolerance testing

To examine the impact of DMSO to TPR1-HSP70 direct binding assay 10% DMSO was added and kD calculated. To corning black non-binding 384-well plates (3820) 20 µL of FP buffer 70 was added to wells A1-F1 through to A20-F20. To wells A1-F1 20 µL of 400 µM TPR2A protein was added and serially diluted down to A20-F20 with final dilution discarded. To this 16 µL of 50 nM long unlinked tracer made up in FP buffer 70 was added to all A-C wells with mixing via pipette. Wells D-F 16 µL FP buffer 70 added as control. Finally, 4 µL of DMSO added to all wells. Rows G-L filled as section 2.2.6.3.1 as a no DMSO control direct titration. Plates incubated for 4 hours at room temperature before reading.

2.2.6.3.3 Competition assay & peptide SAR development

To demonstrate the potential for a small molecule inhibitor to out compete fluorescein labelled HSP70 peptide from TPR1, an increasing concentration of unlabelled HSP70 peptide was used as a positive control. This method was also used to test potential HTS hit compounds and test synthesised peptides. To corning black non-binding 384-well plates (3820) 20 µL of FP buffer 70 was added to wells A2-F2 through to A16-F16. To wells A1-F1 and A2-F2 20 µL of 1 mM unlabelled HSP70 peptide was added and serially diluted down wells A2-F2 to A16-F16 with final dilution discarded. Rows A-C filled with 20 µL of protein tracer solution (25 µM TPR1, 40 nM long unlinked Tracer, FP buffer 70) with mixing. Rows D-F filled with FP buffer 70 with 20 µL protein solution (25 µM TPR1, FP buffer 70), with mixing. Plates incubated for 4 hours at room temperature before reading. This methodology was repeated for rows G-L for synthesised peptide testing with rows A-F containing original control unlabelled peptide for standardisation. Plates incubated for 4 hours at room temperature before reading.

2.2.6.3.4 Fragment screening carboxylic acids

The activity of carboxylic acid containing fragment compounds was explored in relation to TPR1-HSP70 PPI. For fragment screening a direct titration control was conducted analogous to section 2.2.6.3.1 but only across 4 rows A-D rather than 6. Rows E-J were filled with 20 µL of FP buffer 70 from column 1 to column 16. Wells E1-J1 were filled with 20 µL of 100 mM fragment compound (FP buffer 70, pH ≈ 7.6) and serially diluted down the plate to E16-J16. Rows E-G filled with 20 µL of protein tracer solution (25 µM TPR1, 40 nM long unlinked Tracer, FP buffer 70) with mixing. Rows H-I filled with 20 µL protein solution (25 µM TPR1, FP buffer 70) with mixing. Plates incubated for 4 hours at room temperature before reading.

2.2.6.3.5 Fragment screening tetrazole

The activity of tetrazole containing fragment compounds was explored in relation to TPR1-HSP70 PPI. Wells A1-C1 to A16-C16 filled with 36 µL of protein tracer solution (13.9 µM TPR1, 22.2 nM long unlinked Tracer in FP buffer 70). Wells D1-F1 to D16-F16 filled with 36 µL of protein solution (13.9 µM TPR2A, in FP buffer 70). A 16-fold serial dilution of 10 µL 500 mM stock of tetrazole into 10 µL of DMSO. Well A1-F1 4 µL of undiluted 500 mM tetrazole stock added and repeated for serial diluted stocks down plate. Plate incubated for 4 hours at room temperature before reading.

2.2.6.3.6 Z'

A Z' assay was carried out to investigate the efficacy of TPR1-HSP70 FP assay for HTS screening. This is a statistical measure of assay window, variability and the potential of false positives and negative results. Two master mixes were made up in FP buffer 70: negative control containing 12.5 µM TPR1 and 20 nM long unlinked tracer and positive control containing only 20 nM long unlinked tracer. These solutions were placed in alternating wells. Plates were incubated for 4 hours at room temperature before reading.

2.2.6.3.7 High throughput screening

This method was used to screen of MCCB library compound in triplicate as potential SM inhibitors of TPR1-HSP70 PPI. Three sets of control wells were randomly selected in blocks of 10 and these wells covered with foil blockers. Wells A1-A20 down to N1-N20 excluding control wells were filled with 38 µL of HTS master mix (13.2 µM TPR2A, 21.1 nM Tracer in FP buffer 70) to these wells 2 µL of 2 mM MCCB compounds were added with mixing in repeating triplicate sets of compounds. Compound identity was logged per each well. DMSO was added to HTS master mix wells without compounds as DMSO control wells. Control wells had 30 µL of master mix added (16.7 µM TPR2A, 26.6 nm Tracer in FP buffer 70) to

this 10 µL 1mM unlabelled HSP70 peptide or FP buffer 70 buffer added with mixing. Plates incubated for 4 hours at room temperature before reading.

2.2.7   Peptide synthesis

2.2.7.1   Solid phase synthesis

Peptides were synthesised using the following general methodology outlined below to be tested as TPR1-HSP70 PPI disruptors. Utilising CEM Liberty Blue peptide synthesizer synthesis quantities were calculated per peptide for single deprotection single coupling reactions. All reactions were carried out on a 0.25 mMol scale with 5 equivalent amino acid excess utilising DIC and Oxyma as coupling reagents with quantities determined by CEM Liberty Blue synthesizer calculator. Chlorotrityl aspartic acid preloaded resins were resuspended and preswelled in 10 mL of DMF (HPLC grade) with vigorous mixing for 10 minutes. All amino acids reagents were FMOC protected and dissolved in respective quantities of DMF alongside DIC and Oxyma. Reagents were then loaded onto machine and synthesis run to completion. Deprotection solution contained 20% (w/v) piperidine in DMF.

2.2.7.2   Peptide purification

Peptides were purified for downstream applications via the following procedure. Resins were collected from CEM Liberty Blue peptide synthesizer and washed 3 X 10 mL of DMF, DCM, Diethyl ether. Cleavage of peptide from resins was carried out in 5 mL of deprotection cocktail (95% Trifluroacetic acid, 2.5% Triisopropyl silane and 2.5% H_2O) with rotation for 2 hrs. Cleaved product was filtered and 2 mL of deprotection cocktail added for washings. Solutions were blown with N_2 untill 3 mL of solution achieved, any observed suspension/oil was redissolved to allow for effective precipitation of product. To each peptide solution, 10 mL of ice-cold diethyl ether were added and precipitate observed with addition of diethyl ether to total volume of 45 mL and incubated at −18 °C overnight.

Solution was centrifuged for 7 minutes at 4,000 x *g* with pellet obtained. Diethyl ether was removed and the remaining pellet dried via N_2 and resuspended in 5 mL of resuspension cocktail (49.5% H_2O 49.5% Acetonitrile and 0.1% formic acid). The solution was frozen and placed in vented vessel on a freeze drier till fluffy powder obtained. Sample underwent further purification via preparative high pressure liquid chromatography (HPLC).

2.2.7.2.1 N-terminus acetylation

To acetylate the N-terminus of peptides the following approach was employed. Peptides still bound to resin post synthesis were washed 3 X DMF then resuspended in 10 mL DMF. Acetic anhydride and DIPEA added at 1.5 molar excess and stirred at room temperature for 4 hours. Purification then carried out analogous to 2.2.7.2.

2.2.7.2.2 Preparative high pressure liquid chromatography (HPLC)

To further purify peptides preperative HPLC was utilised. Freeze dried crude products were dissolved in 50:50 H_2O:ACN in a maximum volume of 5 mL. Solution was then loaded onto an Aglient 1290 Infinity II preparative HPLC system with mass spectrometer (LC/MSD XT) fitted with Agilent Technologies PLRP-S, 300Å, 8 uM particle size column. A scouting run (also known as the analytical run) for desired molecular weight of product was performed before a preparative run utilising advised mobile phase gradients of H_2O:ACN. Fractions containing the desired mass were collected and flash frozen and freeze dried using above methodology. Products were characterised via analytical HPLC and high resolution mass spectrometry (outlined in 2.2.7.3.1).

2.2.7.3 Peptide analysis

2.2.7.3.1 Analytical HPLC

Analytical HPLC was utilised by Dr Jeanine Williams to determine purity of peptide products. Peptide was dissolved in 50:50 H_2O:ACN at a concentration of approximately 1 mg/mL. 1 µL of this solution was loaded onto an Aglient 1290 Infinity II preparative HPLC system with mass spectrometer (LC/MSD XT) fitted with Agilent Technologies PLRP-S, 300Å, 8 uM particle size column at 40 °C. Mobile phase was a gradient detailed in Table 26 at a flow rate of 0.5 mL/minute. Detection of peptides via 220 nM UV light.

Table 26: Mobile phase solvent gradient utilised during analytical HPLC for peptide purity determination.

Time (mins)	H_2O, 0.1% TFA (%)	ACN, 0.1% TFA (%)
0	95	5
10	5	95
11	0	100
12	95	5

2.2.7.3.2 High resolution mass spectrometry

To confirm identity of synthesised peptides high resolution mass spectrometry was utilised. Peptides were dissolved into 1 mg/mL solutions with 18 Ω deionised water. If peptide failed to dissolve ≈ 20 µL volumes of acetonitrile were added till solubility achieved. From stock

solution 30 µL was diluted into 970 µL of 18 Ω deionised water. From this diluted stock 1 µL was loaded onto Bruker impact II for positive electrospray ionisation.

Chapter 3

~

Investigating the role of HOP during KSHV lytic replication

3   Investigating the role of HOP during KSHV lytic replication

3.1   Introduction

Multiple recent studies detail the key roles of HSP70/90 in relation to their essential roles in virus-mediated pathogenesis, including during both KSHV latent and lytic replication phases (detailed in section 1.2.1.3). Surprisingly despite this, no studies have investigated the role of the molecular co-chaperone, HOP, in viral replication and its potential as an antiviral target. However, some reports have suggested it has a role in cancer and protein aggregation disorders (Zhai et al., 2018; Bhattacharya and Picard, 2021). We therefore wished to explore the role of HOP during KSHV lytic replication and its suitability as a pharmaceutical target. The initial approach taken involved using two KSHV-latently infected cell lines that could be induced into the lytic replication phase to examine the effect on HOP expression and sub-cellular localisation. Following this, shRNAs specifically targeting knockdown of HOP were utilised to determine whether HOP was necessary for KSHV lytic replication. Finally, a low throughput screen of potential inhibitors of the TPR2A-HSP90 PPI identified from an *in-silico* screen was performed to assess for any antiviral activity.

Initially, the study of endogenous HOP expression was assessed in two independent KSHV-infected cell lines, namely BCBL-1 TREx-Rta and rKSHV.219 cells (Clone 9). BCBL-1 TREx-Rta cells are B cell line containing an engineered KSHV episome that can be induced into the lytic replication cycle via addition of doxycycline (Nakamura et al., 2003). Whereas Clone 9 cells are derived from HEK-293T cells that contain a KSHV-BACmid with a puromycin selection marker inserted into the viral genome. Reactivation in Clone 9s occur by the addition of the chemical inducing agents sodium butyrate and TPA (Vieira and O'Hearn, 2004).

3.2   Assessing the impact of KSHV lytic replication on HOP expression.

3.2.1   HOP mRNA levels are increased during KSHV lytic replication.

To characterise HOP mRNA expression during KSHV infection, KSHV latently-infected TREx BCBL1-Rta and Clone 9 cell lines were reactivated to induce lytic replication. Cells were then harvested at a latent time point (0h) and post reactivation (24h and 48h). The viral early lytic gene, ORF57, was used as a marker to confirm induction of the KSHV lytic replication cycle. ORF57 is used as a marker of lytic replication, as it encodes an essential multifunctional posttranscriptional regulator, increasing viral RNA nuclear export, stability, splicing and translation (Majerciak and Zheng, 2015).

Figure 19: RT-qPCR analysis of (A) HOP (B) ORF57 mRNA levels compared to 48 hr scramble and relativised to mRNA levels of GAPDH housekeeping in endogenous BCBL-1 TREx-Rta cells. KSHV lytic replication was induced, and cells collected at 24 hours and 48 hours. Error bars represent SD, n = 3 biological repeats. N = 2 technical repeats of qPCR data with no difference greater than 0.5 ct values between technical repeats utilised. Significance calculated by unpaired t test.
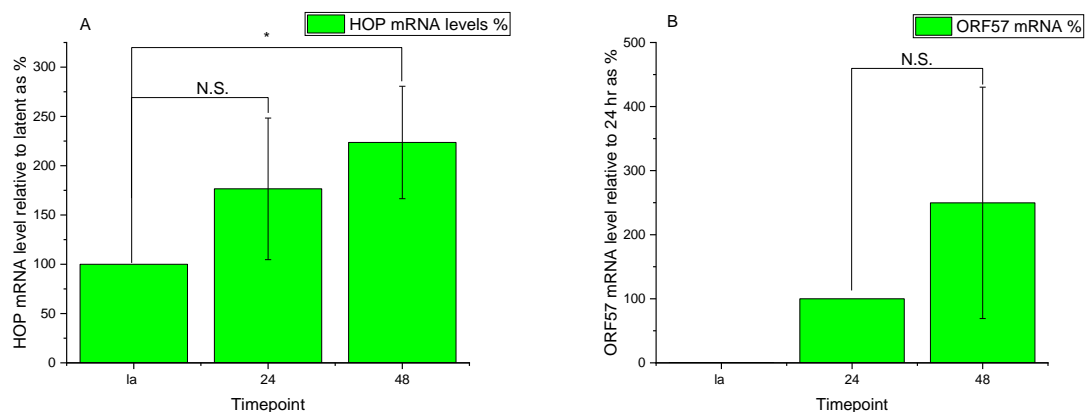
Figure 20: RT-qPCR analysis of (A) HOP (B) ORF57 mRNA levels compared to 48 hr scramble and relativised to mRNA levels of GAPDH housekeeping in endogenous clone 9 cells. KSHV lytic replication was induced, and cells collected at 24 hours and 48 hours. Error bars represent SD, n = 3 biological repeats. N = 2 technical repeats of qPCR data with no difference greater than 0.5 ct values between technical repeats utilised. Significance calculated by unpaired t test.

To initially determine if KSHV reactivation induces an increase in HOP mRNA levels, total RNA was extracted and quantified using two-step qRT-PCR to determine relative mRNA fold change of HOP and viral transcripts to compare expression during latent and lytic KSHV infection. Results showed a significant increase in HOP gene expression at 24h post-reactivation compared to the latent sample in TREx BCBL1-Rta of 1.7 fold (Figure 19) and in Clone 9 of 1.6 fold increase, although this was deemed insignificant (Figure 20). At 48h post-reactivation, there was a higher variability in HOP mRNA levels observed across

independent repeats and cell lines, although overall results showed sustained expression compared to latency in TREx BCBL1-Rta cells and a further significant 2-fold increase in Clone 9 cells. As expected, ORF57 fold change significantly increased compared to the latent sample in both TREx BCBL1-Rta and Clone 9 cells (Figure 19 & Figure 20). Together, these results confirm successful KSHV reactivation and showed HOP mRNA levels increased or at least maintained during early KSHV lytic replication.

3.2.2 Western blot analysis suggest HOP protein levels are maintained during KSHV lytic replication.

To further characterise HOP expression during KSHV infection, western blot analysis was used to analyse HOP protein production. It would be anticipated that the increase in HOP mRNA levels would lead to increased protein levels, however the majority of host cell proteins are decreased during the later stages of KSHV lytic replication due to KSHV-mediated host cell shutoff mechanisms. Western blot analysis shows an increase in viral ORF57 protein levels, confirming efficient reactivation of KSHV lytic replication cycle in both TREx BCBL1-Rta and Clone 9 cells (Figure 21 & Figure 22). Interestingly, however using a HOP-specific antibody which identifies the presence of the 63 kDa HOP protein, levels of HOP protein differs in the respective cell lines. Results suggest that HOP levels are reduced slightly in TREx BCBL1-Rta cells (Figure 21), whereas in Clone 9 cells HOP protein levels are increased 2 fold at 48 hours of KSHV lytic replication cycle (Figure 22). This may suggest that HOP resists or partially resists host-cell shut off during KSHV lytic replication at both the RNA and protein level. Caution should be taken however when comparing results between Clone 9 and TREx BCBL1-Rta cell lines. This is due to different induction of lytic reactivation methods and thus efficiency of reactivation occuring.
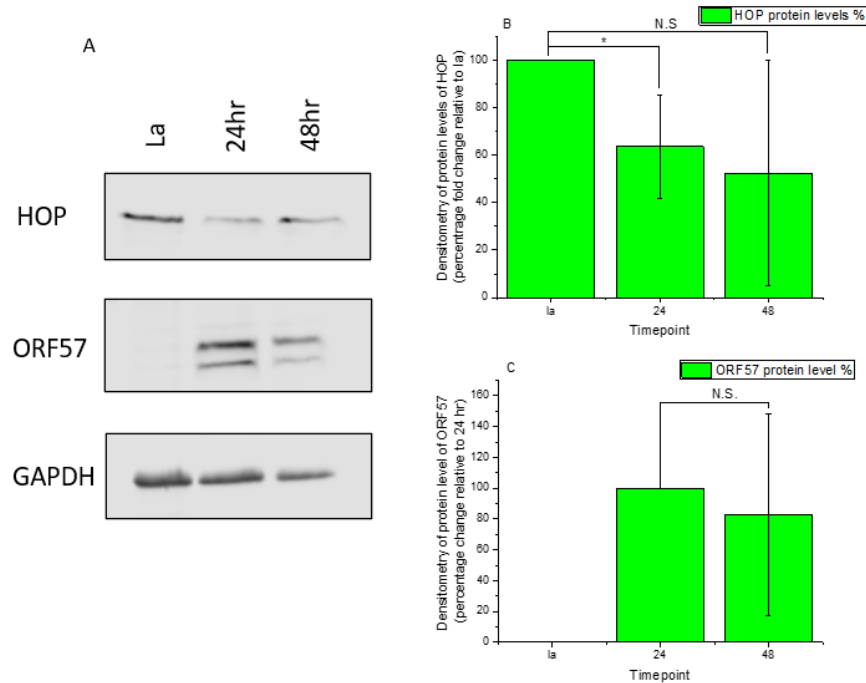
Figure 21 (A) Western blot of BCBL-1 TREx-Rta cells and reactivation of KSHV lytic replication cycle induced and timepoints taken at 24 hours and 48 hours. (B,C) Densitometry of HOP and ORF57 from three biological repeats and relativised to GAPDH housekeeper. Error bars represent SD, n = 3 biological repeats. Significance calculated by unpaired t test.
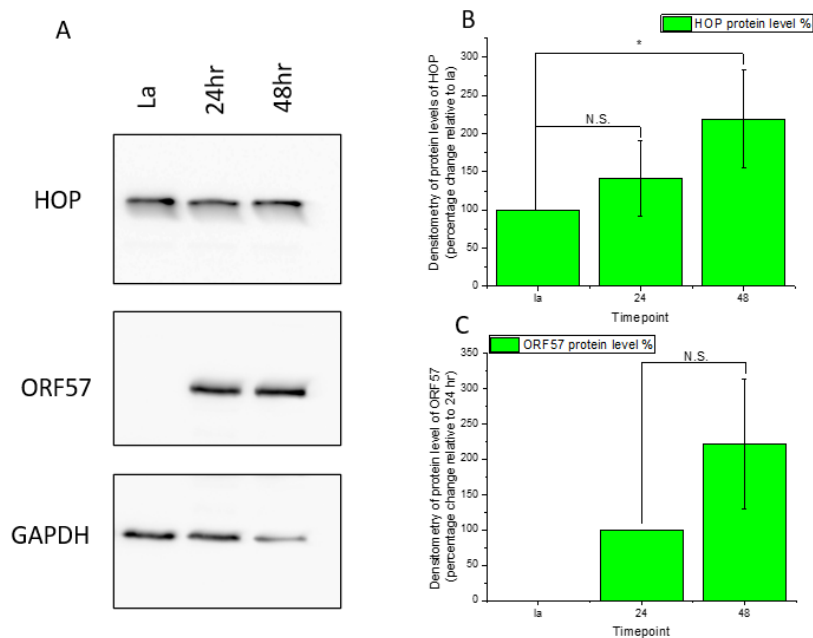
Figure 22 (A) Western blot of Clone 9 cells and reactivation of KSHV lytic replication cycle induced and timepoints taken at 24 hours and 48 hours. (B,C), Densitometry of HOP and ORF57 from three biological repeats and relativised to GAPDH housekeeper. Error bars represent SD, n = 3 biological repeats. Significance calculated by unpaired t test.

3.2.3 Immunofluorescence analysis suggests HOP is redistributed into the nucleus during KSHV lytic replication.

Previously it has been reported that HSP70 is redistributed from the cytoplasm to the nucleus, specifically into vRTCs during KSHV reactivation (Baquero-Perez and Whitehouse, 2015). Therefore, as HOP functions as a co-chaperone for HSP70, experiments were performed to assess if HOP was also relocalised to the nucleus during lytic replication. Confocal immunofluorescence microscopy was used to identify any changes in subcellular localisation of HOP over the course of lytic replication in TREx BCBL1-Rta cells. Post reactivation, cells were fixed, then permeabilised at 0h and 24h post-reactivation, then stained with HOP and ORF57-specific antibodies and localisation identified using fluorescent secondary antibodies. The nucleus was also stained with DAPI. In the latent sample, HOP predominantly localised to the cytoplasm of the cell, as shown by the clear localisation of HOP around the DAPI stained nuclei (Figure 23). At 24h post-reactivation, ORF57 staining shows the presence of large globular structures identified as the replication and transcription complexes (vRTCs) formed within the nucleus. vRTCs are essentially KSHV replication centres, supporting viral gene expression, viral DNA synthesis and capsid assembly. Notably, there is a redistribution of HOP into the nucleus and specifically a proportion of HOP is observed localising with ORF57 in the vRTCs at 24h. This further indicates that HOP may be utilized in the KSHV lytic replication phase.
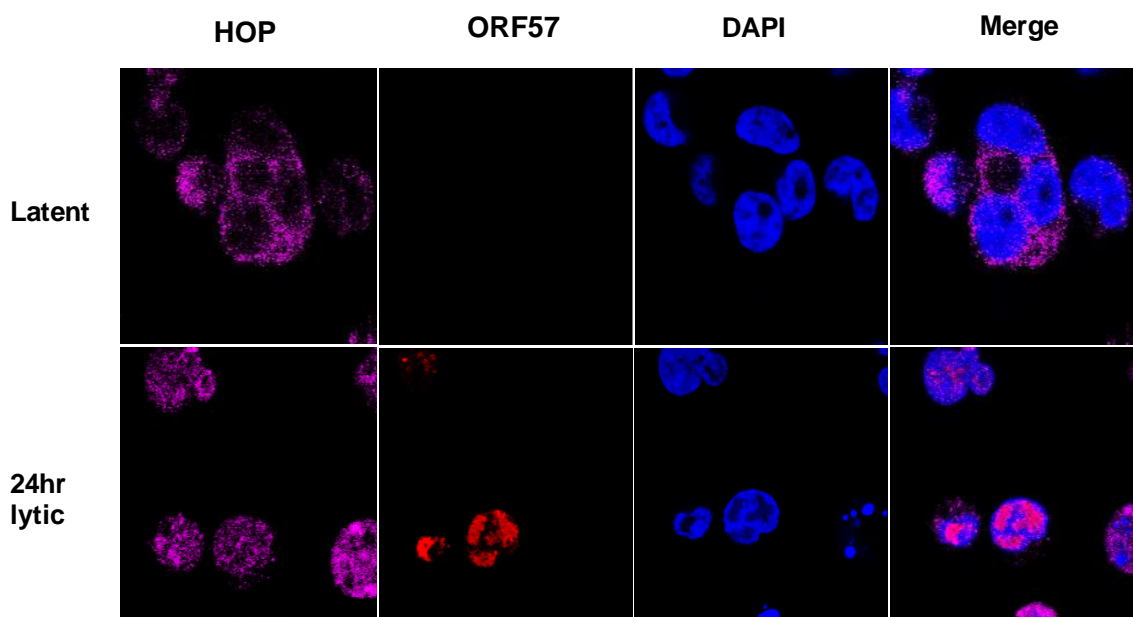
Figure 23: Immunofluorescence of BCBL-1 TREx-Rta during latency and 24 hours in lytic replication showing localisation of HOP to nucleus during KSHV lytic replication. Cells were fixed and permeabilised. Cells were probed for HOP (purple), ORF57 (red) and nucleus via DAPI (Blue). Images captured by Miss Ella Dimascio.

3.3 Assessing lentiviral shRNA-mediated depletion of HOP on KSHV lytic replication.

Due to the observed redistribution of HOP into nuclear vRTCs in confocal microscopy studies and the stability of the transcript and protein levels during infection, it was important to determine whether HOP was required for KSHV lytic replication. Therefore, stable depletion of HOP in TREx BCBL1-Rta cells using lentivirus-transduced HOP targeting-shRNAs was utilised. Plasmids containing HOP-targeting shRNAs were kindly provided by Professor Edkins, Rhodes University, South Africa.

3.3.1 HOP depletion does not affect cell proliferation of TREx BCBL1-Rta cells.

Prior to assessing the impact of HOP knockdown on KSHV lytic replication, it was first essential to determine the impact of HOP depletion on TREx BCBL1-Rta cellular fitness. Obviously if HOP depletion resulted in a deleterious impact on cell growth and viability this in turn could result in false positive phenotypic changes being observed on KSHV lytic replication. HOP knockdown was performed using a lentivirus-based shRNA methodology due to the low transduction efficiency of siRNAs into TREx BCBL1-Rta cells. Upon lentivirus transduction, latently-infected cells were selected in puromycin for one week prior to HOP knockdown being analysed by qPCR and western blot analysis. Both qPCR and western blot analysis confirmed efficient knockdown on HOP RNA and proteins levels compared to a scrambled control cell line (Figure 24 & Figure 25).
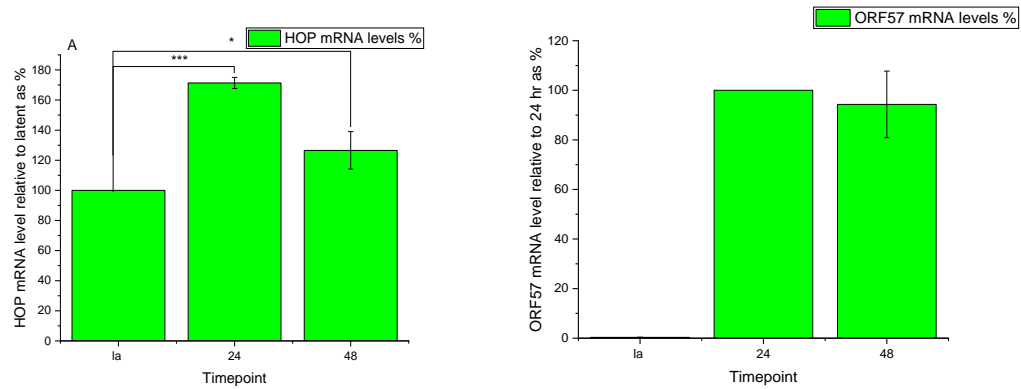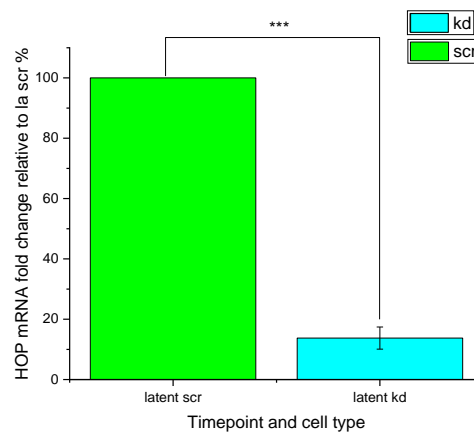

Figure 24: RT-qPCR analysis of HOP mRNA levels compared to latent scramble and relativised to mRNA levels of GAPDH housekeeping in BCBL-1 TREx-Rta cells. These cells contain scramble or HOP targeting shRNAs. Error bars represent SD, n = 3 biological repeats. N = 2 technical repeats of qPCR data with no difference greater than 0.5 ct values between technical repeats utilised.. Significance calculated by unpaired t test.
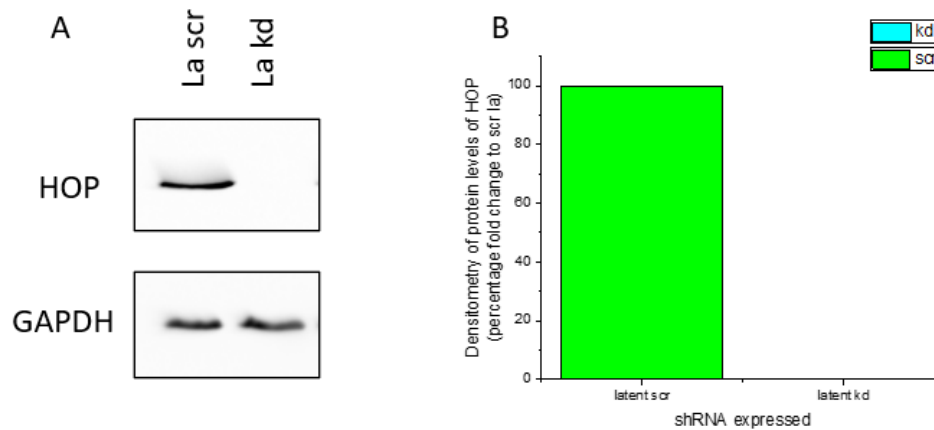
Figure 25: (A) Western blot of BCBL-1 TREx-Rta cells containing either scramble or HOP targeting shRNAs. (B) Densitometry of HOP n = 3 three biological repeats, relativised to GAPDH housekeeper. No t test could be successfully completed on HOP scramble vs knock down as no knock down protein signal detected by densitometry.

To investigate whether HOP knockdown had any impact on TREx BCBL1-Rta cell growth, proliferation assays were performed comparing the proliferation rates of scrambled versus HOP knockdown cells. Here cells were seeded into a 6-well plate at 0.2 x 10^6 cells/well with 2 mL fresh RPMI selection media. Cells were grown for 48 hours and counted at 24 hour intervals. Results show that scrambled and HOP knockdown cells had similar proliferation rates, suggesting that depletion of HOP had little if any effect on TREx BCBL1-Rta cell growth and viability (Figure 26).
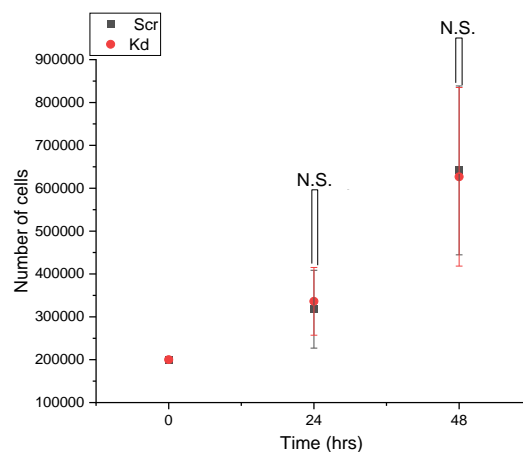
Figure 26: Cell proliferation assay. BCBL-1 TREx-Rta cells containing scramble or HOP targeting shRNAs were seeded and counted at 0, 24 and 48 hours incubation time. Error bars represent SD, n = 3 biological repeats. Significance calculated by unpaired t test.

3.3.2 HOP knockdown impacts KSHV lytic replication.

Once effective HOP depletion had been confirmed in TREx BCBL1-Rta cells during latency, we next determined whether HOP depletion affected KSHV lytic replication. Here HOP and ORF65 transcript levels were analysed in HOP-knockdown TREx BCBL1-Rta cells versus scrambled control at 0h, 24h and 48h post reactivation. Results showed a significant decrease in ORF65 mRNA levels compared to the scramble control at both 24h and 48h (Figure 27). ORF65 mRNA levels was utilised in this assay to analyse later time points during the lytic replication cycle.
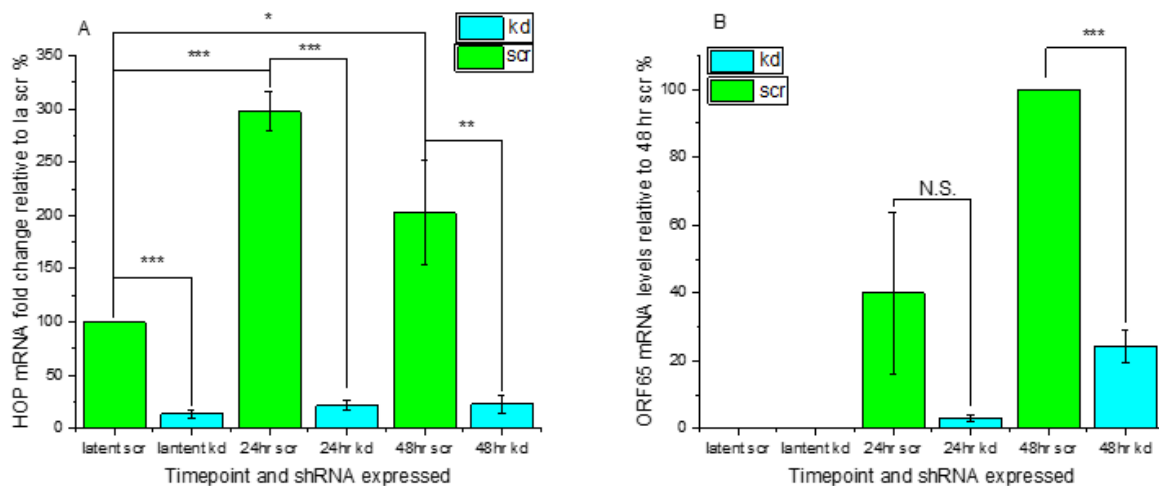
Figure 27: RT-qPCR analysis of (A) HOP & (B) ORF65 mRNA levels compared to 48 hr scramble and relativised to mRNA levels of GAPDH housekeeping in BCBL-1 TREx-Rta cells. These cells contain scramble or HOP targeting shRNAs and KSHV lytic replication was induced and cells incubated 24 hours and 48 hours. Error bars represent SD, n = 3 biological repeats N = 2 technical repeats of qPCR data with no difference greater than 0.5 ct values between technical repeats utilised. Significance calculated by unpaired t test.

Furthermore, western blot analysis was performed on HOP-depleted cell lysates compared to scrambled control cells using HOP, ORF57 and ORF65-specific antibodies. The HOP western confirms near complete knockdown of HOP protein levels and importantly, results show reduced levels of both ORF57 and ORF65 proteins by 80% and 85%, respectively in HOP-knockout TREx BCBL1-Rta cells compared to scrambled control (Figure 28). Together, these results show that KSHV gene expression at both early and late time points is significantly reduced in the absence of HOP, suggesting it has an important role in enhancing KSHV lytic replication.
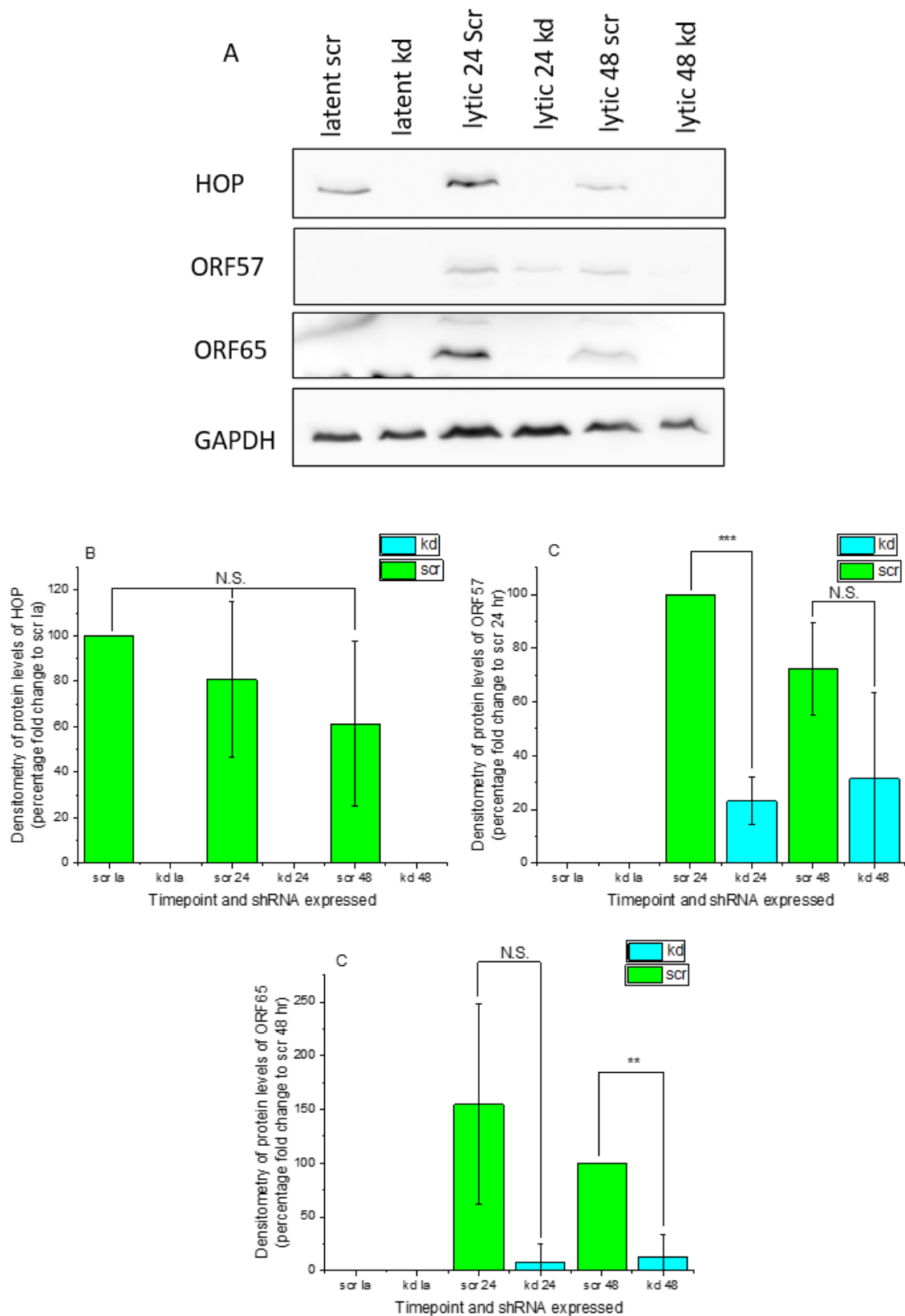
Figure 28: (A) Western blot of BCBL-1 TREx-Rta cells containing either scramble or HOP targeting shRNAs with reactivation of KSHV lytic replication cycle induced and timepoints taken at 24 hours and 48 hours. (B,C,D) Densitometry of HOP, ORF57 and ORF65 from three biological repeats, relativised to GAPDH housekeeper.

Error bars represent SD, n = 3 biological repeats. Significance calculated by unpaired t test. No t test could be successfully completed on HOP scramble vs knock down as no knock down protein signal detected by densitometry.

To further confirm a potential role of HOP in viral replication, viral genome copy number was analysed using a viral load assay (Figure 29). During lytic replication, viral genome number is greatly enhanced before being packaged into new infectious virion particles. Therefore, qPCR was performed on DNA extracted from scramble control and HOP depleted cells at 0 and 72 hours post reactivation. qPCR primers specific to the ORF57 gene was used as a representative of the KSHV genome. ORF57 DNA levels significantly decreased in HOP depleted cells at 72h compared to the scramble control.
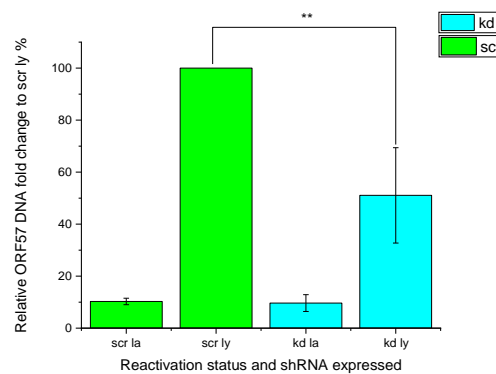
Figure 29: qPCR of a viral load assay, this data shows viral DNA production via ORF57 primers relativised to host GAPDH housekeeping gene DNA in BCBL-1 TREx-Rta cells. These cells contain scramble or HOP targeting shRNAs and KSHV lytic replication was induced, and cells incubated for 72 hours. Error bars represent SD, n = 3 biological repeats. N = 2 technical repeats of qPCR data with no difference greater than 0.5 ct values between technical repeats utilised.. Significance calculated by unpaired t test.

Finally, the effect of HOP-depletion was analysed via *de novo* infection of naïve 293T cells. Here scrambled and HOP depleted cells were induced for 72 hours before being spun down and the supernatant used to infect naïve 293T cells. 24 hours after addition of supernatant, cells were harvested, and RNA extracted. qPCR analysis was then performed to measure KSHV ORF57 levels as an indicator of relative 293T infection with KSHV from either scramble and HOP depleted cells. Results show a significant reduction by >80% in ORF57 levels upon infection from HOP-knockdown TREx BCBL1-Rta cells, suggesting a dramatic reduction in infectivity of HOP- knockdown supernatant. This could be due to a number of factors such as virion fitness or total virion count (Figure 30). Together these results confirm that HOP is important for KSHV lytic replication.
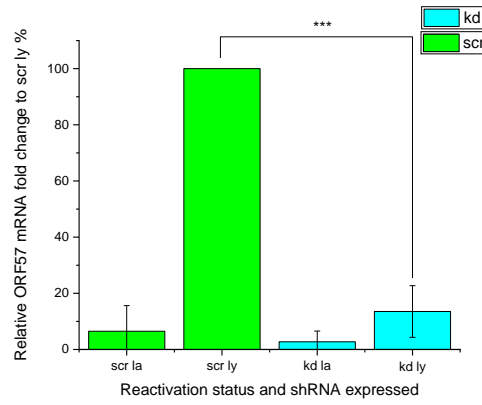
Figure 30: Results of reinfection assays measured via RT-qPCR of viral ORF57 mRNA produced by naïve HEK-293T cells infected with media supernatant of 72 hour induced BCBL-1 TREx-Rta cells. These BCBL-1 TREx-Rta cells contain either scramble or HOP targeting shRNAs. GAPDH mRNA was utilised to relativise ORF57 levels. Error bars represent SD, n = 3 biological repeats. N = 2 technical repeats of qPCR data with no difference greater than 0.5 ct values between technical repeats utilised. Significance calculated by unpaired t test.

3.4 Initial testing of the MCCB library guided by *in-silico* screening to inhibit TPR2A-HSP90 PPI.

3.4.1 A low throughout assay to test inhibitory compounds from an *in-silico* screen

Results above demonstrate the requirement of HOP for efficient KSHV lytic replication cycle. This is emphasised by HOP redistribution to vRTCs and the deleterious effect of HOP knockdown on KSHV gene expression and infectious virion production. Aligned with the previous evidence of the critical role of the HSP network to KSHV replication outlined in chapter 1, the ability to modulate this network via small molecules may provide future treatments of KSHV and its associated pathologies. However, although ATPase inhibition of HSP70 and HSP90 has been demonstrated, there are known downsides with this approach including system redundancy and toxic side effects (Trepel et al., 2010). To date, despite large bodies of research and multiple trials of inhibitory compounds targeting the HSP90 ATPase site, only one compound has reached phase III clinical trials but eventually failed to progress further (Li and Luo, 2023). Based upon these findings, we aimed to develop a more finessed approach to target the chaperone network via HOP, specifically targeting the direct protein-protein interactions between HOP and its HSP partners.

3.4.2 Phenotypic screening of potential TPR2A-HSP90 PPI inhibitors

To develop small molecule inhibitors targeting the essential role of HOP in the chaperone network, we aimed to specifically target the tetratricopeptide repeats (TPR), as HOP has no characterised ATPase or catalytic site (Yamamoto et al., 2014). The TPR domains are defined HSP interacting regions, allowing HOP to function as a scaffold protein for the transfer of clients between HSP70 and HSP90. Therefore, these TPR domains are the key sites of protein-protein interactions with HSP partners (Scheufler et al., 2000; Carrigan, 2006). An advantage of this approach is that the X-ray crystal structure of HOP TPR1 and TPR2A interacting with HSP70 and HSP90, respectively have been published (pdb files 1ELW and 1ELR) (Scheufler et al., 2000) (Figure 31).
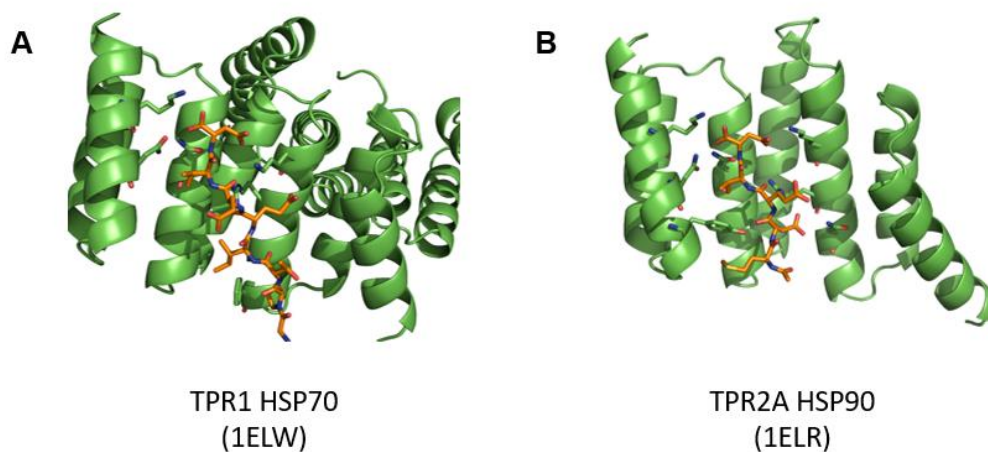
Figure 31: Representative depictions of X-ray crystal structure of (A) TPR1 HSP70 and (B) TPR2A HSP90 PPI interactions. HOP TPR domains modelled as ribbon diagrams with HSP peptides as ball and stick. Data from (Scheufler et al., 2000) images generated by Foster group, University of Leeds.

These structures depicting full-length domains of HOP interacting with HSP partners modelled as small peptides were utilised to develop SMI of these PPI interactions. These short HSP peptides have identified the key "hot spot" for PPI interactions, acting as a major contributor for HSP-TPR binding. Therefore, they are considered the best interaction to target during PPI inhibitor development (Scheufler et al., 2000 Lu et al., 2020). Our collaborators in the Foster group, Department of Chemistry, University of Leeds utilised an *in-silico* approach using Schrodinger Glide software. This involved generation of a receptor grid and the removal of the bound peptides followed by virtual docking of compounds from the MCCB library into the resultant pocket. From this *in-silico* approach, an initial 1000 highest scoring (glide score) target compounds from the MCCB library for both TPR1 and TPR2A were identified (Figure *32*).

TPR1 HSP70
(1ELW)

TPR2A HSP90
(1ELR)
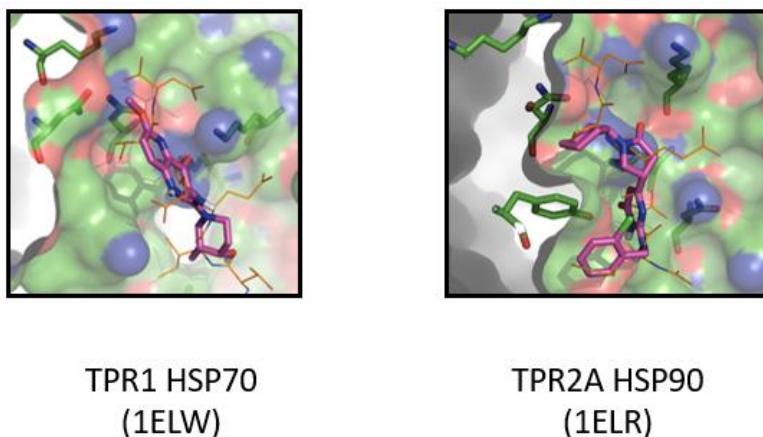
Figure 32: Example image (Foster group, Department of Chemistry, University of Leeds) of Schrodinger Glide docking of MCCB compound library molecule into TPR1 and TPR2A domain structures from X-ray crystal structure (Scheufler et al., 2000). Glide docking undertaken by Foster group, Department of Chemistry, University of Leeds with grid generation based upon co-crystalised HSP peptides. Compounds ranked by generated Glide score.

To assess any potential antiviral activity of the MCCB compounds identified by the *in-silico* approach, we initially tested a small number of compounds selected to bind the TPR2A-HSP90 pocket. Due to the low throughput nature of the KSHV replication assay, we prioritised the 36 highest scoring *in-silico* screen compounds ranked by glide score from a specific compound supplier within the MCCB library. These selected compounds were first assessed for cytotoxicity via an MTS assay to identify suitable non cytotoxic concentrations to be used in the screen over a 48-hour period. An example of the MTS assay is shown in Figure 33 for compound C2, showing an increase in cell toxicity at higher concentrations. This compound was therefore utilised at 1 μM concentration.
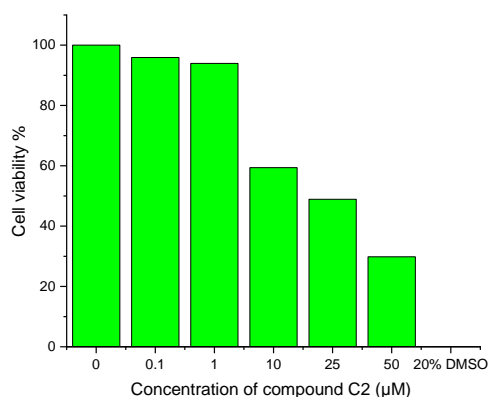
Figure 33: MTS assay of compound C2 utilised during phenotypic screening of BCBL-1 TREx-Rta cells. Concentration of compound C2 selected for phenotypic screening of 1 μM.

From the 36 prioritised compounds 14 were shortlisted by availability for repicking from the Leeds MCCB library stocks. These compounds were tested to determine whether they had an ability to inhibit KSHV lytic replication. Selected compounds and a DMSO control were incubated with latently-infected BCBL-1 TREx-Rta cells at non-cytotoxic concentrations prior to the cells being reactivated for 48 hours. Cell lysates were then probed with an ORF65-specific antibody to assess for late KSHV protein production. Of these 14 screened compounds, two showed consistent antiviral activity, C2 and D2 (Figure 34 & Figure 35).

C2   D2
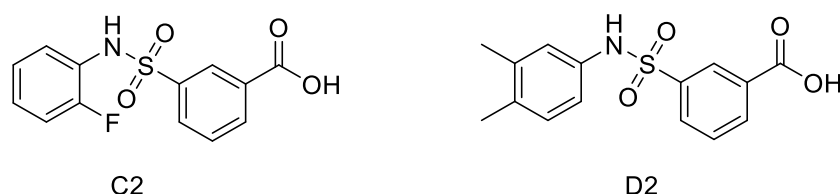
Figure 34: Chemical structures of compounds C2 and D2 that demonstrated antiviral activity against KSHV in BCBL-1 TREx-Rta cells.
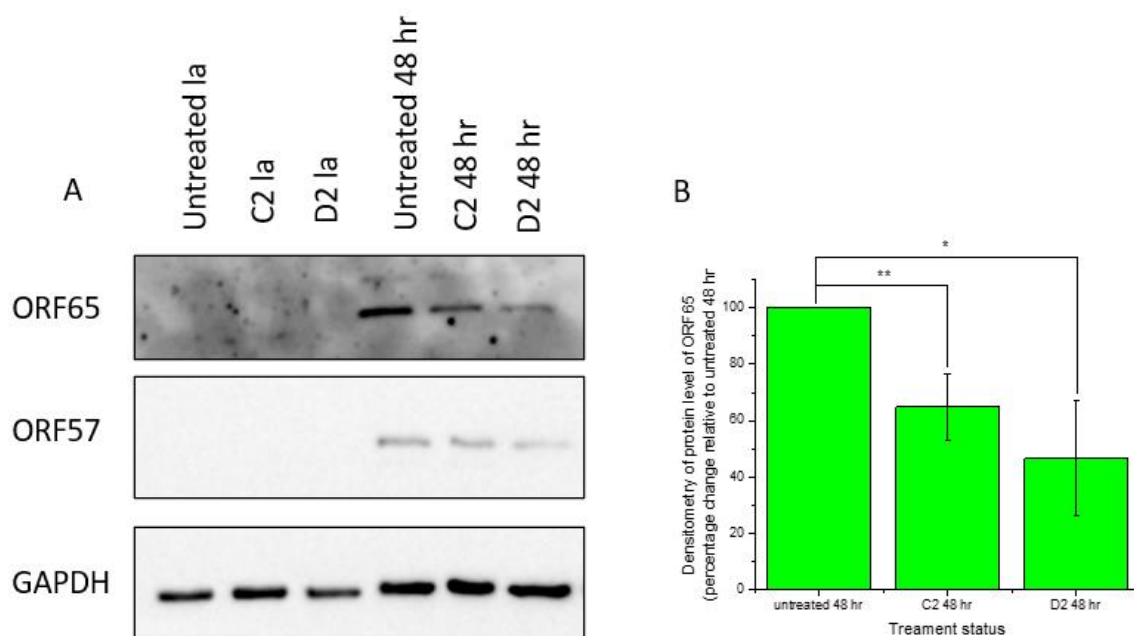
Figure 35: (A) Western blot of compounds C2 and D2 during phenotypic screening of KSHV reactivation in BCBL-1 TREx-Rta cells via ORF65 levels. (B) associated densitometry of three biological repeats of ORF65 levels, relativised to GAPDH housekeeper. Error bars represent SD, n = 3 biological repeats. Significance calculated by unpaired t test.

Results shown in Figure 35, both compounds C2 and D2 demonstrated a phenotypic response by reducing levels of the KSHV protein ORF65, which is suggestion of a potential

102

inhibitory activity. However, the issue with this phenotypic screening approach was twofold. Firstly, it failed to demonstrate disruption of TPR2A-HSP90 PPI definitively with off target effects potentially being responsible for the reduced ORF65 protein levels. Secondly this was a very low throughput method requiring large amounts of reagents and time to screen a small number of compounds. To alleviate these issues, the next chapter describes the development of a high throughput screen that would allow us to economically test compounds at a higher rate and also demonstrate definitive disruption of TPR-HSP PPIs.

3.5 Discussion

This chapter details our approaches to developing an understanding of the role of HOP during KSHV lytic replication and its suitability as an antiviral candidate, alongside early screening approaches. It is clear that HOP plays an important role in KSHV lytic replication, with knock down studies clearly indicating that it has some kind of function in allowing KSHV to effectively undergo lytic reactivation. This reinforced our belief that targeting its PPI interactions with HSP70 and HSP90 would be appropriate and that a successful inhibitor could possess antiviral activity. It has been well documented that both the latent and lytic replication cycle are key in driving KSHV-mediated oncogenesis. Thus, replicating the HOP knockdown phenotypes deleterious effect on lytic replication via small molecule inhibitors could provide a potential route to a future pharmaceutical against KSHV-associated malignancies. Further support to this approach, was highlighted by KSHV induced redistribution of HOP into the nucleus and a proportion localisation to vRTCS, which is highly analogous to the redistribution of its partner, HSP70, during KSHV infection. Small molecule inhibition utilising HSP70 ATPase inhibitors demonstrated a significant impact of KSHV ability to undergo lytic replication and gives credence to the hypothesis of targeting HOP in an antiviral context (Baquero-Pérez and Whitehouse, 2015).

However, it should be noted that the work in this chapter does not definitively prove that inhibition of the TPR1/2A domains of HOP interaction with its HSP partners would work as an antiviral. Several potential factors could contribute to this shortcoming, such as HOP possessing an unknown function independent from its HSP scaffolding via TPR1/2A domains that is critical to KSHV replication. In addition, our knockdown studies removed all HOP domains simultaneously as opposed to selective inhibition of the specific TPR domains. Specific HOP mutant studies could provide an improved way of validating antiviral activity of targeting specific PPIs. Furthermore, the TPR2B domain which we do not attempt to develop inhibitors of, interacts much more weakly with both HSP70 & HSP90 in a supporting role to TPR1/2A and may be of importance in relation to KSHV infection (Bhattacharya and Picard, 2021). Finally, cell type specificity may prove a factor with HOP antivirals, as an upregulation

of HOP at a protein level was seen in Clone 9 cells unlike BCBL-1 TREx-Rta cells. This upregulation could ameliorate phenotypic response upon treatment with a TPR-HSP PPI inhibitor.

However, results herein demonstrate that HOP clearly plays a key role in KSHV lytic replication and as demonstrated in the literature across a large number of conditions (Pimienta et al., 2011; Zhai et al., 2018; Bhattacharya and Picard, 2021). Thus, development of specific PPI inhibitors would be a useful tool molecule for developing a greater understanding of HOP biology across a wide range of contexts and as a potential future treatment for KSHV and its associated malignancies.

The aforementioned issues of our low throughput phenotypic approach of failing to demonstrate mechanism of action and slow screening rate led us to consider alternative approaches in screening of *in-silico* hit compounds. To test these potential inhibitors a high throughput screening campaign based upon demonstrating TPR-HSP PPI inhibition would be incredibly beneficial. A wealth of literature has detailed the use fluorescent polarisation in HTS screens particularly for the development of PPI inhibitors (Lea and Simeonov, 2011; Hall et al., 2016). The next chapter covers our approach to the development of two HTS FP assays that would allow for efficient, economic and specific testing of TPR-HSP inhibitors. In section 4.2.2.5.2 testing of compounds C2 and D2 failed to show disruption of the TPR2A-HSP90 PPI. Due to this no further work was undertaken with these copounds as the antiviral phenotype was believed to be due to off target effects.

Chapter 4

~

High throughput screening of the MCCB library for inhibitors of HOPs PPIs with HSP90 and HSP70

4 High throughput screening of the MCCB library for inhibitors of HOPs PPIs with HSP90 and HSP70

4.1 Introduction

As outlined in Chapters 1 and 3, the importance of the chaperone network to KSHV infection and a wide variety of pathologies has been outlined. However, we now wished to optimise our approach to screening of compounds firstly to ensure specificity of TPR-HSP inhibition and to develop an effective high throughput approach to test the large number of *in-silico* predicted inhibitors. To this end, we chose to utilise a fluorescent polarisation assay, a literature validated approach for HTS screening of PPI inhibitors (Lea and Simeonov, 2011; Hall et al., 2016). This chapter covers the production of purified TPR1/2A domains of HOP and fluorescent polarisation (FP) assay validation, optimisation, and utilisation with their respective HSP partners.

A high yielding, high purity protein expression system for both TPR1 and TPR2A would be critical to allow for effective development and use of a fluorescent polarisation-based assay. For this reason both TPR1 and TPR2A underwent trials to optimise conditions for maximal production of pure protein via a recombinant bacterial-based expression system. Upon production of protein, assays would then require validation through direct titration, competition and Z' experiments to demonstrate assay suitability before beginning a HTS screen of MCCB compounds. In addition, we present the importance of tracer (fluorescently labelled peptide) design and validation, to generate an effective model of the desired PPI. Finally, we show results of our HTS screens and also testing of a literature-reported inhibitory compound.

4.1.1 Introduction to fluorescent polarisation and its utilisation in high throughput screening

Visible light is part of the electromagnetic spectrum, it is a transverse wave comprised of electrical and magnetic field components. These electrical and magnetic oscillations travel perpendicular to the direction of travel of the light wave. By convention, polarised light only contains light in which the electrical fields are travelling in the same direction. This can be generated via a polarising filter which only allows light to pass with the correct orientation of the electrical field.
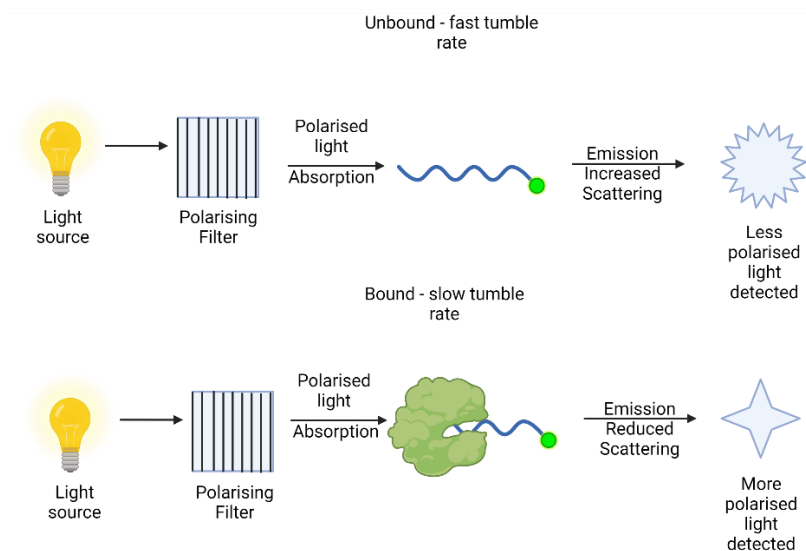
Figure 36: Schematic of principles of a fluorescent polarisation assay. In an unbound state tracer tumble rate in solution is fast resulting in the emission spectrum having less polarised light detected. When the tracer is in a bound state the complex formed is much larger resulting in a slower tumble rate, so the emission spectrum has more polarised light detected.

Polarisation of light can therefore be utilised for an FP assay, a biochemical assay that demonstrates the binding of a smaller fluorescently labelled component, referred to as a tracer, to a larger unlabelled component. A pulse of light is directed onto a polarising filter thus generating polarised light at a fixed wavelength. This polarised light is then absorbed by the small fluorescently labelled component of the system. In solution all molecules are dynamic, moving and rotating at varying rates depending on factors such as size, shape, viscosity of solution, and temperature. For FP, the rotation or "tumble rate" is the key and allows for relative size change comparisons. If the tracer is unbound, its tumble rate in solution will be comparatively quick, however if the tracer is bound to the larger component (i.e. a protein) it will have a much slower tumble rate. During emission from the tracer, a faster tumble rate results in more scattering of light occurring. A secondary polarising filter either perpendicular or parallel to the first filter results in two intensities at a longer wavelength light (due to stokes shift) being detected, defined as the S and P channel intensity. A completely bound system will have a much greater overall polarisation than an unbound system and this differential in polarisation can be used to examine binding (Lea and Simeonov, 2011; Hall et al., 2016; Daviter et al., 2022).

Fluorescent polarisation has been employed for numerous HTS campaigns as a primary or secondary screen involving small molecule inhibition of PPIs (Hall et al., 2016; Hua et al.,

2023). In PPI models, a small fluorophore-labelled peptide represents one binding partner whilst the larger component is an unlabelled protein or protein domain. Yi and Regan previously employed FP as a secondary non-HTS confirmational screen of the TPR2A-HSP90 interaction, in which the full-length TPR2A domain of HOP was used as the large component, with fluorescently labelled HSP90 C-terminus peptide as the tracer (Yi and Regan, 2008). From this basis, we elected to begin a HTS campaign utilising FP as a primary screen with HSP peptide tracers and respective binding domains of HOP as protein components. All polarisation measurements were taken utilising a Perkin Elmer EnVision™ 2103 MultiLabel plate reader.

4.2   TPR2A-HSP90 Fluorescent polarisation assay development and HTS screening

The overall aim of this section was the development of a HTS FP screen to discover novel inhibitors of the TPR2A-HSP90 PPI. This would require the development, optimisation, and validation of an effective and reproducible assay to test MCCB compounds highlighted by the aforementioned *in-silico* screening of the PPI. Work would begin with development of an effective high yield and purity protein expression system of the TPR2A domain.

4.2.1   *E.coli*-based protein production of the TPR2A domain

The first stage of the development of the FP assay was the preparation of suitable quantities of the TPR2A domain at high purity to allow effective development and utilisation of the technique in compound screening. A repeatable, high yield and high-purity protein expression system is of great benefit during a HTS campaign to allow effective screening to occur. An *E.coli* based expression system was selected as the preferred route with a variety of purification tags, media, bacterial strains, and temperatures trialled utilising Hamilton and Promega MagneHis purification system. POPin F plasmid was selected as the most suitable, with a hexahistidine tag (HIS-tag) transformed into Lemo21 *E. coli* strain (Figure 37). Temperature trials at 18 ˚C and 25 ˚C resulted in no observable difference, so a room temperature of 22 ˚C was selected to minimise environmental impact relating to heating and cooling during expression.
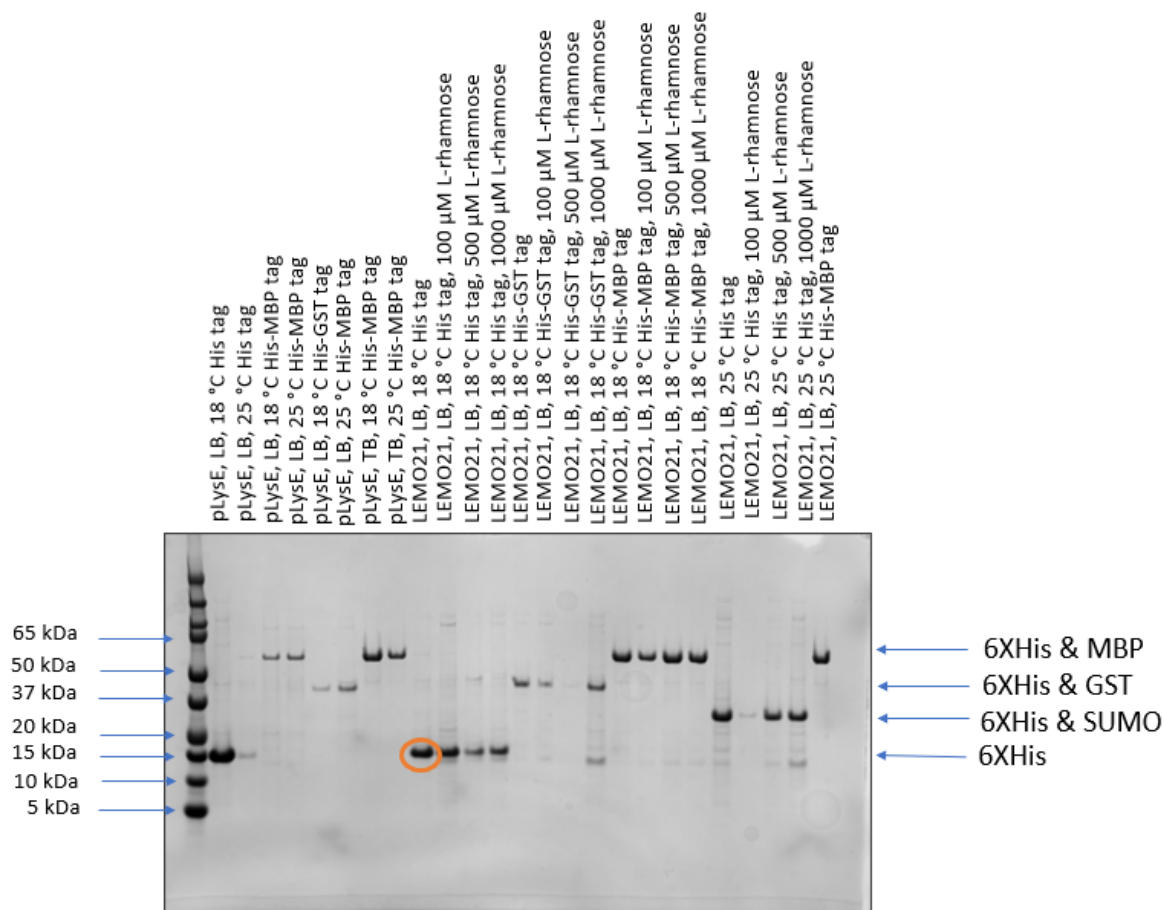
Figure 37: Example SDS-PAGE and Coomassie blue staining of small-scale expression trial of TPR2A protein purification. Orange circle highlights optimal/selected conditions of LEMO21 E.coli strain transformed with POPin F construct expressing 6XHIS tagged TRP2A.

Once the expression conditions of TRP2A were optimised, large-scale batch expression was conducted with a four-step purification process to obtain purified protein (Figure 38). Interestingly, attempts to remove the tag resulted in lower yields, however trypsin digest LC/MS analysis of purified protein excised from the Coomassie acrylamide gel showed autocleavage of the tag occurring (Figure 68). Protein concentration was determined using a Bradford assay and BSA controls (Figure 39). A Bradford assay was selected to determine concentration due to the use of DTT as a buffer additive during the protein production process. Moreover, the TRP2A domain has a low number of aromatic residues therefore protein concentration could not be determined via 280 nM UV or copper-based concentration assays. DTT is frequently utilised in the literature when expressing the TPR2A domain and is beneficial during HTS screening of small molecules (Scheufler et al., 2000; Yi and Regan, 2008; Lee et al., 2012). Yields of protein we produced up to ≈ 24 mg per litre of culture.
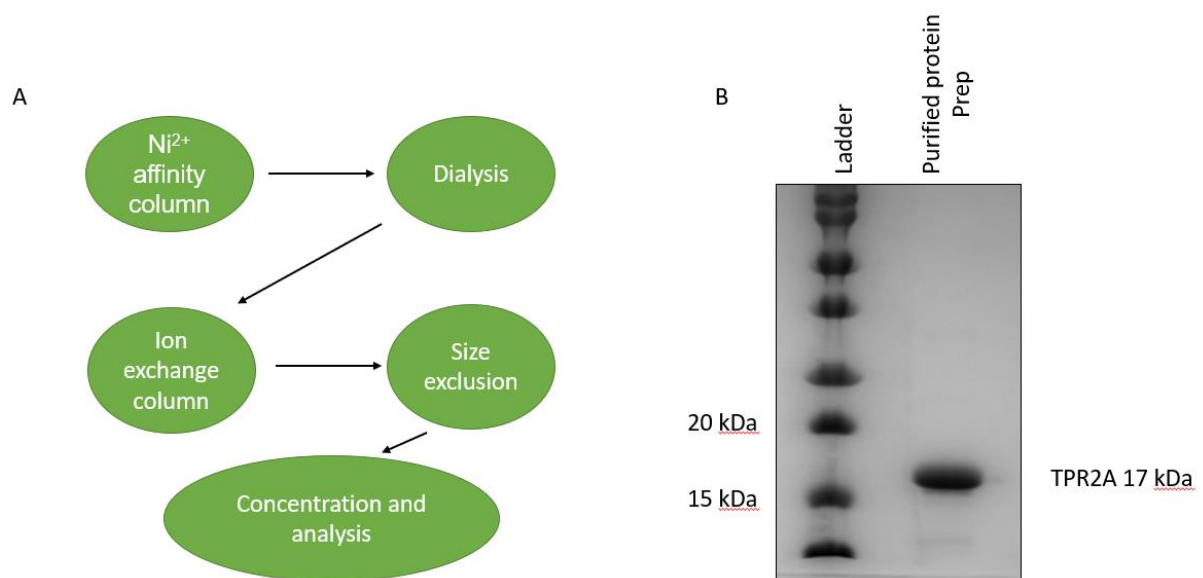
Figure 38: A) Schematic of purification of TPR2A domain of HOP. B) SDS-PAGE and Coomassie blue staining of purified concentrated product
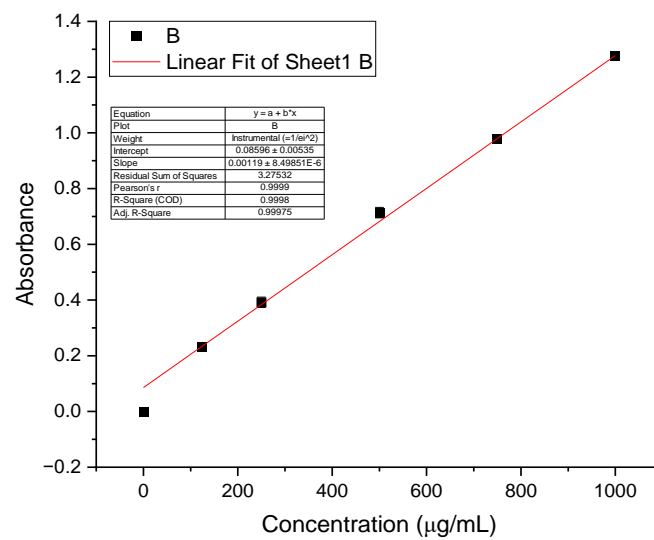
Figure 39: Bradford assay calibration plot. Increasing concentration of BSA standard resulting in increasing absorbance at 595 nM. The absorbance of TPR2A purified protein measured and concentration calculated utilising line of best fit. Error bars represent SD, n = 3 technical repeats.

4.2.2   Fluorescent polarisation experiments of TPR2A-HSP90 interaction

To validate an appropriate FP assay, several stages of development were required which are covered in the following sections.

4.2.2.1   Direct titration and tracer selection

A key control experiment in a FP HTS campaign is a direct titration demonstrating binding between tracer peptide and protein domain by varying protein concentration at a fixed concentration of tracer peptide. As the concentration of TPR2A protein increases more of the unbound fluorescein labelled HSP90 tracer being bound resulting in an increase in polarisation of the system (Lea and Simeonov, 2011). Results in Figure 40 confirm that as TRP2A concentrations increase, it complexes with free tracer until complete binding is observed, thus increasing the polarisation of system.
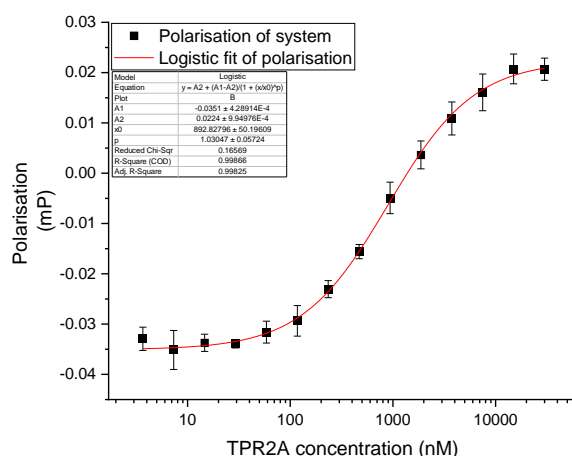
Figure 40: Direct titration experiment of an increasing concentration of TPR2A interacting with HSP90 C terminus tracer and the associated polarisation of the system. Error bars represent SD, n = 3 technical repeats.
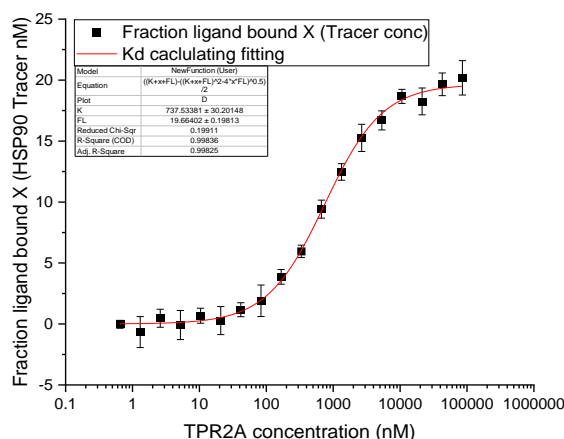
Figure 41: Direct titration experiment of an increasing concentration of TPR2A interacting with HSP90 C terminus tracer (ligand) resulting in an increase in the fraction of ligand bound. Error bars represent SD, n = 3 technical repeats. K parameter is Kd or equilibrium dissociation constant in nM.

Data generated by the Perkin Elmer EnVision™ 2103 MultiLabel plate reader gives two intensity values: the perpendicular intensity (P) and parallel intensity (S). This data was processed following previously published methodology (Azzarito et al., 2012; Hóbor et al., 2022) and is detailed below to give a Kd or equilibrium dissociation. S and P intensity from control wells containing no tracer were averaged for each column and subtracted from individual test wells. The corrected intensity of test wells was used in Equation 1, giving a total intensity I for each well. Three technical repeats were utilised for both control and test wells. Total intensity for each well was then converted to polarisation via Equation 2. Test wells anisotropy values were averaged, and standard deviation calculated. These polarisation values and error were plotted against associated protein concentration (see Figure 40) and fitted in OriginPro 2020b with a logistic sigmodial fit Equation 3 giving r_{min} and r_{max} (seen as A1 and A2 in Figure 40). The values r_{min} and r_{max} are the calculated lower and upper bounds of polarisation in the system, respectively. These polarisation limits were applied to Equation 4 to calculate a fraction of ligand bound, which was then multiplied by tracer concentration. This ligand bound multiplied by tracer concentration was plotted against protein concentration and fitted against Equation 5 as seen in Figure 41 with Kd given as K in nM.

$$\text{Equation 1: } I = (2PG) + S$$

$$\text{Equation 2: } r = \frac{(S - PG)}{I}$$

$$\text{Equation 3: } y = r_{max} + \frac{r_{min} - r_{max}}{1 + (\frac{x}{x_0})^p}$$

$$\text{Equation 4 } F_b = \frac{r - r_{min}}{(\lambda(r_{max} - r) + (r - r_{min})}$$

$$\text{Equation 5: } y = \frac{Kd + x + (FL) - \sqrt{Kd + x + (FL)^2 - 4x(FL)}}{2}$$

Table 27: Reference sheet for fluorescent polarisation equations.

Symbol	Meaning
P	Perpendicular intensity
S	Parallel intensity
G	Instrument factor set to 1
I	Overall intensity
r	Polarisation
F_b	Fraction ligand bound
λ	Ratio of unbound to bound ligand and equals 1
r_{min}	Minimum polarisation of system
r_{max}	Maximum polarisation of system
FL	Tracer concentration (nM)
Kd	Equilibrium dissociation constant

An important consideration in FP is the impact of the tracer fluorophore to binding. To interrogate the impact of the fluorophore on binding, a linker can be utilised. In this case a polyethylene glycol double repeat unit (PEG2) between the HSP90 peptide and fluorophore was introduced. This moves the fluorophore away from the TPR2A binding site and a comparative Kd via direct titration can be measured. As seen in Figure 42 similar direct titration curves were produced for unlinked and PEG2 fluorophores. In addition, results in Table 28 showing Kd values obtained from direct titrations are very similar with unlinked Kd of 777.18 (± 40.91) nM and for PEG2 Kd of 975.85 (± 70.08) nM. Taken together, these results suggest that the overall impact of the fluorophore in the unlinked system was minimal. Due to the inherent conformational motility that the PEG2 linker introduces, the maximal polarisation of

the system is reduced resulting in a greater signal to noise ratio and smaller assay window. Therefore, the PEG2 linker is a less optimal tracer and was not utilised for HTS.
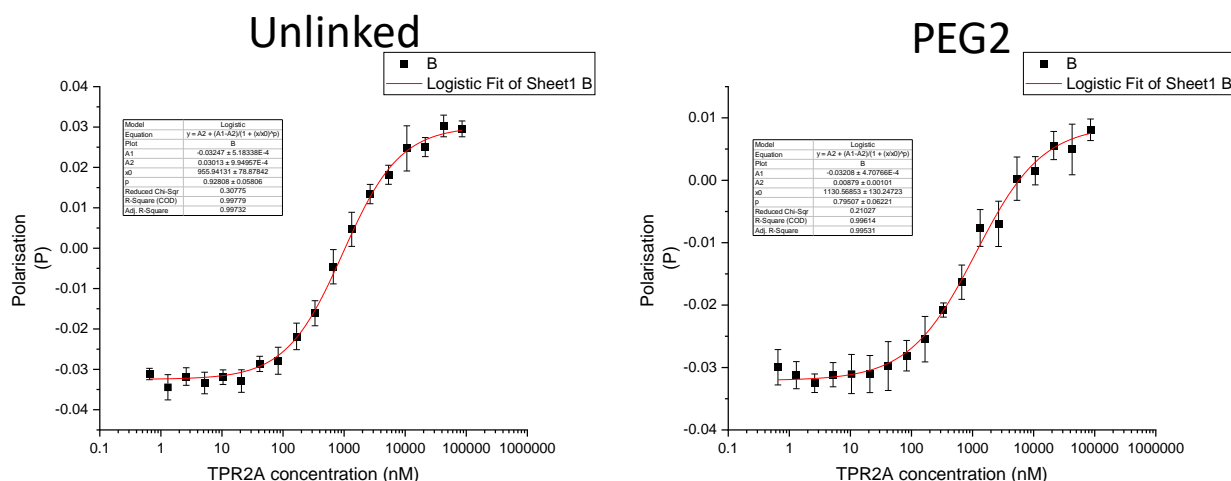
Figure 42: Direct titration experiment of an increasing concentration of TPR2A interacting with both unlinked and PEG2 linked versions of HSP90 C terminus tracer with associated polarisation of system. Error bars represent SD, n = 3 technical repeats.

Table 28 Unlinked vs PEG2 linked HSP90 tracer peptides sequence and direct titration Kd's. Error represent SD, n = 3 biological and n = 9 technical repeats over 1 – 20 hrs.

Peptide	Sequence	Kd (nM)
Unlinked	(5/6-FAM)DDTSRMEEVD	777.18 (± 40.91)
PEG2	(5/6-FAM)(PEG2)DDTSRMEEVD	975.85 (± 70.08)

4.2.2.2 TPR2A-HSP90 direct titration FP assay stability over time.

For repeatability and to reduce false hits, the stability over time of the assay is an important factor to consider. A direct titration assay was plated out for both unlinked and PEG2 tracers. This plate was then repeatedly measured over 1-20 hours to examine changes in Kd calculated. As seen in Figure 43 no significant change in Kd for the two tracers was detected showing stability of the system with Kd maintained at ≈ 700nM for unlinked and ≈ 1000nM for linked respectively.
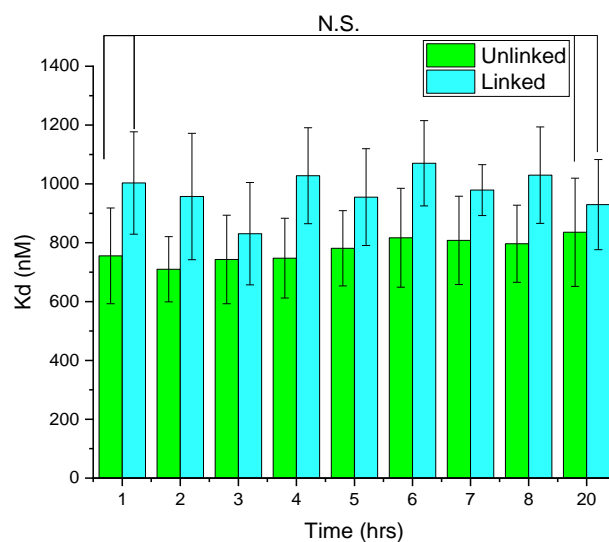
Figure 43: Timepoint titration Kds of unlinked and PEG2 linked HSP90 c-terminus tracer against TPR2A. Error bars represent SD, n = 3 both technical and biological repeats. Significance calculated by unpaired t test.

4.2.2.3 DMSO tolerance testing of TPR2A-HSP90 FP assay.

The MCCB compounds used in the HTS screening are dissolved in DMSO, therefore it was important to interrogate the impact of DMSO on the system before screening to ensure addition of DMSO would not introduce assay artifacts. At this stage, final concentrations for HTS screening had not been elucidated, therefore tolerance testing was carried out at a concentration of 10% however the final concentration in the HTS was only 5%. As seen in Figure 44 there was no significant change in Kd even at these higher concentrations, suggesting the assay was tolerable to the concentrations of DMSO present when using the MCCB compounds.
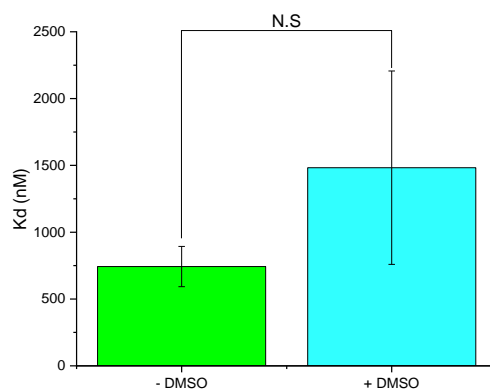
Figure 44: Impact of 10% DMSO to TPR2A FP direct titration calculated Kd. Error bars represent SD, n = 3 technical and biological repeats. Significance calculated by unpaired t test.

4.2.2.4 Competition and Z' FP experiments of the TPR2A-HSP90 interaction.

In section 4.2.2.1, binding of TPR2A to the HSP90 C-terminal tracer was demonstrated. A further key control for a FP HTS are competitive inhibition experiments. Here fixed concentrations of the HSP90 tracer are outcompeted from TPR2A with a known positive control. This is vital as demonstrating compeption by a known positive control shows the system can be inhibited as a hit compound would during HTS screening. The unlabelled form of the HSP90 C-term tracer/peptide was used as this appropriate control and an IC_{50} generated. Analogous to the procedure previously reported (Azzarito et al., 2012), intensity from tracer free wells, S and P channels were averaged per condition and subtracted from tracer containing wells. Utilising Equation 1 and Equation 2, an anisotropy value per well was calculated and averaged. This was plotted against ligand concentration and a logistic fit Equation 3 utilised to calculate an IC_{50} (Figure 45). As seen in Figure 46 no statistical difference in IC_{50} for unlinked vs PEG2 linked tracer was found with IC_{50}s calculated for unlinked of 20.55 ± (1.59) μM and PEG2 17.19 ± (2.34) μM.

A

Unlinked

Model	Logistic
Equation	y = A2 + (A1-A2)/(1 + (x/x0)^p)
Plot	B
A1	0.00563 ± 3.03243E-4
A2	-0.03078 ± 7.17575E-4
x0	19692.37622 ± 1223.77251
p	1.0986 ± 0.05425
Reduced Chi-Sqr	0.15568
R-Square (COD)	0.99753
Adj. R-Square	0.99701

B

PEG2 linked

Model	Logistic
Equation	y = A2 + (A1-A2)/(1 + (x/x0)^p)
Plot	D
A1	-0.00245 ± 4.89908E-4
A2	-0.02127 ± 5.06009E-4
x0	19841.08159 ± 2287.61664
p	1.44825 ± 0.28767
Reduced Chi-Sqr	0.86535
R-Square (COD)	0.99389
Adj. R-Square	0.99205

Figure 45: Competition curves of unlinked (A) and PEG2 (B) variants. An increasing concentration of unlabelled peptide titrated against fixed concentrations of HSP90 Tracer and TPR2A.
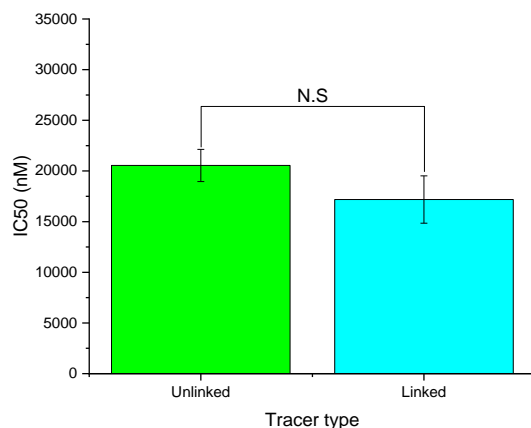
Figure 46: Compiled IC_{50} from competition studies with serial dilution of unlabelled HSP90 c-terminus peptides with both unlinked and linked tracer peptides. Error bars represent SD, n = 3 technical and biological repeats. Significance calculated by unpaired t test.

4.2.2.5 Z' factor of TPR2A-HSP90 HTS FP assay

To determine the efficacy of an FP assay in a HTS role, the Z' factor for the assay is determined utilising Equation 6. This involves filling a plate with alternating wells of solutions to mimic the bound and unbound state of tracer at concentrations utilised during HTS screening. The unbound solution consists of free tracer at screening concentration to mimic complete competition of tracer from TPR2A domain by a compound. The bound solution contrains tracer and TPR2A domain at screening concentration mimicking no competition. The polarisation of these well in then used with Equation 6. The Z' factor incorporates the variation and assay window between bound and unbound state. An assay with a Z' above 0.5 is considered an excellent assay (Zhang et al., 1999). The Z', this assay was found to have a value above 0.5, of 0.70 ± 0.01.

$$\text{Equation 6: } Z' = 1 - \frac{(3\sigma_{c^+} + 3\sigma_{c^-})}{(|\mu_{c^+} - \mu_{c^-}|)}$$

σ_{c^+} = standard deviation positive control polarisation

σ_{c^-} = standard deviation negative control polarisation

μ_{c^+} = mean positive control polarisation

μ_{c^-} = mean negative control polarisation

4.2.2.5.1 **Investigation of the reported TPR2A-HSP90 PPI inhibitor 3-methyl toxoflavin.**
Previous work of Yi and Regan suggested 3-methyl toxoflavin was a potential inhibitor of the TPR2A-HSP90 PPI (Yi and Regan, 2008). Therefore, it was anticipated this compound could act as an excellent control for the FP assay developed herein.
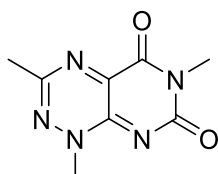
3-methyl toxoflavin

Figure 47: Structure of 3-methyl toxoflavin a reported inhibitor of TPR2A and HSP90 C-terminus peptide.

This compound was therefore trialled in our FP assay. This was done by serially diluting 3-methyl toxoflavin with fixed concentrations of TPR2A and HSP90 tracer. If 3-methyl toxoflavin was active then it would out compete HSP90 tracer, this would result in a decrease in polarisation and a competition curve being generated. However no competition was observed as shown in Figure 48, suggesting this compound failed to block the TPR2A-HSP90 PPI. Furthermore, the toxoflavin family of compounds are known to be "frequent flyer" or PAINS compounds (pan-assay interference) in HTS screen due to redox cycling and production of hydrogen peroxide (dos Santos, 2015; Baell and Nissink, 2018). In addition, 3-methyl toxoflavin is a highly coloured compound and as seen in Figure 49, its UV-Vis absorption overlaps with fluorescein absorption in the 450-475 nM range (Wang et al., 2002). Finally, binding and competition of 3-methyl toxoflavin reported by Yi and Regan to TPR2A/HSP90 PPI is much weaker than the reported 170 nM IC_{50} demonstrated for inhibition of Protein Disulfide Isomerase (Kyani et al., 2018). Due to this combination of factors no further work or development relating to 3-methyl toxoflavin was undertaken.
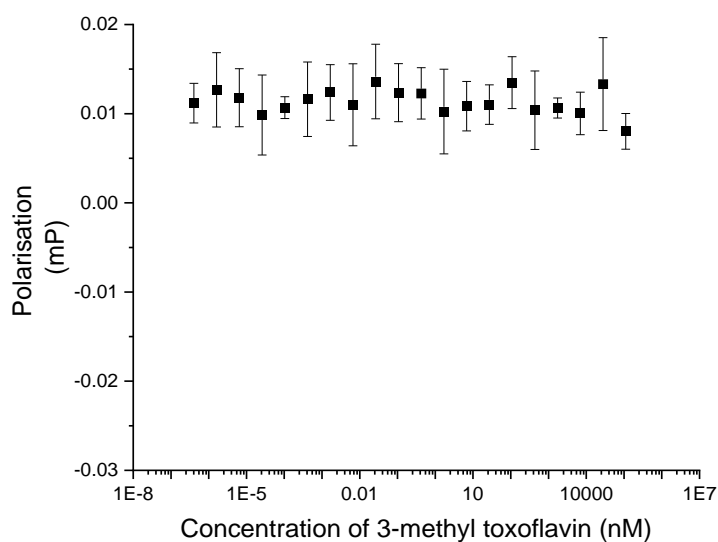
Figure 48: Serial dilution of 3-methyl toxoflavin competition study. Error bars represent SD, n = 3 technical.
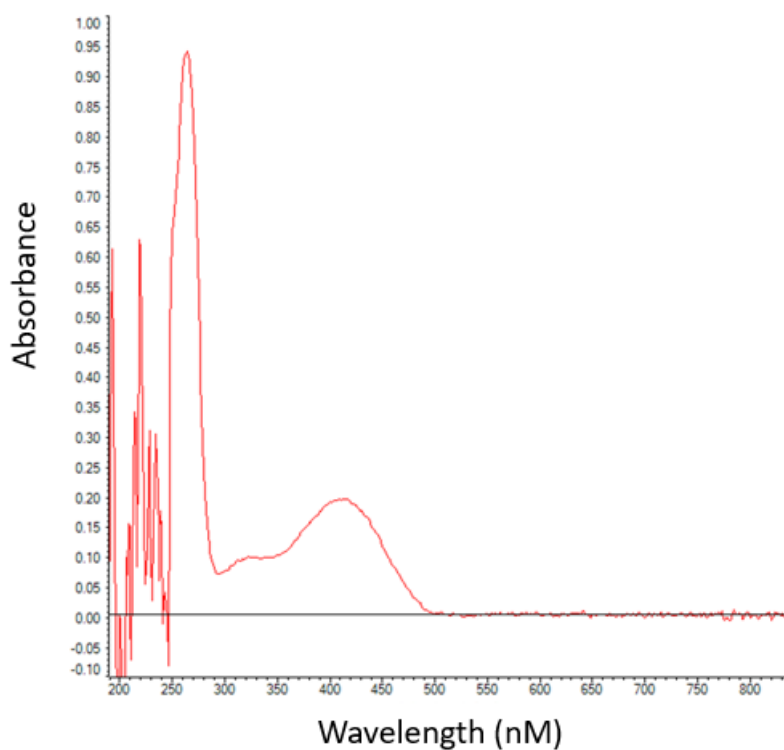
Figure 49: Scanning UV-vis of 3-methyl toxoflavin dissolved in DMSO. UV-vis spectrometer blanked with DMSO.

4.2.2.5.2 Competition studies of Compounds C2 and D2 from cellular screens

Work in chapter 3 demonstrated compounds C2 and D2 possessed some potential antiviral activity. Therefore, we wished to test these compounds in our FP assay to determine if they were successful in inhibiting the TPR2A-HSP90 PPI. Unfortunately, no competition was

demonstrated by either compound (Figure 50). Due to this result no further work was conducted with respect to C2 or D2.
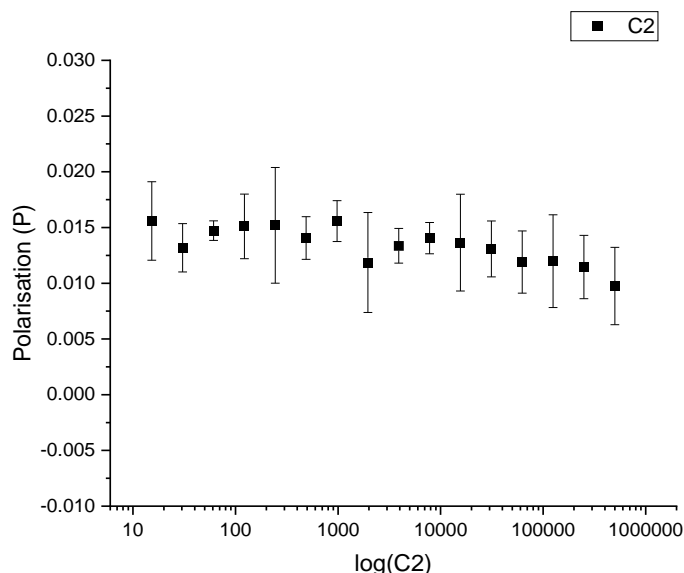
Figure 50: Serial dilution of compound C2 in competition study. Error bars represent SD, n = 3 technical.

4.2.2.6 High throughput screening of MCCB library compounds in TPR2A-HSP90 FP assay

Compounds from the *in-silico* screen were picked from the MCCB library to a compound plate to enable assessment of any inhibitory activity of the TPR2A-HSP90 PPI. Notes were taken of stock characteristics such as colour and presence of precipitation. Compounds were then transferred from the compound plate to a FP measuring plate and tested at 100 µM in triplicate.. Additionally, DMSO positive and negative controls were employed in randomly selected wells on each plate throughout screening. Results were plotted as a raw polarisation value and normalised to average negative control polarisation value, an example of these results is shown in Figure 51. In total approximately 500 compounds were screened in triplicate. Any compound showing activity of 0.75 or lower to normalised negative control was retested via competition curve for activity. Unfortunately, whilst several compounds showed initial activity under 0.75, these failed the competition curve assay therefore were not considered true hits.

121
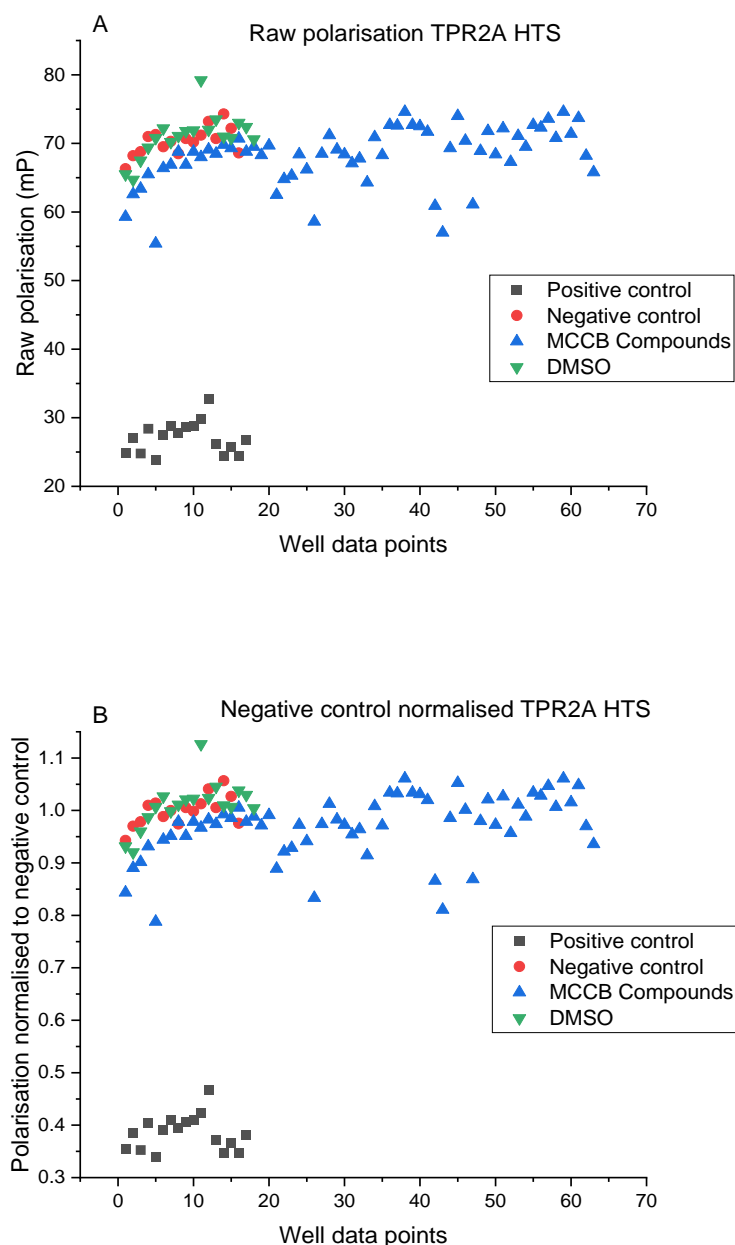
Figure 51: (A) Raw polarisation values and (B) normalised to negative control HTS of MCCB library compounds (blue) FP with TRP2A. Positive controls shown in black, negative controls shown in red, DMSO control shown in green.

4.3 TPR1-HSP70 Fluorescent polarisation assay development and HTS screening

As no compounds screened from the MCCB library demonstrated any inhibitory activity of the TPR2A-HSP90 PPI, a similar approach was used to screen compounds for inhibitory activity of the TPR1-HSP70 PPI.

4.3.1 Protein production and purification of HOP domain, TRP1

As a first step, a high yield and pure recombinant TPR1 domain protein was required. Therefore, to determine the optimal conditions for purification of the TRP1 domain, small scale expression studies were performed trialling temperature and strains with a SUMO-HIS or HIS-tag. The SUMO tag was trialled as it can improve protein expression and solubility resulting in higher yields. However results showed that the hexahistidine-tagged TPR1 expressed in LEMO 21 strain at 22 °C was the most efficient.
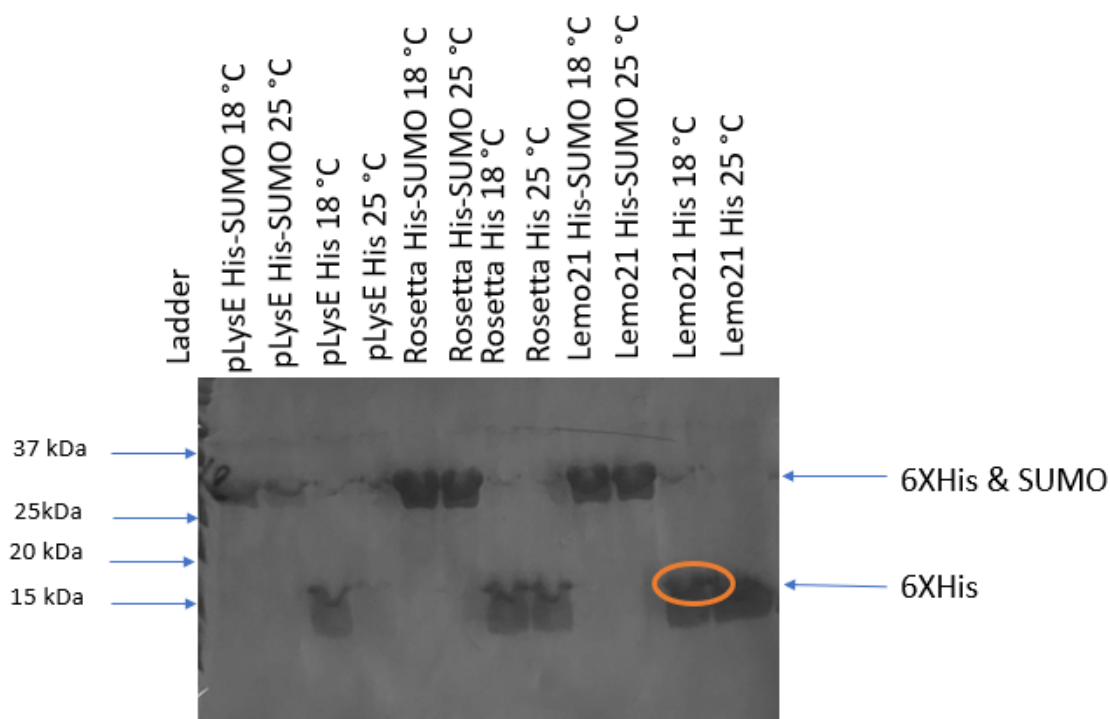
Figure 52 Small scale expression trial of TPR1 domain with either SUMO-HIS of HIS-tag at 18 °C and 25 °C. Orange circle highlights selected conditions.

Using the purification strategy outlined in Figure 53A, a slight impurity was observed that could not be removed despite further purification techniques, such as gel filtration (Figure 53B). Mass spectrometry of this impurity identified the impurity as cAMP-activated global transcriptional regulator CRP of *E.coli* and due to the comparatively low concentration of this impurity, it was decided to utilise the TRP1 product produced and begin FP experiments. To maintain consistency with TPR2A, protein concentration was determined using Bradford assays and yields of protein produced were up to approximately 38 mg per litre of culture.
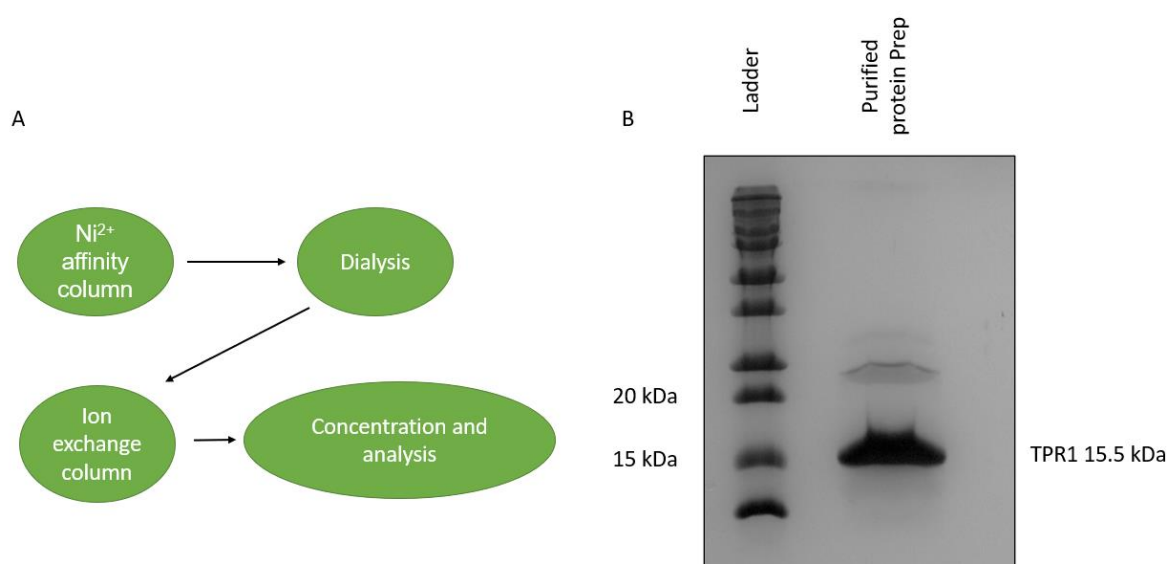
Figure 53: (A) Schematic of purification process of TPR1 domain of HOP. (B) SDS-PAGE and Coomassie blue staining of purified concentrated product. Additionally, note impurity from *E.coli* of cAMP-activated global transcriptional regulator CRP at higher molecular weight than TPR1.

4.3.2 Fluorescent polarisation experiments of TPR1-HSP70 PPI

Analogous to TPR2A-HSP90 FP assay, several stages of development of TPR1-HSP70 FP assay were required which are covered in the following sections.

4.3.2.1 Direct titration and tracer selection

Peptide sequence for the HSP70 tracer was based upon previous ITC data of the truncated HSP70 peptide binding to the TPR1 domain (Scheufler et al., 2000), highlighted in Table 29. Sequence selection was based upon maximal binding with minimum sequence length. Three fluorescein labelled tracer peptides were trialled (Table 30). Tracer design in FP is critical, as reducing tracer size and molecular weight results in a larger mass change upon binding, resulting in a larger tumble rate difference between bound and unbound states. This provides a larger polarisation change and increased assay window however, larger tracers are a more biologically relevant model of PPIs and often produce tighter binding to protein resulting in increased ability to detect binders (Huang, 2003; Hua et al., 2023). Furthermore, the impact of the fluorophore to binding must be accounted for in assay development. Faling to account for fluorophore contribution to binding could result in false positive compounds that disrupt fluorophore-protein binding rather than peptide-protein binding(Hua et al., 2023). Therefore equilibrium dissociation constants (Kd) were calculated utilising procedure outlined in 4.2.2.1.
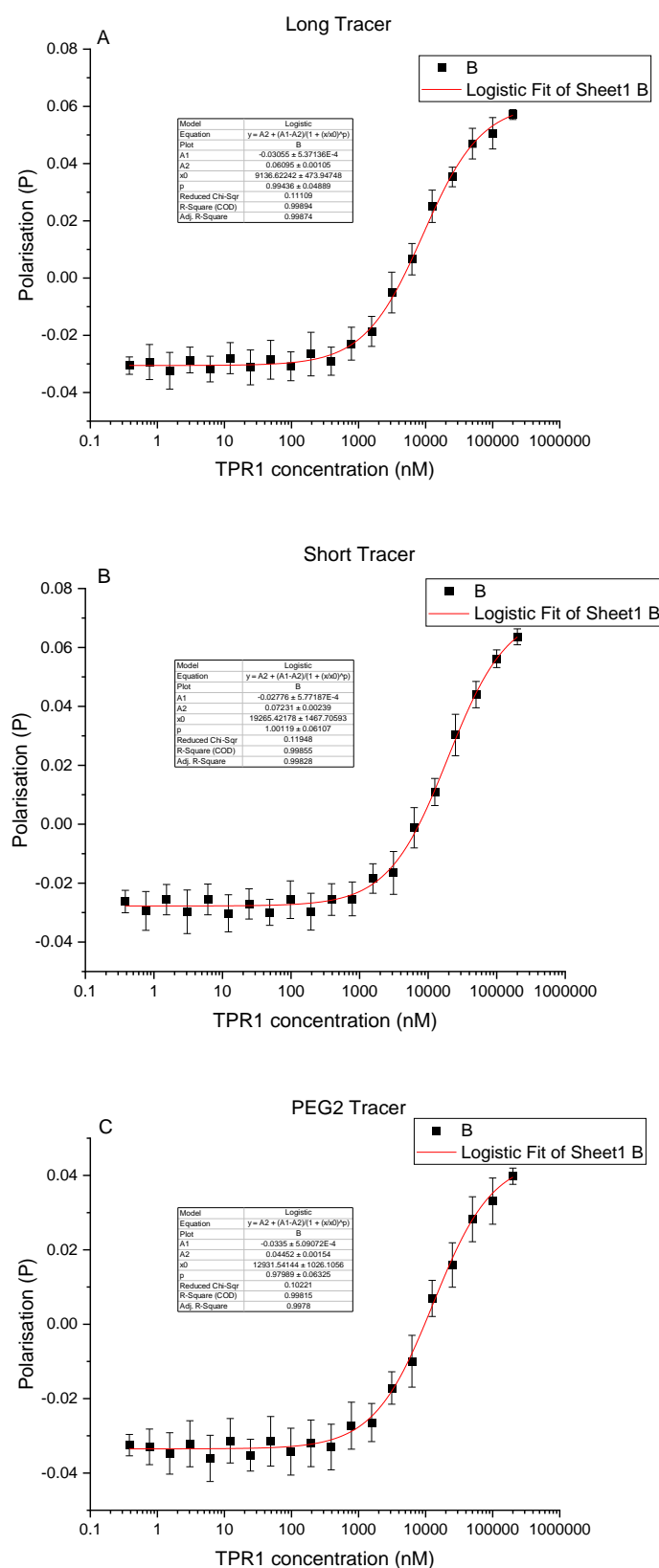
Figure 54: Direct titration experiment of an increasing concentration of TPR1 domain of HOP interacting with both Long (A), Short (B) and PEG2 (C) linked versions of HSP70 C terminus tracer with associated polarisation of system. Error bars represent SD, n = 3 technical repeats.

Table 29 ITC data by (Scheufler et al., 2000) of HSP70 C terminus peptides binding to TPR1 domain of HOP

Peptide Sequence	ITC Kd (µM)
GSGPTIEEVD	14
PTIEEVD	19

Table 30 HSP70 tracers, associated sequence and Kd generated from direct titration binding experiments. Error represents SD, n = 3 technical and biological repeats

Tracer	Sequence	Kd (µM)
Long unlinked	(5/6-FLUO)GSGPTIEEVD	10.95 ± 1.85
Short unlinked	(5/6-FLUO)PTIEEVD	22.61 ± 3.56
Short PEG2 linked	(5/6-FLUO)[PEG2]PTIEEVD	14.05 ± 1.79

Initial tracer sequence design was based upon previous published ITC data, Table 29 (Scheufler et al., 2000). Trialling of TPR1 tracers in Table 30 highlights the impact of fluorophore upon binding, with short unlinked having weaker binding than PEG2 variant, 22.61 ± (3.56) µM vs 14.05 ± (1.79) µM. From these direct titration experiments, the long unlinked tracer with a Kd of 10.95 ± (1.85) µM was selected as the best option for the FP experiments. This was due to a larger assay window than using the short PEG2 linked variant. DMSO tolerance testing was conducted at a concentration of 10% with HTS screening conducted at 5% DMSO concentration with no significance found (Figure 55). Therefore, the assay was tolerable to the concentrations of DMSO present when using the MCCB compounds.
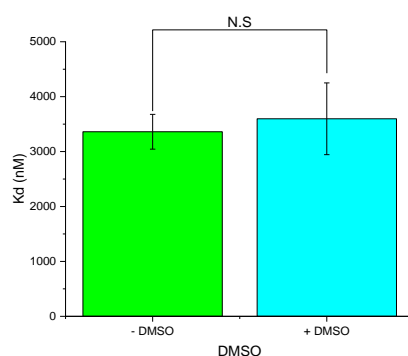
Figure 55: Impact of 10% DMSO to TPR1 FP direct titration calculated Kd. Error bars represent SD, n = 3 technical and biological repeats.

4.3.2.2 Buffer optimisation of TPR1-HSP70 FP assay via direct titration experiments.

Buffer optimisation was carried out for HTS screening. A higher Kd between tracer and protein results in the ability to detect weaker binders (Huang, 2003). Furthermore, the presence of certain additives can reduce assay artefacts and false hits (Feng and Shoichet, 2006; Lee et al., 2012) . Table 31 details buffer changes and resultant changes to tracer protein binding affinity.

Table 31 Composition of buffers utilised during optimisation and associated equilibrium constants calculated from direct titration. Error represent SD, n = 3 technical.

Buffer number	Buffer components	Kd (µM)
1	50 mM NaCl, 20 mM Tris/HCl, pH 8	14.38 ± 0.74
2	50 mM NaCl, 20 mM Tris/HCl, 0.05% TWEEN 20, pH 8	8.34 ± 0.38
3	50 mM NaCl 20 mM Tris/HCl, 1 mM DTT 0.05% TWEEN-20, pH 8	7.37 ± 0.36
4	10 mM NaCl, 20 mM Tris/HCl, 1 mM DTT 0.05% TWEEN-20, pH 8	4.16 ± 0.16

From an initial start point of buffer 1, a DTT free TPR2A FP buffer optimisation resulted in a 3-fold improvement in affinity, resulting in buffer 4 being utilised. Addition of TWEEN-20 was beneficial for binding affinity and is a literature recognised additive in small molecule HTS (Feng and Shoichet, 2006). Buffer 4 not only resulted in a higher protein tracer affinity but also simplified workflow and reduced any potential downstream impacts of ionic strength changes.

4.3.2.3 Competition and Z' FP experiments of the TPR1-HSP70 interaction

Binding of HSP70 tracers to TPR1 was demonstrated in part 4.3.2.1. Therefore, it is then crucial to demonstrate competition of tracers with a positive control to mimic a successful hit in HTS screening. To achieve this an unlabelled version of the long tracer was utilised and generated an IC_{50} by a similar procedure outlined in 4.2.2.4. As seen in Figure 56, as the concentration of unlabelled peptide increases the amount of tracer bound to TPR1 decreases resulting in a decrease in the polarisation of the system. This generated an average IC_{50} value of 7.60 µM ± 3.00 (N=4 biological repeats).
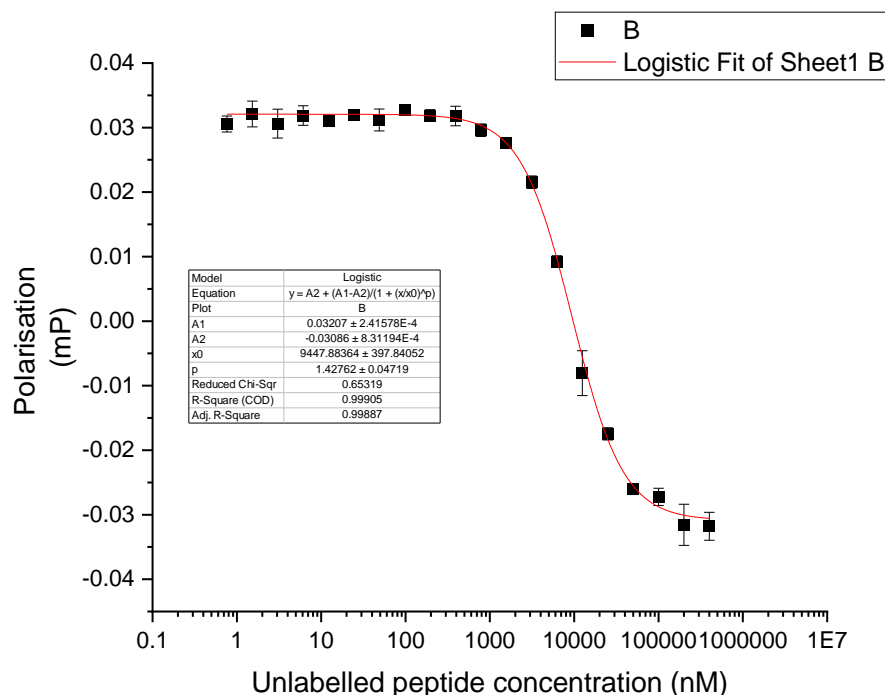
Figure 56: Competition study of TPR1 with long tracer. An increasing concentration of unlabelled peptide tritrated against fixed concentrations of HSP70 Tracer and TPR2A. This results in a decrease in polarisation of system as binding decreases.

The Z' factor was used to test assay suitability for HTS screening (Zhang et al., 1999). Utilising Equation 6, a Z' score of 0.795 ± 0.045 (n = 3 biological repeats) was achieved demonstrating an excellent assay (Zhang et al., 1999).

4.3.2.4 High throughput screening of MCCB library compounds in TPR1-HSP70 FP assay

The previous experiments established efficient controls and concentrations to be used in the HTS. To perform the screen prioritised compounds were transferred from a compound plate to a fluorescent polarisation plate and tested at 100 µM in triplicate. Additionally, DMSO positive and negative controls were employed in randomly selected wells on each plate throughout screening. Results were plotted as a raw polarisation value and relativised to the negative control. In total approximately 500 compounds were screened in triplicate. Any compound showing activity of 0.75 compared to the negative control was retested via competition curve for activity. Whilst several compounds showed initial activity under 0.75, these however failed the competition curve assay therefore were not considered true hits. Figure 58 shows the investigation of a potential hit compound, results show that as the well number increases so does the number of serial dilutions of potential compound and positive control peptide with additional controls of serial dilution of controlled peptide and fixed tracer

concentration wells. Compound dilution with and without tracer (red & black Figure 58) shows a similar change in polarisation of system, indicating that this compound is a false positive from HTS screen.
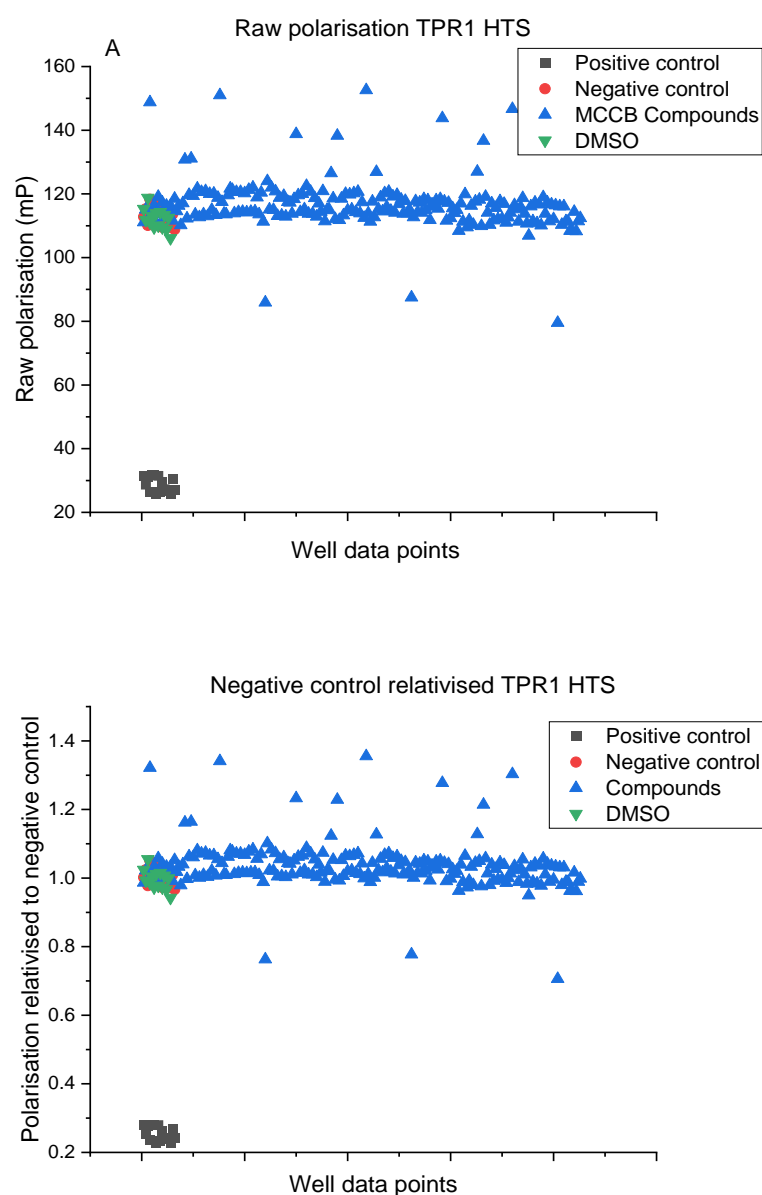
Figure 57: (A) Raw polarisation values and (B) relativised to negative control HTS of MCCB library compounds (blue) FP with TRP1. Positive controls shown in black, negative controls shown in red, DMSO control shown in green. This example depicts a compound showing activity to warrant further investigation.
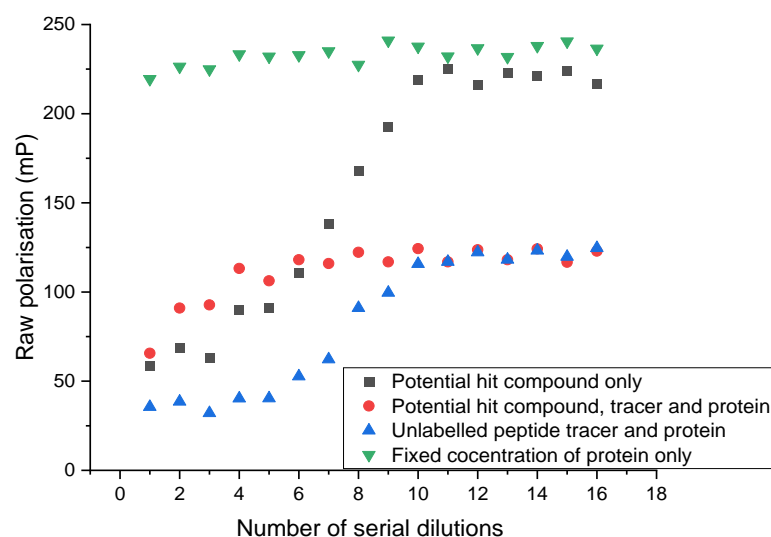
Figure 58: Investigation of potential hit compound, as detected in Figure 57. To determine if the potential hit compound was independently active, or active due to inhibiting tracer-protein binding, the compound was serially diluted either independently (black) or in the presence of a fixed concentration of tracer and protein (red). A positive control peptide was serially diluted with the fixed concentration of tracer and protein (blue) and a fixed concentration of the protein was used as a negative control (green). If compound in isolation shows activity (black) this suggest it is a false positive.

4.4   Discussion

This chapter describes the development and employment of two high throughput fluorescent polarisation assays. Whilst no true positive hit compounds were detected, assay efficacy and effectiveness were demonstrated by successful direct titration, competition, and Z' experiments. In addition, these two validated protein expression and FP assays provide a useful basis for additional work outlined in chapter 5. Based upon previous work, a hit would have been a particularly fortuitous outcome (Yi and Regan, 2008; Darby et al., 2020), especially for TPR2A as combined they blind screened over 150,000 compounds and failed to produce a viable lead molecule. In addition, the challenging druggability of the TPR2A domain has been discussed at great length (Darby et al., 2020). Compounding this, is the inherent challenge of targeting PPI which are well characterised for their difficulty in developing SMIs due to large, diffuse, and open pockets (Lu et al., 2020).

The importance of tracer design is particularly apparent for TPR1. As seen in Table 30, the impact of tracer design on binding is demonstrated, in particular the contribution of the fluorophore. The short, unlinked tracer has a higher Kd and thus a weaker interaction comparative to the PEG2 linked version indicating the fluorophore is causing weaker binding. This result dictated that the short unlinked tracer would not be a suitable in the FP

HTS. The long-unlinked tracer was therefore selected due to a larger assay window comparative to the short PEG2 linked variant. Despite short PEG2 having a lower molecular weight, the motility that PEG2 induces to the fluorophore results in a smaller assay window comparative to long unlinked referred to as the "propeller effect" (Lea and Simeonov, 2011; Hua et al., 2023). In both assays it should be noted that Kd and IC_{50} calculated appeared in the same µM range, this coupled with PEG2 experiments is indicative that overall contribution of fluorophore to binding was minimal (Zhu et al., 2018).

Linker design is based upon a "trade-off" between increasing fluorophore distance from the protein, against tracer mass gain and increasing fluorophore motility (Lea and Simeonov, 2011). The choice of PEG2 as a linker was based upon various factors, including it being the shortest commercially available linker with the lowest molecular weight to combat polarisation loss due to gained molecular mass of tracer, and it is a literature validated linker in FP assays (Kiehstaller et al., 2020; Hua et al., 2023). A potential alternative to PEG2 could be the utilisation of a conformationally constrained linker to reduce loss of maximal polarisation associated with the increased motility.

Competition studies and HTS protein concentrations used gave ratios of 70% tracer binding to protein during direct titration experiments. This falls within the literature guidelines of 50%-80% tracer binding. This range gives a trade-off between assay window and assay sensitivity (Huang, 2003). Following the approach of Zhu et al., 2018, DMSO tolerance testing was undertaken at 10% for both assays despite only 5% DMSO to be used in the screen itself. This ensured any variability of compound addition would be accounted for and gave the possibility for compound screening at higher concentrations. As seen no statistical impact on binding was observed for either assay. The concentration of MCCB compound screened was selected to give a trade off between detection of weak binders versus solubility, based off prior experience within the Foster group of screening the MCCB library. Throughout both screens, compounds were detected with polarisation values above the negative control which we believe is indicative of either solubility, aggregation or autofluorescence interference.

The presence of coloured compounds within the MCCB library resulted in false positives due to autofluorescence/colour based interference. The utilisation of carboxy fluorescein as the fluorophore of choice was due to it being the most frequently utilised fluorophore for HTS within the literature (47%) (Hall et al., 2016). Fluorescein fluorophores encompass several derivatives with the most utilised being FAM and FITC. We utilised FAM due to its smaller molecular weight (Le Guern et al., 2020). A potential alternative group of fluorophores to

combat this autofluorescence issue are the red shifted choices, which have a longer wavelength of excitation and emission. These red shifted fluorophores are argued to reduce autofluorescence false positives in organic compounds screening due to fewer organic molecules having excitation emission peaks at these wavelengths (Banks P et al., 2000).

During development of the TPR1 FP, assay buffer optimisation was undertaken resulting in a buffer that reduced the Kd by 3 fold. This is beneficial as tighter binding demonstrated by a lower Kd reduces the amount of protein required during competition and HTS steps, alongside giving a larger range of hit compounds that could have been identified (Huang, 2003). In addition, use of the detergent Tween 20 reduced Kd and has additional advantages such as reduction of assay artefacts, such as those occurring due to small molecule self-assembly to colloidal aggregates (Feng and Shoichet, 2006). Similarly, utilisation of a reducing agent is of benefit during HTS screening to prevent oxidation of cysteines and covalent binding of HTS ligands to cysteines present in the protein(Lee et al., 2012). Encouragingly, in both FP assays tracer concentration was significantly below the Kds calculated by direct titration. This avoids stoichiometric direct titrations seen when $2Kd \approx$ tracer concentration, which are not considered valid (Huang, 2003).

Moving forward we employed the TPR1 FP assay to trial both full sized drug molecules and fragments in a similar approach to previous used assays (Darby et al., 2020), which highlighted the binding of dicarboxylic acids to the TPR2A-HSP90 binding pocket. This approach is further supported by the observation that the carboxylic acid bio-isotere tetrazole group can inhibit the TPR2A HSP90 interaction (Vaaltyn et al., 2022). Furthermore, the success of utilising our peptide as a control was the starting point for the development of a peptide SAR library towards peptidomimetic compound discovery.

Chapter 5

~

Alternative approaches for the development of TPR1-HSP70 PPI inhibitors

5   Alternative approaches for the development of TPR1-HSP70 PPI inhibitors

Chapter 4 detailed the development and utilisation of high-throughput FP assays to screen TPR2A-HSP90 & TPR1-HSP70 PPIs with shortlisted compounds from *in-silico* screens from the MCCB library. Unfortunately however, no hit compounds were detected with any sufficient inhibitory activity to ultimately test for activity against KSHV in a cellular context. This is not surprising as hit rates in previous random compound screening of TPR2A-HSP90 PPI have been poor and HTS screening particularly against PPIs is often challenging (Yi and Regan, 2008; Darby et al., 2020). Therefore, this chapter details alternative approaches to develop TPR1-HSP70 PPI of inhibitors, which included fragment screening, peptide SAR development and selective functional group screening.

Functional group screening was our final attempt to find a small molecule inhibitor from the MCCB library. By shortlisting functional groups that had shown some activity in previous studies to prevent the TPR2A-HSP90 interaction, we hoped to maximise our chance of finding a compound with inhibitory activity towards the TPR1-HSP70 PPI (Darby et al., 2020; Vaaltyn et al., 2022). This functional group compound screen also included bio-isosteres to see if any new chemical motifs demonstrated activity and to maximise our chances of a hit. Our fragment screening approach similarly was based upon literature activity in a TPR2A-HSP90 context applied to TPR1-HSP70 interaction (Darby et al., 2020; Vaaltyn et al., 2022). We wished to see if any activity was present towards the TPR1-HSP70 interaction using similar fragments and also if this could be utilised in helping with future work towards small molecule inhibitor development and peptide SAR development. Finally, development of peptide SAR would allow us to begin with a known inhibitor and attempt to optimise it further for greater activity, with a view for future work to be undertaken to develop peptidomimetic compounds. To achieve a successful peptidomimetic compound would be beyond the scope of this work but could lay the foundational knowledge required for future attempts. With this in mind, we also explored the feasibility of delivering the FP assay tracer peptides into human cell lines to validate their uptake and potential to disrupt the TPR-HSP PPIs as a pharmaceutical target.

5.1   Selective screening of carboxylic acid and bio-isostere containing compounds from the MCCB library in the FP assay

Previously published work has shown that dicarboxylic acid and tetrazole containing compounds had some inhibitory activity, albeit weak, of the TPR2A-HSP90 PPI (Darby et al., 2020; Vaaltyn et al., 2022). We therefore wished to screen compounds from the MCCB library containing these functional groups, to determine if these compounds had a similar effect on the TPR1-HSP70 PPI using the FP assay. We were particularly interested in the

tetrazole functional group, as it is a literature recognised bio-isostere of carboxylic acid. Tetrazoles are frequently utilised during SAR development to improve the poor pharmacokinetic properties associated with carboxylic acids (Ballatore et al., 2013). An ideal advantage of bio-isosteres as functional groups is that they maintain similar shapes, volumes within the chemical space and physicochemical properties, which allow for similar interactions to occur with a biological target (Malik et al., 2014). Therefore, a screen was performed using a range of carboxylic acid and bio-isostere containing compounds, these included tetrazoles, sulfonamides, sulfamides and sulfonates (Figure 59). A further aim was also to test a range of other known carboxylic acid bio-isosters, such as hydroxamic acids and isoxazole-3-ols, however unfortunately, no compounds containing these functional groups were identified in the MCCB library (Bredael et al., 2022).
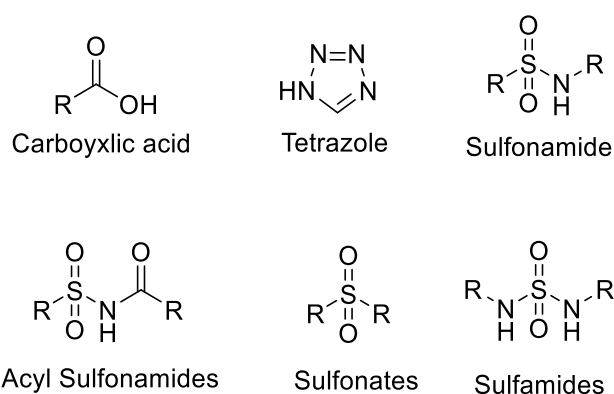
Figure 59: Functional groups of compounds from MCCB library chosen for selective screening at 500 µM and 100 µM in TPR1 FP assay.

To provide a higher chance of detecting potential weak inhibitors in this selective functional group screen, the method described in Chapter 4 for HTS FP screening was modified slightly. We elected to screen each MCCB compound once at a higher concentration of 500 uM and twice at 100 uM. This is different from our previous approach of screening the same compound three times at at 100 µM. By utilising this functional group approach, we could chemically target our screening and also potentially demonstrate a new chemical motif with inhibitory activity. Interestingly compounds C2 and D2 from section 3.4.2 contained both an acyl sulfonamide and carboxylic acid group suggesting our initial *in-silico* screen utilised was a valid starting point in previous screenings.

Compounds were identified using SMILE code searches of the MCCB library. Utilising similar conditions described for the MCCB TPR1-HSP70 HTS FP campaign in chapter 4, a further 226 compounds were screened in triplicate with one screen being performed at 500 µM concentration, whereas the remaining 2 screens were performed at 100 µM compound

concentrations. Figure 60 shows an example of the TPR1-HSP70 HTS assay conducted against carboxylic acid and bio-isostere compounds identified from MCCB library. It also highlights the trade-off of screening at higher concentrations, with an increased number of compound wells showing polarisation values larger than negative controls in the first triplicate. This is likely due to solubility issues of compounds at higher concentrations. Unfortunately, whilst several compounds showed some initial activity under 0.75, these potential hits failed the competition curve assay and were therefore not considered true hits.
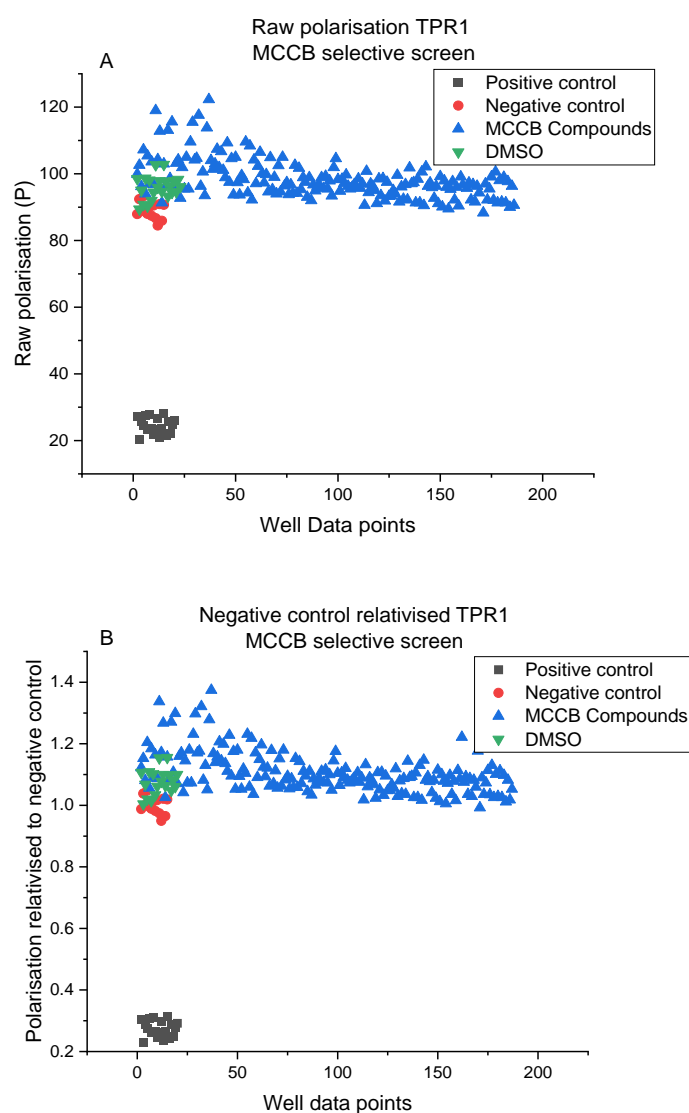
Figure 60: (A) Raw polarisation values and (B) relativised to negative control HTS of carboxylic acid and bio-isostere MCCB library compounds (Blue) FP with TRP1. Positive controls shown in black, negative controls shown in red, DMSO control shown in green.

5.2   Fragment Screening of carboxylic acids and tetrazoles against TPR1-HSP70 PPI

As previously highlighted published work suggested the potential activity of dicarboxylic acid and tetrazole fragments in disrupting the TPR2A-HSP90 PPI (Darby et al., 2020; Vaaltyn et al., 2022). We therefore next examined if any inhibitory activity could be identified with fragment compounds containing these functional groups in relation to the TPR1-HSP70 PPI. This could provide insights into SAR similarities and also highlight any potential differences between the TPR2A and TPR1 PPI domains, which could ultimately aid in future inhibitor development. Importantly, due to the smaller size of fragment-based compounds and their known weaker effect upon PPI inhibition, the fragment-based screen utilised a higher concentration of 25 mM of compound in TPR1-HSP70 FP competition studies. To select compounds, the University of Leeds Chemistry department compound inventory was searched for carboxylic acids and tetrazoles and pure synthetic stocks of these compounds utilised due to comparatively high concentration required.

To perform the screen, carboxylic acid fragments were initially dissolved in standard TPR1-HSP70 FP buffer, neutralised to pH 7, then diluted to 50 mM. Fragments were then screened in an analogous way to our competition studies outlined in section 4.3.2.3. This involved a serial dilution with a starting fragment concentration of 25 mM. However importantly, neutralisation of fragments was crucial to prevent any denaturing of the protein and pH-induced artifacts in competition studies. Here sodium hydroxide was used to neutralise carboxylic acid fragments, although this resulted in a much higher ionic strength, in particular of sodium ions, than had previously been utilised in FP assay. With a dicarboxylic acid at 50 mM we approximated the sodium ion concentration to be around 100 mM, and obviously this led to concerns regarding how this would impact the TPR1-HSP70 peptide interaction. Therefore, to control for this increase in ionic strength a competition study using the unlabelled HSP70 peptide control with a serial dilution of 100 mM salt was trialled against previous conditions (Figure 61). This resulted in comparative IC_{50} values of 9.88 ± (0.47) μM and 8.22 ± (0.75) μM for higher salted vs unmodified. This was viewed as an acceptable change and given the consistent presence of higher sodium ion concentrations for all carboxylic acids screened, the screen proceeded using these parameters.

Model	Logistic
Equation	y = A2 + (A1-A2)/(1 + (x/x0)^p)
Plot	D
A1	0.02931 ± 5.84849E-5
A2	-0.02951 ± 0.0012
x0	8224.86592 ± 745.73516
p	1.44649 ± 0.11051
Reduced Chi-Sqr	0.7147
R-Square (COD)	0.99752
Adj. R-Square	0.9969

Model	Logistic
Equation	y = A2 + (A1-A2)/(1 + (x/x0)^p)
Plot	B
A1	0.03206 ± 6.32011E-4
A2	-0.03106 ± 3.43236E-4
x0	9882.23777 ± 474.49943
p	1.39483 ± 0.06773
Reduced Chi-Sqr	0.3808
R-Square (COD)	0.99897
Adj. R-Square	0.99872
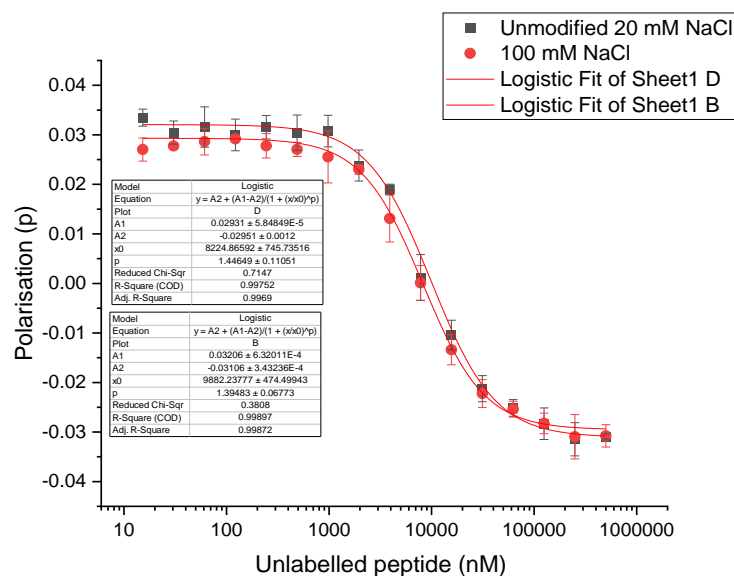
Figure 61: Ionic strength and sodium ion control run (red) vs unmodified buffer system (grey) for TPR1-HSP70 FP assay competition experiment.

Upon screening a range of di,tri and quadcarboxylic acids fragments it was clear that none of the fragments reached the end point of dissociation of the competition assay, in which tracer is effectively unbound and free in solution (Figure 62). This highlighted a major issue in the approach, as the logistic sigmoidal fit equation Equation 3 r_{max} required the end point of dissociation for values to be comparative across different plates. Therefore, to address this issue and provide a modelled endpoint for dissociation, an individual direct titration was carried out for every screened fragment. This resulted in a polarisation value for fully unbound tracer that could then be utilised to model the end point (r_{max}) during fitting and allow comparison between results. Figure 62 shows two fittings of a malonic acid fragment (A) without a modelled end point and (B) with a modelled end point. Clearly (B) incorporating the modelled end point results in a better fitting of data points. These different fittings resulted in a large difference in IC_{50} generated of 8.8 ± (0.66) mM vs 27.25 ± (0.72) mM respectively, however we believe (B) is the most appropriate way to utilise the data and also resulted in a smaller percentage error.
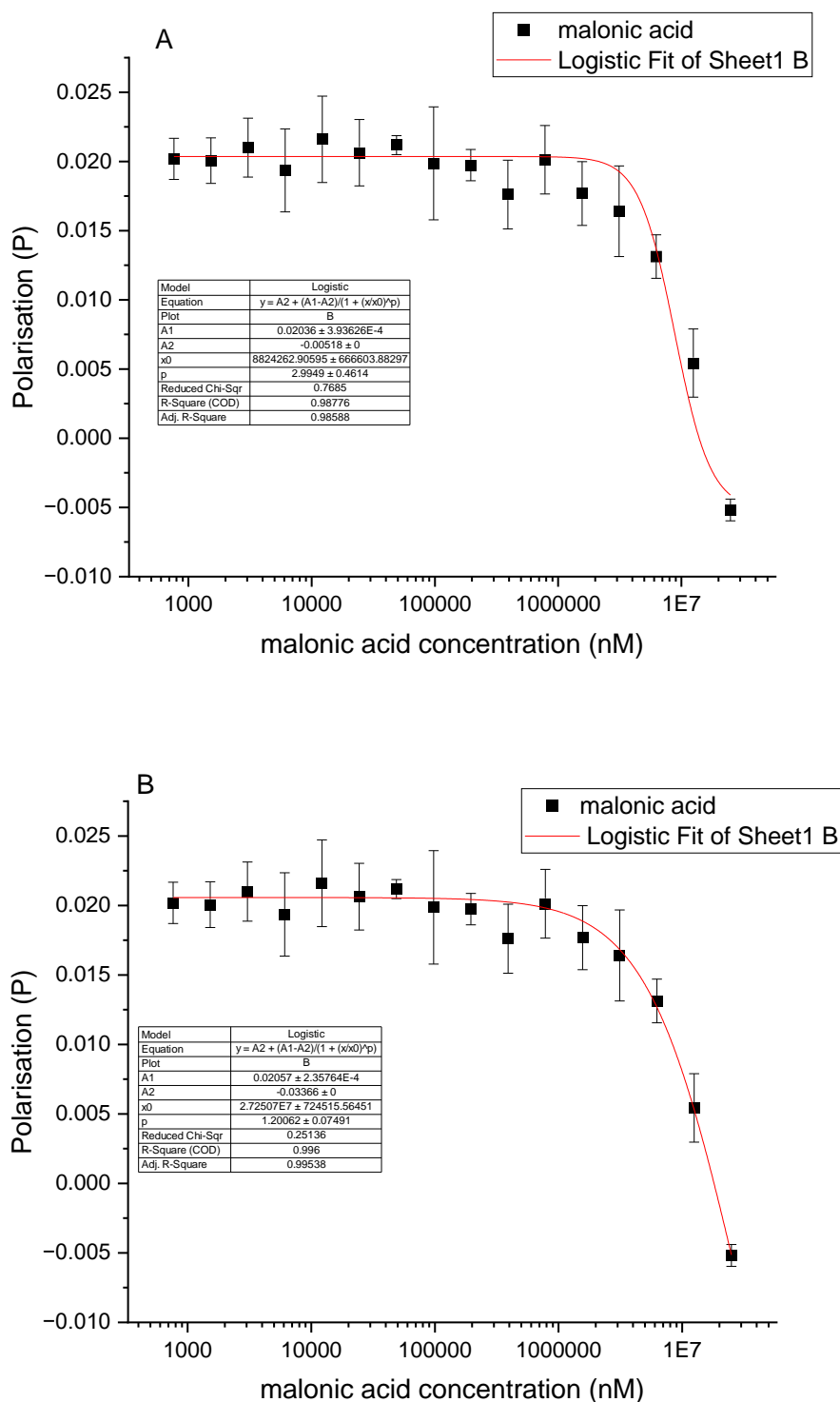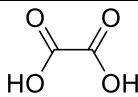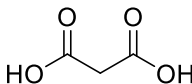
Figure 62: Competition fragment screening of malonic acid in our TPR1-HSP70 FP assay. (A) logistic fitting without a direct titration modelled endpoint vs (B) logistic fitting with a direct titration endpoint.
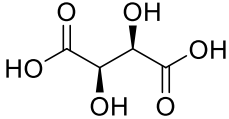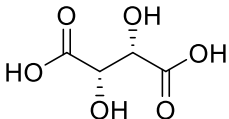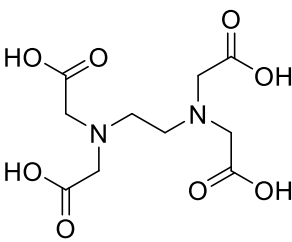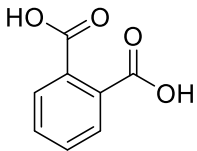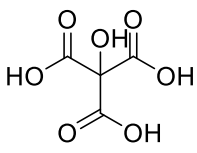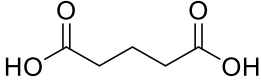
Results of the fragment screen are shown in Table 32, which details the carboxylic acid containing fragments screened and their associated IC_{50}s. Several interesting observations

were noted. Firstly, oxalic acid was the simplest fragment screened, resulting in an IC_{50} of 22.16 ± (0.71) mM. It is interesting to note that extension of the carbon chain whilst maintaining this simple diacid motif, such as malonic acid and pentanedioic acid resulted in increased IC_{50}s of 27.25 ± (0.72) mM and 53.62 ± (9.26) mM, respectively. This result suggests that the small oxalate motif may have potential and an interesting starting point to develop compounds with the ability to disrupt the TPR1-HSP70 PPI. Secondly, the introduction of alpha hydroxy groups to carboxylic acids in the cases of D-tartaric acid and L-tartaric acid also resulted in an increase in inhibitory activity compared to simple diacids like oxalic and malonic despite increasing chain length, with IC_{50} values calculated of 14.35 ± (0.44) mM and 17.65 ± (0.32) mM, respectively. The modest preference for R chirality of D-tartaric acid acids may be of interest in future SAR developments of this motif with selection of this enantiomer being beneficial, although further fragment screening is required to confirm this observation. Aligned with this observation is results using the conformationally constrained and relatively planar pthalic acid, which demonstrated no inhibitory activity, indicating that the mere presence of diacid is not sufficient for activity. Building on this observation, it would be interesting to trial *cis* & *trans*-butenedioic acid for a further exploration of competition with spatially constrained diacids.

EDTA was also trialled in the assay due to it being a readily available quadcarboxylic acid and it allowed experiments to assess whether increasing the number of carboxylic acid groups effected activity. However, results showed only a modest improvement over oxalic acid (IC_{50} = 19.27 ± (1.03) mM). Citric acid showed the best activity with an IC_{50} 11.63 ± (0.41) mM, which we believe is due to it being triacid and also containing the alpha hydroxyl group that tartaric acid fragments had indicated increased activity. Together, this small fragment screen has provided some interesting results to be taken forward in the development of early SAR relating to carboxylic acids. However, more compounds are required to generate a better understanding of the specific binding motif of the TPR1 pocket.

Table 32: Carboxylic acid fragment screen by TPR1-HSP70 FP competition assay with structures and calculated IC_{50} values of fragments. Error n = 3 technical repeats.

Fragment name	Fragment structure	IC_{50} (mM)
Oxalic Acid		22.16 ± 0.71
Malonic acid		27.25 ± 0.72

D-tartaric acid		14.35 ± 0.44
L-tartaric acid		17.65 ± 0.32
EDTA		19.27 ± 1.03
Pthalic acid		No competition observed
Citric acid		11.63 ± 0.41
Pentanedioic acid		53.62 ± 9.26

In a similar approach as above, a range of tetrazole containing fragments were also assessed. Unfortunately and a little surprisingly, no tetrazole compound demonstrated any activity in our fragment screen (Table 33 & Figure 63). Although it must be noted that only 3 fragments were used and screening of more fragments is required to confirm this lack of activity.
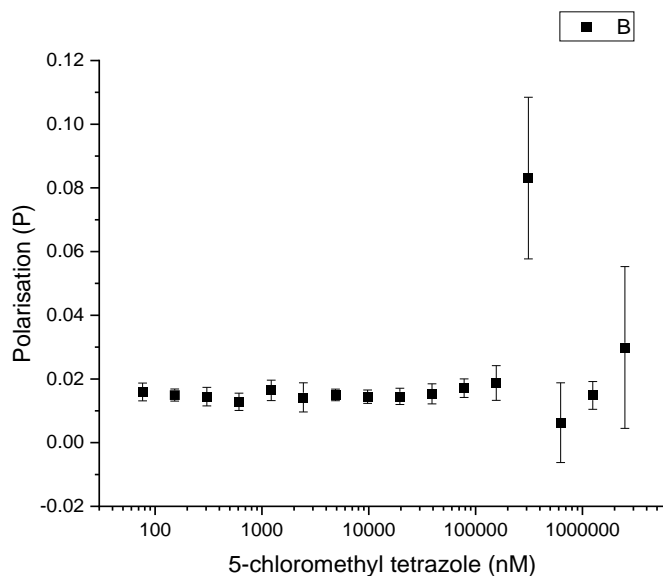
Figure 63: Fragment screening FP competition study of 5-chloromethyl tetrazole against TPR1-HSP70 interaction. This fragment showed no activity in disrupting TPR1-HSP70 binding. Error bars N = 3 technical repeats.

Table 33: Name and structure of tetrazole fragments screened in TPR1-HSP70 FP competition assay. All tetrazole fragments trialled failed to demonstrate any activity. N = 3 technical repeats

Name	Structure
2-(tetrazol-5-yl) phenyl boronic acid	
5-chloromethyl tetrazole	
5-amino tetrazole	

5.3   Creation of a peptide SAR library for future peptidomimetic compound development

Given the challenges faced thus far with development of small molecule inhibitors targeting the HOP TPR domains, we focussed on exploring peptide SAR of the TPR1-HSP70 interaction. Peptide SAR work could then be utilised as a platform towards the future generation of peptidomimetic compounds. Peptidomimetic compounds generally contain a pharmacophore that mimics the natural peptide but have been iteratively altered to generate

a compound with increased biological stability, target selectivity and bioavailability for utilisation as a therapeutic. Numerous peptidomimetic compounds have been trialled in the clinic, and the success of this approach is highlighted by Indinavir, a protease inhibitor used as a component of highly active antiretroviral therapy to treat HIV/AIDS (Lenci and Trabocchi, 2020).

The pipeline for early peptidomimetic drug discovery follows a generalised workflow of developing SAR from an identified biologically active peptide which binds the target protein of choice. Initial SAR begins with simple peptide truncation to identify the shortest, most active substrate. This is then followed by alanine-scanning mutation studies to identify the key residues of interaction and suitable sites for modification. Finally, modification of substituent groups is used to improve binding and pharmacokinetic properties, generating a lead molecule.

Initial studies for peptide SAR of the TPR1-HSP70 was based on previous work by Scheufler *et al.* which identified the shortest and most active HSP70 peptide which could bind the TPR1 domain within HOP (Scheufler et al., 2000). This was further coupled with results by Brinker *et al.* who screened combinatorial peptide libraries against TPR1-HSP70 as a starting point of peptide SAR work (Brinker et al., 2002). However, this work failed to identify tryptophan containing peptides, which have recently been demonstrated to improve the binding of HSP70 and HSP90 truncated peptides to the TPR-containing co-chaperone, CHIP (Ravalin et al., 2019). Therefore, based upon the combinatorial approach giving limited SAR specificity and the lack of validation of tryptophan containing peptides, we decided to individually synthesise and test natural amino acid substitutions of HSP70 peptides, for their ability to inhibit binding of the TPR1-HSP70 in our FP competition assay. A further aim was to complement this approach with *in-silico* docking of HSP70 peptides into the TPR1 domain (1ELR PDB) using the Schrodinger Glide docking software as a further guide for SAR development. Glide docking software is a software package used to simulate the interaction of ligands into proteins via modelled intermolecular interactions and is employed in *in-silico* drug discovery. From these modelled intermolecular interactions between ligands and receptor, it generates a glide score to rank energetic favourability of interaction. However, despite several rounds of protein and ligand preparation with increasing number of conformational and bond constraints, no docking results provided a suitable correlation with the 1ELR peptide binding structure. This meant no effective baseline of native peptide binding could be modelled. Thus alteration of ligand peptide sequence and subsequent docking would not be informative for SAR development, so disappointingly this worked was discontinued.

5.3.1 Solid phase peptide synthesis based off HSP70 C-terminus

To develop peptide SAR, a range of desired peptides were first synthesised. This synthetic approach utilised solid phase peptide synthesis with aspartic acid conjugated chlorotrityl resins. Chlorotrityl resins were chosen as this would produce a final product with both unprotected carboxylic acid groups associated with the terminal aspartic residue. This is key as it produces a peptide which is analogous to the natural final amino acid of the HSP70 C-terminus being modelled. Importantly, this residue interaction is critical to the carboxylic clamp activity of TPR-HSP interactions (Vaaltyn et al., 2022). Figure 64 gives an overview of the processing of peptides from synthesis to testing in the TPR1-HSP70 FP competition assay.
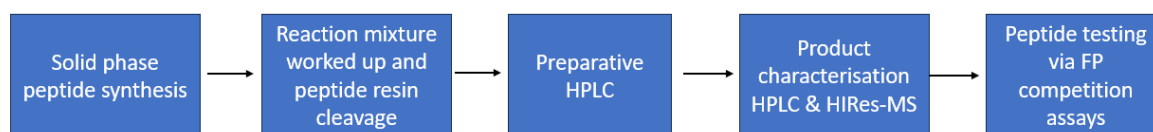
Figure 64: A generalised flow through of peptide SAR library synthesis, purification, characterisation, and testing.

To summarise, peptide reaction mixtures were washed, the peptides were cleaved from the resins and reaction mixture were "worked up" to generate a crude product. Freeze dried crude products were then purified by preparative HPLC. Isolated peptides were then freeze dried and characterised for purity via analytical HPLC and high-resolution mass spectrometry to confirm product identity. Each peptide was then assessed for activity in TPR1-HSP70 competition FP assays. Our externally purchased unlabelled GSGPTIEEVD HSP70 peptide from section 4.3.2.3, was used as a positive control (Figure 65). The IC_{50} generated from each synthesised peptide was then relativised to our purchased control native peptide which matched tracer amino acid sequence to reduce cross plate variability.
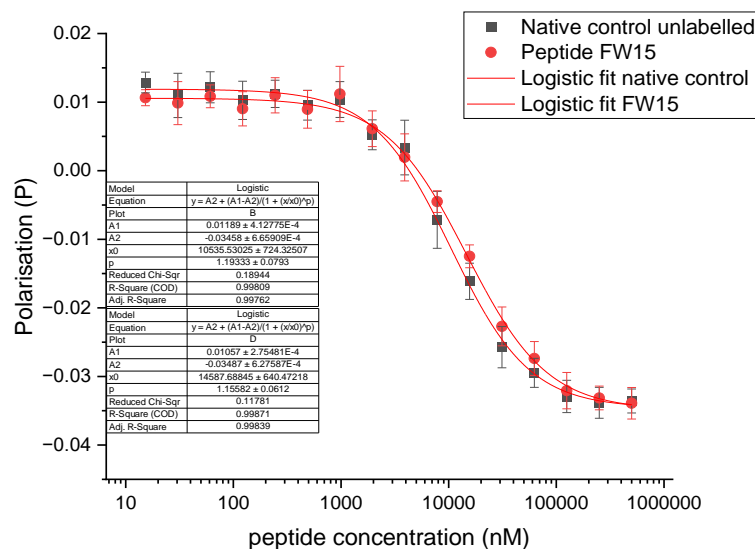
Figure 65: TPR1-HSP70 FP competition assay of native control peptide grey and synthesised peptide FW15 outcompeting HSP70 tracer peptide. Polarisation values plotted and logistic fit employed to generate IC_{50} value. Relative IC_{50} to native control peptide for FW15 was 1.38 indicating weaker inhibition of TPR1-HSP70 PPI. Error bars represent n = 3 technical repeats

Table 34 details the peptide sequences synthesised to explore peptide SAR and the relativised IC_{50} of these peptides to our purchased control peptide. Notably, high resolution mass spectrometry to confirm peptide identity is included, alongside a theoretical mass. An error of 5 ppm in high resolution mass spectrometry is the standard cutoff for structure determination, correlating to an error of 0.05 daltons in a 1000 dalton compound (Gross, 1994). All peptides synthesised and presented with high resolution mass spectrometry data in Table 34, fall within these guidelines compared to their theoretical mass, highlighting successful synthesis of desired products. However, some peptides, such as FW8 and FW18, failed to produce any solid purified product, instead a gel was produced probably as a result of coelution of DMSO with the peptide post preparative HPLC, this prevented their use due to the difficulties of effective concentration determination.

Table 34: This table details aspects of peptide synthesis, characterisation of peptides and IC_{50} from TPR1-HSP70 FP competition studies that were relativised to purchased unlabelled HSP70 peptide GSGPTIEEVD which was ran concurrently with each sample.

Lab code	Sequence	Crude product isolated	Purity	IC_{50} relative to purchased unlabelled	Theoretical mass	HiRes mass
FW1	GSGPTIEEVD	Y	95	1.15	1003.4578	1003.4608
FW2	PTIEEVD	Y	99	1.16	802.3829	802.3858
FW3	ATIEEVD	Y	98	1.47	776.3672	776.3685
FW4	PAIEEVD	Y	95	2.01	772.3724	772.3723
FW5	PTIEAVD	Y	96	1.71	744.3774	744.3776
FW6	PTIAEVD	Y	94	1.84	744.3774	744.3777
FW7	PTIEQVD	Y	82	FP Interference	801.3989	801.3989
FW8	PTIEKVD	Y	85	Solid not obtained	-	-
FW9	PTIEDVD	Y	90	1.19	788.3672	788.3666
FW10	PTIEEID	Y	96	2.64	816.3985	816.3988
FW11	PSIEEVD	Y	93	1.76	788.3672	788.3681
FW12	PTIEELD	Y	97	3.82	816.3985	816.3988
FW13	PTVEEVD	N	-	-	-	-
FW14	PTLEEVD	N	-	-	-	-
FW15	Ac-PTIEEVD	Y	92	1.38	844.3935	844.3932
FW16	PTLWWPD	N	-	-	-	-
FW17	LWWPD	Y	95	FP interference	716.3402	716.3401
FW18	PTIEWVD	Yes	-	Solid not obtained	-	-
FW19	YYILDVD	Y	83	0.72	900.4349	900.4359
FW20	WWWLDVD	Y	86	0.56	1019.4621	1019.4625
FW21	YWWLDVD	Y	95	0.95	996.4462	996.4462
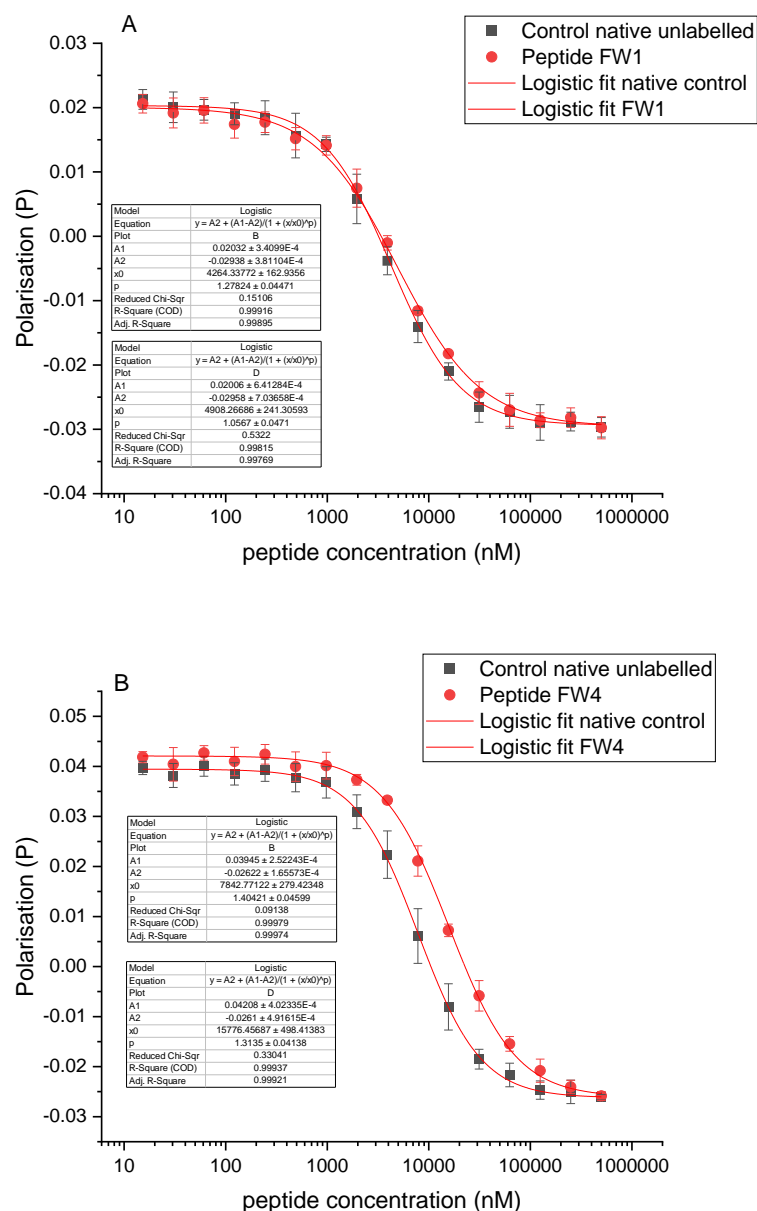
Figure 66: TPR1-HSP70 FP competition assay of control peptide grey and synthesised peptide (A) FW1 & (B) FW4 with associated logistic fits generating IC$_{50}$ data. FW1 IC$_{50}$ much closer to value to FW 4 as demonstrated by overlap to control peptide. Error bars represent n = 3 technical repeats

Each peptide was then assessed for activity in TPR1-HSP70 competition FP assays to generate an appropriate IC$_{50}$ value (Table 34). Importantly, validation that the synthesised peptides were functioning correctly was confirmed by analysing peptide FW1. This peptide has the identical sequence to the purchased control peptide and a relative IC$_{50}$ was achieved close to 1, suggesting the synthesised approach was valid (Figure 66 A). Furthermore, peptide FW2 is the shortest natural HSP70 peptide that Scheufler *et al.* demonstrated

maintained a good binding affinity for the TPR domain (Scheufler et al., 2000). Again, results from the FP assay correlate closely showing a similar relativised IC_{50} to FW1.

Following on from these initial results, FW2 was prioritised as the smallest truncated peptide for further SAR development. However, the C-terminal Aspartic acid was left unmodified as this has previously been shown to be essential for binding to the TPR domain (Brinker et al., 2002). Firstly, peptides FW3-FW6 were generated consisting of single alanine mutations. Results showed that replacement of the threonine residue in FW4 resulted in the most deleterious effect on competition with a doubling of the IC_{50} value (Figure 66 B). Interestingly, replacement of either glutamic acid residue in peptides FW5 and FW6, resulted in a similar IC_{50} reduction suggesting neither plays a more dominant role than the other in TPR domain binding.

Next, peptides were synthesised which contained single point mutations incorporating non-alanine amino acids. FW7 was first utilised to determine how deleterious the introduction of a positive charge would be to TPR binding. Unfortunately, the final product was contaminated with an unidentified coloured contaminant, which prevented a FP competition curve from being generated. Other peptide SAR however provided important information, for example replacement of valine with other alkyl chains in FW10 and FW12 resulted in the largest reduction in IC_{50} values, of nearly 4 fold, for any modification. This emphasised that valine was critical for peptide binding to the TPR domain. Two further peptides gave rather surprising results in their loss of activity. Replacement of threonine with a chemically similar serine residue in peptide FW11, resulted in a 75% decrease in the IC_{50} value. In addition, peptide FW15 which contained an acetylated terminal amine, to investigate if removal of this exposed polar amine improved binding, also resulted in a 40% reduction in activity. Moreover, the previously published combinatorial screen suggested that peptide FW19 would be more active than the natural sequence (Brinker et al., 2002). Results indeed confirmed this theory, with a 20% reduction in relative IC_{50} demonstrated. However, most notable, was analysis of peptides incorporating tryptophan residues, FW20 and FW21, which resulted in the most improvement in IC_{50} values, of nearly a 50% reduction (Table 34). This suggested that a tryptophan/indole motif should be further explored in any future peptidomimetic compound.

Taken together this preliminary exploration of peptide SAR demonstrates that bulky N-terminus aromatic substituents enhanced binding, with relatively few other modifications being tolerated. Development of future SAR should therefore include synthetic amino acids to mimic these groups. Alongside this replacement of segments of peptide backbone to

reduce the peptidic nature of molecule and towards a more drug like biologically stable structure should also be attempted. In addition, modifications such as peptide stapling which chemically constraint peptides to reduce entropic change upon binding should also be explored to maximise binding efficiency.

5.3.2   Assessment of tracer peptide delivery into mammalian cells

As outlined in chapters 1 and 3, the molecular chaperones HSP70/HSP90 and the co-chaperone HOP, have important roles in enhancing KSHV lytic replication. Therefore, the overall aim of this thesis was to demonstrate that specific disruption of the HOP-HSP70 or HOP-HSP90 PPIs would inhibit KSHV lytic replication, validating them as suitable therapeutic targets going forward. Unfortunately, no appropriate small molecular inhibitors targeting the HOP-HSP interaction were identified. In contrast, the peptide SAR experiments highlighted the potential of a peptidomimetic compound approach to inhibit KSHV lytic replication. However, therapeutic peptides have two intrinsic drawbacks, namely poor cell membrane permeability and poor *in vivo* stability, which represent major stumbling blocks for peptide drug development. Therefore, we wished to investigate whether it was possible to efficiently deliver peptides into KSHV-infected cells and if so, did they have any efficacy in preventing KSHV lytic replication. To address these questions, preliminary experiments were performed to assess whether the tracer peptides used in the FP assays could be efficiently delivered into human cells. The tracer peptides were used as they were already conjugated with a fluorescein fluorophore, which allowed direct visualisation using fluorescent confocal microscopy. Moreover, the anionic nature and molecular weight of peptides meant they could be bound by cationic lipid nanoparticle carriers, such as lipofectamine, to enhance transfection efficiency into human cells. Therefore, HEK 293T cells were transfected with either HSP70 and HSP90 tracer peptides incubated with lipofectamine 2000. After 24 hours cells were fixed, stained with the nuclear marker DAPI and tracer peptide fluorescent directly visualised. Figure 67 shows that HSP90 and HSP70 tracer peptides can be delivered into HEK 293T cells. Further work is now required to determine this exact location within cells where the peptides are accumulating using co-localisation studies with distinct subcellular and organelle markers. In addition, key experiments need to be performed in KSHV latent and lytically replicating cells to determine whether peptides can gain entry to the nucleus and more specifically localise to the vRTCs, as importantly HOP and HSP70 are both redistributed into vRTCs during lytic replication. Aligned with vRTC targeting, a key experiment will be to assess the ability of these peptides to inhibit the TPR-HSP PPIs in KSHV-infected cells.
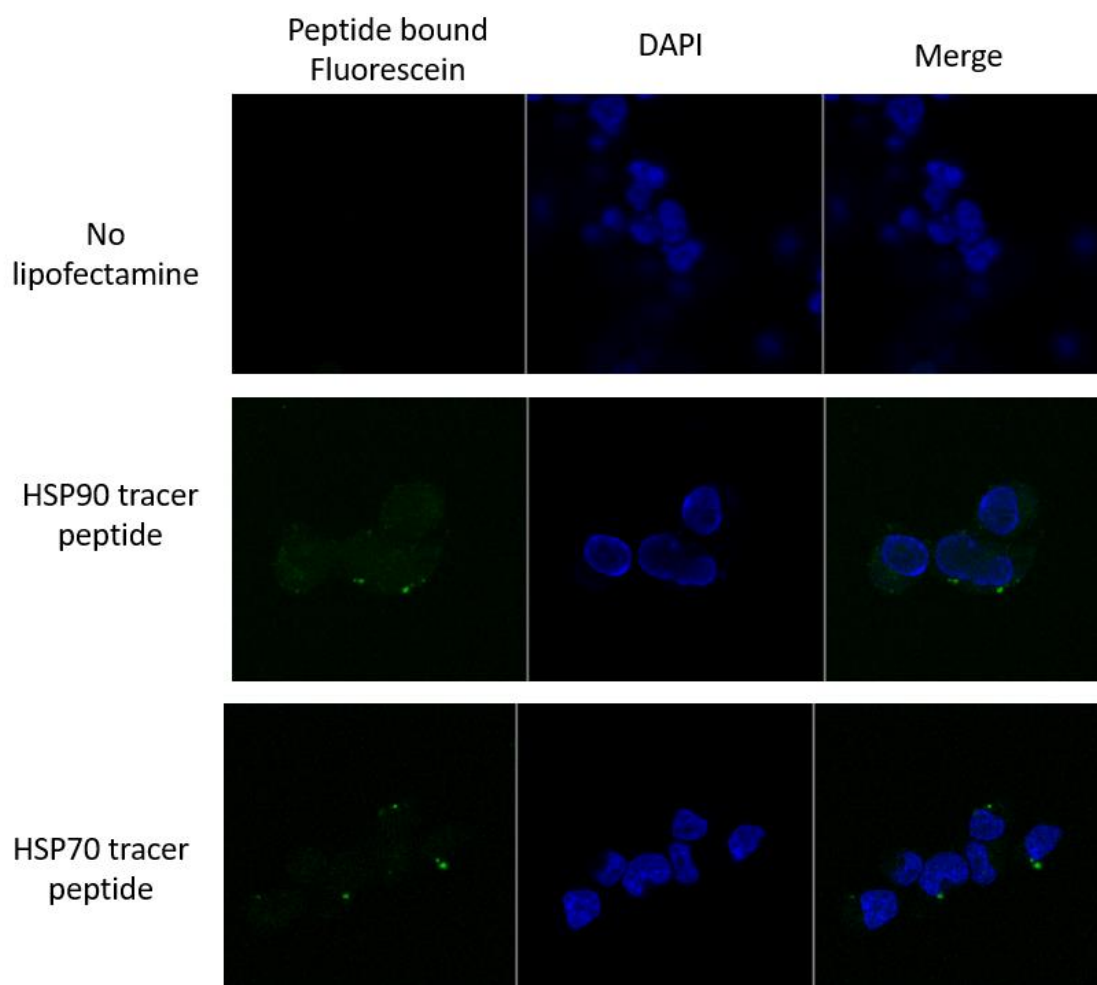
Figure 67: Confocal microscopy of HEK293T cells treated with lipofectamine and HSP70/90 fluorescein labelled C-terminus peptide showing uptake of peptide into cells. Cells additionally stained with nuclear marker DAPI.

5.4   Discussion

This chapter details alternative approaches towards the development of inhibitors of TPR1-HSP70 PPI using a variety of methodologies. Unfortunately, chapter 4 detailed the unsuccessful attempts to identify a selective high affinity small molecule from the MCCB library prioritised by *in-silico* screening approaches. This chapter extends the MCCB screen but focusses on carboxylic acid and bio-isostere containing compounds. These compounds were prioritised due to previous work reporting that they had some, albeit weak activity, in the inhibition of the TPR2A-HSP90 PPI (Darby et al., 2020; Vaaltyn et al., 2022). However, results herein failed to identify any activity against the TPR1-HSP70 interaction. Screening was therefore extended to use a fragment-based approach containing carboxylic acid and tetrazole functional groups. Results from this screen provided some interesting preliminary results to be taken forward in the development of early SAR relating to carboxylic acids in relation to TPR1-HSP70 interaction. Expanded fragment screening of this functional group is now required however before firm conclusions can be drawn. Results highlighted no

inhibitory activity of the tetrazole functional group, this was rather surprising given its bio-isosteric nature to carboxylic acid. Although, a further extended screen of tetrazole fragments would be required before this can be definitively proven for TPR1. We believe that further development of this fragment screen approach of carboxylic acids and other bio-isosteres may be of use in future inhibitor development and may also aid in rational design in peptide SAR development. Screening of alternative carboxylic acid bio-isosteres would be of particular interest due to pharmacokinetic challenges associated with the carboxylic acid group.

Finally, a peptide SAR approach was utilsed, in an attempt to improve on the binding affinity of the natural amino acid peptide, as the first stage in the development of a peptidomimetic compound. Results showed an improvement of IC_{50} value generated, particularly upon the addition of tryptophan residues. This work could be continued beginning with the introduction of synthetic amino acids and conformational constraint of peptides following the pipeline outline by Lenci and Trabocchi (Lenci and Trabocchi, 2020). This could hopefully progress towards the development of peptidomimetic compound. However, barriers still need to be overcome to address issues of efficient delivery into mammalian cells and the correct nuclear localisation of any peptide-based approach. Although delivery of the tracer peptide was observed in some cells, its localisation and stability needs to be confirmed. Interestingly the online prediction tool protparam (Expasy) gives vastly different half lives in mammalian cells of the HSP70 and HSP90 peptides used of 30 hours and 1.1 hours, respectively. This highlights a key point that fluorescence signal detected in cells may not truly represent full peptide conjugated to tracer but tracer only with peptide having been metabolised. Again further experiments will need to be performed to test any *in vivo* stability.

Chapter 5

~

Discussion

6   Discussion

The role of molecular chaperones across a wide swathe of pathologies is well documented, especially in viral infection (Rosenzweig et al., 2019; Aviner and Frydman, 2020; Li and Luo, 2023). KSHV, like many other viruses, utilise the host cell heat shock protein (HSP) machinery to alter the cellular microenvironment, enhancing both its latent and lytic replication cycles. This is highlighted by work showing HSP70 is crucial for the recruitment RNA polymerase II to viral DNA promoters, whereas HSP90 and the viral protein vFLIP combine to inactivate the IKK complex, allowing NF-kB transcription factor activation which is essential for KSHV infection (further outlined in section 1.2.1.3) (Field et al., 2003; Baquero-Pérez and Whitehouse, 2015). Therefore, modulating HSPs activity may be a suitable antiviral therapeutic strategy in certain contexts. This is supported by observations, where inhibiting the direct ATPase site of HSP70 and HSP90, using VER-155008 and geldanamycin, result in effective inhibition of the KSHV lytic replication cycle. Unfortunately however, utilisation of these HSP specific ATPase inhibitors is not a clinically viable approach, as redundancy in the HSP network exists and toxic side effects have been observed in several clinical trials (Zuehlke et al., 2018; Li and Luo, 2023). Thus, alternative approaches to modulating the HSP70 and HSP90 system via small molecules is an active area of research for pharmaceutical development.

An alternative approach to modulating protein function is using small molecule-mediated inhibition of PPIs. This approach has been validated by examples such as the clinically approved Venetoclax, a PPI inhibitor which disrupts interactions between the anti-apoptotic B-cell lymphoma-2 (Bcl-2) protein and pro-apoptotic proteins, such as BAK and BAX, leading to programmed cell death of chronic lymphocytic leukemia cells (Ran and Gestwicki, 2018). Both HSP70 and HSP90 interact with the co-chaperone HOP which facilitates the transfer of client proteins from HSP70 to HSP90. Studies specifically investigating the role of HOP have implicated it in the development of cancer and neurodegeneration (Zhai et al., 2018; Bhattacharya and Picard, 2021). However, surprisingly, no previous studies have investigated the role of HOP in virus infection. Hence this research project aimed to investigate the role of HOP in the context of KSHV lytic replication and to develop small molecule inhibitors of HOP-HSP PPIs, as a potential novel antiviral approach.

6.1   KSHV lytic replication effects HOP abundance and distribution

In chapter 3 we investigated whether HOP had any role in enhancing KSHV lytic replication. Interestingly, results showed that induction of the KSHV lytic replication resulted in an upregulation of HOP mRNA expression in two KSHV-infected cell lines; BCBL-1 TREx-RTA and Clone 9 cells. This increase in expression was also observed at protein level in clone 9

cells, in contrast to BCBL-1 TREx-RTA cells. The increase in HOP expression occurs despite KSHV eliciting a wide host cell shutoff mechanism during lytic replication, which reduces the expression of many cellular genes as the lytic replication cycle proceeds. Viruses strategically exploit various cellular mechanisms to downregulate host gene expression for their own benefit. To inhibit host gene expression, KSHV encodes the shutoff and exonuclease (SOX) protein (KSHV ORF37) (Glaunsinger and Ganem, 2004), increasing the rate of cytoplasmic mRNA degradation. SOX causes host shutoff in combination with the cellular 5'-3' exonuclease, Xrn1 (PACMAN), resulting in cytoplasmic transcript degradation (Covarrubias et al., 2011). It is hypothesised that SOX internally cleaves target transcripts in at specific degenerate sequence motifs. Then Xrn1 binds to SOX cleavage sites and completes degradation (Gaglia et al., 2015; Mendez et al., 2018). How HOP overcomes SOX-mediated degradation is currently unknown. However, recent findings have shown that host cell resistant RNAs, such as the transcript encoding interleukin-6 (IL-6), escape SOX-induced cleavage through a 3' UTR RNA regulatory element that overrides the SOX targeting mechanism (Muller and Glaunsinger, 2017). It will be of interest to determine if a similar 3' UTR element also functions in the HOP transcript.

However, although the mechanism by which HOP expression is maintained during KSHV infection is unknown at present, it does indicate that HOP may be important in enhancing KSHV lytic replication. This is further supported by the redistribution of HOP to the nucleus during KSHV lytic replication, with a proportion of HOP residing in vRTCs. Similar results have been observed for its binding partner, HSP70 (Baquero-Pérez and Whitehouse, 2015). HSP90 was also shown to be abundant within both the nucleus and cytoplasm during KSHV infection (Chen et al., 2012). HOP and HSP70 are recruited relatively early, by 24 hours, post reactivation into vRTCs and the previous use of HSP70 inhibitors which prevent vRTC formation, suggest that have an important role in the assembly and activation of pre-initiation complexes on the origin of viral DNA replication. Similar results have been seen in other viruses such as human papillomavirus-11 and Herpes simplex virus 1 (Liu et al., 1998; Le Gac and Boehmer, 2002; Lin et al., 2002). Furthermore, HSP70 may have a potential role in KSHV capsid assembly, having been identified within the mature virion (Bechtel et al., 2005). Therefore, key future aims would be to determine the exact client proteins that are preferentially chaperoned by HOP and HSP70 in vRTCs. Moreover, how HOP is specifically redistributed to the nucleus and targeted to vRTCs is unknown. Interestingly, mouse studies have demonstrated that localisation of a HOP ortholog was controlled by phosphorylation of serine 189 and Threonine 198 residues, with phosphorylation promoting a nuclear or cytoplasmic distribution, respectively (Longshaw et al., 2005).

Knockdown studies of HOP have demonstrated that HOP has a key role in the ability of KSHV to undergo its lytic replication cycle, with an observed dramatic reduction in the production of viral mRNA, proteins, viral DNA and infectious virions. As mentioned above the exact role of HOP/HSP70 is yet to be determined, potentially having a role in viral genome replication and capsid assembly. However, considering the localisation of HOP-HSP70 during KSHV lytic replication and the impact of HOP knockdown in the context of KSHV it is particularly fascinating to consider an alternative model. Recent work has demonstrated that HOP appears to promote degradation via the proteosome, rather than refolding as initially expected (Bhattacharya et al., 2020). Furthermore, in HOP knockdown cells a HSP70-HSP90 complex independent of HOP formed, which was found to promote folding more efficiently than the canonical HOP dependent system. These results could indicate that the role of HOP in KSHV lytic replication is not in promoting the folding of proteins, but instead causing the degradation of specific clients via the proteasome. KSHV has been demonstrated to utilise the proteasome heavily during its replication cycle, altering the cellular environment to suit its requirements and it would be interesting to have a better mechanistic understanding of the specific role of HOP during KSHV lytic replication and whether there is a link between HOP and the proteasome (Ashizawa et al., 2012). However, although mechanistic details have not been fully elucidated, results clearly show in chapter 3 that HOP is critical to KSHV lytic replication. Therefore, these results support the pharmaceutically targeting HOP as a valuable endeavour, both in relation to KSHV lytic replication and across a wider range of other pathologies.

6.2   Targeting of HOP and screening of the MCCB library

The approach throughout this body of work was to inhibit the functionality of HOP, through preventing its interactions with HSP70 and HSP90, via its TPR1 and TPR2A domains. In chapter 3, our initial cellular screening of *in-silico* predicted inhibitors of the TPR2A-HSP90 interaction showed two compounds that demonstrated some antiviral activity. However, further testing of these compounds in our TPR2A-HSP90 FP assay failed to demonstrate any specific activity. These compounds do feature in patent literature however, specifically relating to calcium ion channel inhibition and this may be responsible for the phenotypic response (Qingwei et al., 2011). This is of interest as intracellular calcium (Ca^{2+}) transport is involved in inducing lytic replication (Zoeteweij et al., 2001). Moreover, recent work in the Whitehouse laboratory have shown that an extracellular source of Ca^{2+} is required for KSHV lytic replication and Mibefradil, a specific inhibitor of T-type voltage-gated Ca^{2+} channels, dramatically reduced the levels of KSHV lytic replication (Whitehouse personal communication). Therefore, to confirm a potential role of C2 and D2 compounds in calcium mobilisation, experiments to measure Ca^{2+} influx into TREx BCBL1-RTA cells during KSHV

lytic replication could be performed using the ratiometric Ca^{2+} dye Fura-Red. Although this low-throughput screen may have stumbled on an interesting link to calcium channels, this cellular screening approach was not a suitable way of screening compounds effectively due to the low throughput nature and it also failed to effectively demonstrate direct inhibition of the PPI. Due to these caveats, a focus of Chapter 4 was to develop a HTS FP assay, to directly assess the inhibition of HOP TPR-HSP interactions.

In chapter 4 the development, validation, and utilisation of two HTS FP assays allowed for effective HTS screening of the PPIs. These assays could provide useful tools for future studies of the HOP TPR-HSP interaction and the development of inhibitors. In addition, our protein expression systems generated high yields of protein that could be utilised for a wider variety of techniques. Of particular interest was the importance of tracer design in our TPR1-HSP70 FP assay. The introduction of PEG2 linker resulted in an approximately 40% stronger binding compared to the unlinked variant, indicating the deleterious contribution of the fluorophore to binding in our short peptide variant. The importance to properly control for this during assay development is essential to prevent assay artifacts or invalidate entire screens.

A further optimisation for our FP assays could be to incorporate far-red fluorophores. These have been demonstrated to reduce false positives associated with compound fluorescence, a clear problem encountered in HTS screening of the MCCB library (Banks P et al., 2000). Unfortunately, HTS screening of the MCCB library guided by an *in-silico* screen failed to generate any hit compounds for either TPR1-HSP70 or TPR2A-HSP90 FP assays. However, the challenging nature of targeting HOP TPR domains is abundant in the literature, with two large unbiased small molecule HTS screens also failing to identify an effective hit compound for the TPR2A-HSP90 interaction (Yi and Regan, 2008; Darby et al., 2020). As such, in chapter 5 work was undertaken to perform a functional group screen of the MCCB library in our TPR1-HSP70 FP assay, which again unfortunately failed to generate any hit compounds. We had hoped that by selecting for functional groups that had demonstrated previous activity in the literature for the TPR2A-HSP90 PPI, this would maximise the likelihood of finding a hit compound.

6.3   Fragment screening and Peptide SAR development

In chapter 5, two alternative approaches were utilised to begin exploring potential SAR of the TPR1-HSP70 interaction. Firstly, the fragment screening approach was based upon previously published findings that demonstrated inhibitory activity of dicarboxylic acids and tetrazole fragments against the TPR2A-HSP90 interaction. These fragments disrupted the five amino acid carboxylic clamp of TPR domains that is key for HSP binding via the terminal

aspartic acid (Brinker et al., 2002). Interestingly, results highlighted that only the carboxylic acid fragments demonstrated any potential activity, with tetrazoles failing to demonstrate any competition in the FP assay. It should be noted however, our tetrazole testing used comparatively few compounds, due to the lack of availability of tetrazole containing molecules for screening in the MCCB library. Notably however, the inhibitory activity demonstrated by carboxylic acid fragments began to give rise to some early SAR, although screening of more fragments will be required before any overall conclusions can be elucidated. The presence of an α-hydroxyl group between the two carboxylic acids in fragments resulted in the best activity suggesting this may provide a useful motif to build upon. However, the trade-off with the introduction of the polar hydroxyl group could present pharmacokinetic challenges with cell permeability at later stages of any potential inhibitor development. Interestingly the constrained planar phthalic acid despite containing the dicarboxylic acid motif demonstrated no activity. This we believe demonstrates some conformation motility is required for activity.

Secondly, the peptide SAR approach gave an early insight into the activity of natural amino acid peptides which may have the potential to disrupt the TPR1-HSP70 interaction. Notably, the tryptophan containing peptide developed herein demonstrated the best activity and improved on the previous literature example (Brinker et al., 2002). Tryptophan contains an α-amino group, an α-carboxylic acid group, and a side chain indole, making it a polar molecule with a non-polar aromatic beta carbon substituent. It is interesting to note that the indole group is also present in the best TPR2A inhibitor previously developed (Darby et al., 2020). An exploration of this indole activity with other heteroaromatics may provide a useful point of future inhibitor development. Together, these results support further development and optimisation of the peptide SAR, which may provide the opportunity for the development of peptidomimetic compounds in the future. The optimisation of TPR1-HSP70 peptide inhibitory activity, could include the incorporation of synthetic amino acids and conformationally constrained peptides. The use of synthetic amino acids gives potential to explore areas of chemical space that natural amino acids cannot access and additional improvements in metabolic stability. The advantage of conformationally constraining peptides is twofold, firstly in reducing the entropic loss during peptide binding events resulting in higher affinity binding and secondly increasing the metabolic stability of the peptide (Bozovičar and Bratkovič, 2021). However careful consideration of conformational restriction is required to prevent losses in activity due to the reduction of peptide-target interactions. In addition, future work will also be needed in a cellular context, to explore the best delivery system by comparing lipofectamine transfections with other delivery systems such as cell penetrating tags (Horibe

et al., 2011). Furthermore, nuclear targeting of the peptides will need to be demonstrated due to the redistribution of HOP and HSP70 into vRTCs during KSHV lytic replication.

6.4   Future perspectives and final conclusions

This study has presented data that demonstrates the critical role of HOP in the KSHV lytic replication cycle. However, the exact mechanism of action of HOP has not been fully elucidated. Several experiments, detailed below, would be particularly interesting in respect to developing a better understanding of the intricacies of the role of HOP leading to future pharmaceutical targeting. From a pharmaceutical perspective the development of knock out and over-expression HOP truncation mutants, comprising specific TPR and DP domains, in KSHV-infected cell lines could provide valuable insight. This could provide a better understanding of which domains are key for KSHV lytic replication, versus those that are possibly redundant. Results would be particularly useful for target validation.

The elucidation of the specific client proteins that HOP is mediating the transfer between HSP70 and HSP90 during lytic reactivation would be particularly interesting to investigate further. Mass spectrometry-based proteomic approaches-coupled with quantitative tandem mass tagging approaches using a HOP overexpression cell line could give insight into specific virally-encoded and cellular client proteins. This could provide opportunities for targeting of these specific clients based on their biological relevance. Furthermore, from a fundamental molecular biology perspective developing a better understanding of the role of HOP in relation to client proteins during KSHV lytic replication would be of interest. In particular, a key question to address is whether KSHV's requirement for HOP is linked to client proteins access to the HSP network or alternative to enhance for proteasomal degradation via the HSP70-HSP90 axis.

Finally, the development of small molecule inhibitors of the HOP TPR domains has proved challenging for both ourselves and others. However, the ability to selectively modulate the HSP70-HSP90 chaperone system holds great promise for a wide range of pathologies. Further fragment screening to identify novel active functional groups alongside expanding existing understanding of fragment SAR could be useful. In addition, utilisation of alternative methods for the development of inhibitors of HOP-HSP interactions could involve the use of affimer screening, which has been applied to challenging targets, such as "the previously undruggable" RAS protein (Haza et al., 2021). Affimers allow rapid isolation of reagents capable of blocking PPIs, based on a constant small 91 residue scaffold protein containing two randomised nine residue variable regions for molecular recognition. Phage display screening then isolates reagents that readily target PPIs with high specificity. A longer term

objective would be to co-crystallise the Affimers in combination with the HOP domains and use the constraints as a template to guide small molecule design mimicking the Affimer-HOP interactions. This is due to small molecules representing better therapeutic options over Affimers owing to their ability to penetrate cellular membranes.

In conclusion, this work demonstrates that HOP is intrinsically involved in KSHV lytic replication and may provide future pharmaceutical opportunities. However, it is clear that targeting TPR-HSP interactions is a challenging medicinal chemistry problem. The development of small molecules that have high affinity and selectively to disrupt this interaction will require further dedicated campaigns, but success could pave the way for novel pharmaceuticals treating a wide range of conditions.

7 References

Abere, B., Li, J., Zhou, H., Toptan, T., Moore, P.S. and Chang, Y. 2020. Kaposi's sarcoma-associated herpesvirus-encoded circrnas are expressed in infected tumor tissues and are incorporated into virions. *mBio*. **11**(1).

Acker, T.M., Gable, J.E., Bohn, M.F., Jaishankar, P., Thompson, M.C., Fraser, J.S., Renslo, A.R. and Craik, C.S. 2017. Allosteric Inhibitors, Crystallography, and Comparative Analysis Reveal Network of Coordinated Movement across Human Herpesvirus Proteases. *Journal of the American Chemical Society*. **139**(34), pp.11650–11653.

Alvira, S., Cuéllar, J., Röhl, A., Yamamoto, S., Itoh, H., Alfonso, C., Rivas, G., Buchner, J. and Valpuesta, J.M. 2014. Structural characterization of the substrate transfer mechanism in Hsp70/Hsp90 folding machinery mediated by Hop. *Nature Communications*. **5**.

American Cancer Society 2023. *Kaposi Sarcoma Early Detection, Diagnosis and Staging*.

Aneja, K.K. and Yuan, Y. 2017. Reactivation and lytic replication of Kaposi's sarcoma-associated herpesvirus: An update. *Frontiers in Microbiology*. **8**(APR).

Ardi, V.C., Alexander, L.D., Johnson, V.A. and McAlpine, S.R. 2011. Macrocycles that inhibit the binding between heat shock protein 90 and TPR-Containing proteins. *ACS Chemical Biology*.

Arias, C., Weisburd, B., Stern-Ginossar, N., Mercier, A., Madrid, A.S., Bellare, P., Holdorf, M., Weissman, J.S. and Ganem, D. 2014. KSHV 2.0: A Comprehensive Annotation of the Kaposi's Sarcoma-Associated Herpesvirus Genome Using Next-Generation Sequencing Reveals Novel Genomic and Functional Features. *PLoS Pathogens*. **10**(1).

Arvin A, Campadelli-Fiume G, Mocarski E and Davison Andrew J 2007. *Human Herpesviruses: Biology, Therapy, and Immunoprophylaxis. Overview of classification* (Roizman Bernard, ed.). Cambridge: Cambridge University Press.

Ashburner, M. and Bonnert, J.J. 1979. *The Induction of Gene Activity in Drosophila by Heat Shock*.

Ashizawa, A., Higashi, C., Masuda, K., Ohga, R., Taira, T. and Fujimuro, M. 2012. The ubiquitin system and Kaposi's sarcoma-associated herpesvirus. *Frontiers in Microbiology*. **3**(FEB).

Assimon, V.A., Southworth, D.R. and Gestwicki, J.E. 2015. Specific Binding of Tetratricopeptide Repeat Proteins to Heat Shock Protein 70 (Hsp70) and Heat Shock Protein 90 (Hsp90) Is Regulated by Affinity and Phosphorylation. *Biochemistry*. **54**(48), pp.7120–7131.

Aviner, R. and Frydman, J. 2020. Proteostasis in viral infection: Unfolding the complex virus–chaperone interplay. *Cold Spring Harbor Perspectives in Biology*. **12**(3).

Azzarito, V., Prabhakaran, P., Bartlett, A.I., Murphy, N.S., Hardie, M.J., Kilner, C.A., Edwards, T.A., Warriner, S.L. and Wilson, A.J. 2012. 2-O-Alkylated para-benzamide α-helix mimetics: The role of scaffold curvature. *Organic and Biomolecular Chemistry*. **10**(32), pp.6469–6472.

Baell, J.B. and Nissink, J.W.M. 2018. Seven Year Itch: Pan-Assay Interference Compounds (PAINS) in 2017 - Utility and Limitations. *ACS Chemical Biology*. **13**(1), pp.36–44.

Ballatore, C., Huryn, D.M. and Smith, A.B. 2013. Carboxylic Acid (Bio)Isosteres in Drug Design. *ChemMedChem*. **8**(3), pp.385–395.

Banks P, Gosselin M and Prystay L 2000. Impact of a red-shifted dye label for high throughput fluorescence polarization assays of G protein-coupled receptors. *Journal of Biomolecular Screening*. **5**(5), pp.329–334.

Baquero-Pérez, B. and Whitehouse, A. 2015a. Hsp70 Isoforms Are Essential for the Formation of Kaposi's Sarcoma-Associated Herpesvirus Replication and Transcription Compartments. *PLoS Pathogens*. **11**(11).

Baquero-Pérez, B. and Whitehouse, A. 2015b. Hsp70 Isoforms Are Essential for the Formation of Kaposi's Sarcoma-Associated Herpesvirus Replication and Transcription Compartments. *PLoS Pathogens*. **11**(11), pp.1–42.

Bechtel, J.T., Winant, R.C. and Ganem, D. 2005. Host and Viral Proteins in the Virion of Kaposi's Sarcoma-Associated Herpesvirus. *Journal of Virology*. **79**(8), pp.4952–4964.

Beraldo, F.H., Soares, I.N., Goncalves, D.F., Fan, J., Thomas, A.A., Santos, T.G., Mohammad, A.H., Roffé, M., Calder, M.D., Nikolova, S., Hajj, G.N., Guimaraes, A.L., Massensini, A.R., Welch, I., Betts, D.H., Gros, R., Drangova, M., Watson, A.J., Bartha, R., Prado, V.F., Martins, V.R. and Prado, M.A.M. 2013. Stress-inducible phosphoprotein 1 has unique cochaperone activity during development and regulates cellular response to ischemia via the prion protein. *The FASEB Journal*. **27**(9), pp.3594–3607.

Bhattacharya, K. and Picard, D. 2021. The Hsp70–Hsp90 go-between Hop/Stip1/Sti1 is a proteostatic switch and may be a drug target in cancer and neurodegeneration. *Cellular and Molecular Life Sciences*. **78**(23), pp.7257–7273.

Bhattacharya, K., Weidenauer, L., Luengo, T.M., Pieters, E.C., Echeverría, P.C., Bernasconi, L., Wider, D., Sadian, Y., Koopman, M.B., Villemin, M., Bauer, C., Rüdiger, S.G.D., Quadroni, M. and Picard, D. 2020. The Hsp70-Hsp90 co-chaperone Hop/Stip1 shifts the proteostatic balance from folding towards degradation. *Nature Communications*. **11**(1).

Bose, S., Weikl, T., Bügl, H. and Buchner, J. 1996. Chaperone Function of Hsp90-Associated Proteins. *Science*. **274**(5293), pp.1715–1717.

Bouvard, V., Baan, R., Straif, K., Grosse, Y., Secretan, B., El Ghissassi, F., Benbrahim-Tallaa, L., Guha, N., Freeman, C., Galichet, L., Cogliano, V. and WHO International Agency for Research on Cancer Monograph Working Group 2009. A review of human carcinogens–Part B: biological agents. *The Lancet. Oncology*. **10**(4), 321—322.

Bozovičar, K. and Bratkovič, T. 2021. Small and simple, yet sturdy: Conformationally constrained peptides with remarkable properties. *International Journal of Molecular Sciences*. **22**(4), pp.1–25.

Bredael, K., Geurs, S., Clarisse, D., De Bosscher, K. and D'hooghe, M. 2022. Carboxylic Acid Bioisosteres in Medicinal Chemistry: Synthesis and Properties. *Journal of Chemistry*. **2022**.

Brinker, A., Scheufler, C., Von Der Mülbe, F., Fleckenstein, B., Herrmann, C., Jung, G., Moarefi, I. and Ulrich Hartl, F. 2002. Ligand discrimination by TPR domains. Relevance and selectivity of EEVD-recognition in Hsp70·Hop·Hsp90 complexes. *Journal of Biological Chemistry*. **277**(22), pp.19265–19275.

Broussard, G. and Damania, B. 2020. Regulation of KSHV Latency and Lytic Reactivation. *Viruses*. **12**(9).

Calderwood, S.K. and Gong, J. 2016. Heat Shock Proteins Promote Cancer: It's a Protection Racket. *Trends in Biochemical Sciences*. **41**(4), pp.311–323.

Carbone, A., De Paoli, P., Gloghini, A. and Vaccher, E. 2015. KSHV-associated multicentric Castleman disease: A tangle of different entities requiring multitarget treatment strategies. *International Journal of Cancer*. **137**(2), pp.251–261.

Carrigan, P.E. 2006. Domain:domain interactions within Hop, the Hsp70/Hsp90 organizing protein, are required for protein stability and structure. *Protein Science*. **15**(3), pp.522–532.

Casper, C., Krantz, E.M., Corey, L., Kuntz, S.R., Wang, J., Selke, S., Hamilton, S., Huang, M.L. and Wald, A. 2008. Valganciclovir for suppression of human herpesvirus-8 replication: A randomized, double-blind, placebo-controlled, crossover trial. *Journal of Infectious Diseases*. **198**(1), pp.23–30.

Cattamanchi, A., Saracino, M., Selke, S., Huang, M.L., Magaret, A., Celum, C., Corey, L., Wald, A. and Casper, C. 2011. Treatment with valacyclovir, famciclovir, or antiretrovirals reduces human herpesvirus-8 replication in HIV-1 seropositive men. *Journal of Medical Virology*. **83**(10), pp.1696–1703.

Cesarman, E., Damania, B., Krown, S.E., Martin, J., Bower, M. and Whitby, D. 2019. Kaposi sarcoma. *Nature Reviews Disease Primers*. **5**(1).

Chandran, B. 2010. Early Events in Kaposi's Sarcoma-Associated Herpesvirus Infection of Target Cells. *Journal of Virology*. **84**(5), pp.2188–2199.

Chang, Y., Cesarman, E., Pessin, M.S., Lee, F., Culpepper, J., Knowles, D.M. and Moore, P.S. 1994. Identification of herpesvirus-like DNA sequences in AIDS-associated Kaposi's sarcoma. *Science*. **266**(5192).

Chen, W., Sin, S.H., Wen, K.W., Damania, B. and Dittmer, D.P. 2012. Hsp90 Inhibitors Are Efficacious against Kaposi Sarcoma by Enhancing the Degradation of the Essential Viral Gene LANA, of the Viral Co-Receptor EphA2 as well as Other Client Proteins. *PLoS Pathogens*. **8**(11).

Cheng, C.H. and Hsu, Y.H. 2017. Immune reconstitution inflammatory syndrome-associated disseminated Kaposi's sarcoma in a patient infected with human immunodeficiency virus: Report of an autopsy case. *Tzu Chi Medical Journal*. **29**(1), pp.41–45.

Clerico, E.M., Tilitsky, J.M., Meng, W. and Gierasch, L.M. 2015. How Hsp70 molecular machines interact with their substrates to mediate diverse physiological functions. *Journal of Molecular Biology*. **427**(7), pp.1575–1588.

Covarrubias, S., Gaglia, M.M., Kumar, G.R., Wong, W., Jackson, A.O. and Glaunsinger, B.A. 2011. Coordinated destruction of cellular messages in translation complexes by the gammaherpesvirus host shutoff factor and the Mammalian Exonuclease Xrn1. *PLoS Pathogens*. **7**(10).

Dai, X., Gong, D., Lim, H., Jih, J., Wu, T.T., Sun, R. and Zhou, Z.H. 2018. Structure and mutagenesis reveal essential capsid protein interactions for KSHV replication. *Nature*. **553**(7689), pp.521–525.

D'Andrea, L.D. and Regan, L. 2003. TPR proteins: The versatile helix. *Trends in Biochemical Sciences*. **28**(12), pp.655–662.

Darby, J.F., Vidler, L.R., Simpson, P.J., Al-Lazikani, B., Matthews, S.J., Sharp, S.Y., Pearl, L.H., Hoelder, S. and Workman, P. 2020. Solution structure of the Hop TPR2A domain and investigation of target druggability by NMR, biochemical and in silico approaches. *Scientific Reports*. **10**(1).

Davison, A.J., Eberle, R., Ehlers, B., Hayward, G.S., McGeoch, D.J., Minson, A.C., Pellett, P.E., Roizman, B., Studdert, M.J. and Thiry, E. 2009. The order Herpesvirales. *Archives of Virology*. **154**(1), pp.171–177.

Daviter, T., Johnson, C.M., Mclaughlin, S.H. and Williams, M.A. 2022. *Protein-Ligand Interactions Methods and Applications Third Edition Methods in Molecular Biology 2263* [Online]. Available from: http://www.springer.com/series/7651.

DiMasi, J.A., Grabowski, H.G. and Hansen, R.W. 2016. Innovation in the pharmaceutical industry: New estimates of R&D costs. *Journal of Health Economics*. **47**, pp.20–33.

Dollery, S.J. 2019. Towards understanding KSHV fusion and entry. *Viruses*. **11**(11).

Dollery, S.J., Santiago-Crespo, R.J., Chatterjee, D. and Berger, E.A. 2019. Glycoprotein K8.1A of Kaposi's Sarcoma-Associated Herpesvirus Is a Critical B Cell Tropism Determinant Independent of Its Heparan Sulfate Binding Activity. *Journal of Virology*. **93**(6).

Eder, J., Sedrani, R. and Wiesmann, C. 2014. The discovery of first-in-class drugs: Origins and evolution. *Nature Reviews Drug Discovery*. **13**(8), pp.577–587.

El-Mallawany, N.K., Kamiyango, W., Villiera, J., Peckham-Gregory, E.C., Scheurer, M.E., McAtee, C.L., Allen, C.E., Kovarik, C.L., Frank, D., Eason, A.B., Caro-Vegas, C., Chiao, E.Y., Schutze, G.E., Ozuah, N.W., Mehta, P.S., Kazembe, P.N. and Dittmer, D.P. 2019. Kaposi Sarcoma Herpesvirus Inflammatory Cytokine Syndrome-like Clinical Presentation in Human Immunodeficiency Virus-infected Children in Malawi. *Clinical Infectious Diseases*. **69**(11), pp.2022–2025.

Engel, E.A., Song, R., Koyuncu, O.O. and Enquist, L.W. 2015. Investigating the biology of alpha herpesviruses with MS-based proteomics. *Proteomics*. **15**(12), pp.1943–1956.

Esser, S., Schöfer, H., Hoffmann, C., Claßen, J., Kreuter, A., Leiter, U., Oette, M., Becker, J.C., Ziemer, M., Mosthaf, F., Sirokay, J., Ugurel, S., Potthoff, A., Helbig, D., Bierhoff, E., Schulz, T.F., Brockmeyer, N.H. and Grabbe, S. 2022. S1 Guidelines for the Kaposi Sarcoma. *JDDG - Journal of the German Society of Dermatology*. **20**(6), pp.892–904.

Feng, B.Y. and Shoichet, B.K. 2006. *A Detergent-Based Assay for the Detection of Promiscuous Inhibitors* [Online]. Available from: http://shoichetlab.compbio.ucsf.edu.

Field, N., Low, W., Daniels, M., Howell, S., Daviet, L., Boshoff, C. and Collins, M. 2003a. KSHV vFLIP binds to IKK-γ to activate IKK. *Journal of Cell Science*. **116**(18), pp.3721–3728.

Field, N., Low, W., Daniels, M., Howell, S., Daviet, L., Boshoff, C. and Collins, M. 2003b. KSHV vFLIP binds to IKK-γ to activate IKK. *Journal of Cell Science*. **116**(18), pp.3721–3728.

Le Gac, N.T. and Boehmer, P.E. 2002. Activation of the herpes simplex virus type-1 origin-binding protein (UL9) by heat shock proteins. *Journal of Biological Chemistry*. **277**(7), pp.5660–5666.

Gaglia, M.M., Rycroft, C.H. and Glaunsinger, B.A. 2015. Transcriptome-Wide Cleavage Site Mapping on Cellular mRNAs Reveals Features Underlying Sequence-Specific Cleavage by the Viral Ribonuclease SOX. *PLoS Pathogens*. **11**(12).

Ganem, D. 2010. KSHV and the pathogenesis of Kaposi sarcoma: Listening to human biology and medicine. *Journal of Clinical Investigation*. **120**(4), pp.939–949.

Gasc, J.-M., Renoir, J.-M., Faber, L.E., Delahaye, F. and Baulieu, E.-E. 1990. Nuclear Localization of Two Steroid Receptor-Associated Proteins, hsp90 and p59. *Experimental Cell Research*. **186**, pp.362–367.

Gathers, D.A., Galloway, E., Kelemen, K., Rosenthal, A., Gibson, S.E. and Munoz, J. 2022. Primary Effusion Lymphoma: A Clinicopathologic Perspective. *Cancers*. **14**(3).

Genest, O., Wickner, S. and Doyle, S.M. 2019. Hsp90 and Hsp70 chaperones: Collaborators in protein remodeling. *Journal of Biological Chemistry*. **294**(6), pp.2109–2120.

Glaunsinger, B. and Ganem, D. 2004. Highly selective escape from KSHV-mediated host mRNA shutoff and its implications for viral pathogenesis. *Journal of Experimental Medicine*. **200**(3), pp.391–398.

Gomez-Pastor, R., Burchfiel, E.T. and Thiele, D.J. 2018. Regulation of heat shock transcription factors and their roles in physiology and disease. *Nature Reviews Molecular Cell Biology*. **19**(1), pp.4–19.

Gong, D., Dai, X., Jih, J., Liu, Y.T., Bi, G.Q., Sun, R. and Zhou, Z.H. 2019. DNA-Packing Portal and Capsid-Associated Tegument Complexes in the Tumor Herpesvirus KSHV. *Cell*. **178**(6), pp.1329-1343.e12.

Gregory, S.M., Davis, B.K., West, J.A., Taxman, D.J., Matsuzawa, S.I., Reed, J.C., Ting, J.P.Y. and Damania, B. 2011. Discovery of a viral NLR homolog that inhibits the inflammasome. *Science*. **331**(6015), pp.330–334.

Gross, M.L. 1994. Accurate masses for structure confirmation. *Journal of the American Society for Mass Spectrometry*. **5**(2), p.57.

Grundhoff, A. and Ganem, D. 2004. Inefficient establishment of KSHV latency suggests an additional role for continued lytic replication in Kaposi sarcoma pathogenesis. *Journal of Clinical Investigation*. **113**(1), pp.124–136.

Le Guern, F., Mussard, V., Gaucher, A., Rottman, M. and Prim, D. 2020. Fluorescein derivatives as fluorescent probes for ph monitoring along recent biological applications. *International Journal of Molecular Sciences*. **21**(23), pp.1–23.

Guito, J. and Lukac, D.M. 2012. KSHV Rta promoter specification and viral reactivation. *Frontiers in Microbiology*. **3**(FEB).

Hall, M.D., Yasgar, A., Peryea, T., Braisted, J.C., Jadhav, A., Simeonov, A. and Coussens, N.P. 2016. Fluorescence polarization assays in high-throughput screening and drug discovery: A review. *Methods and Applications in Fluorescence*. **4**(2).

Haslbeck, V., Eckl, J.M., Kaiser, C.J.O., Papsdorf, K., Hessling, M. and Richter, K. 2013. Chaperone-interacting TPR proteins in caenorhabditis elegans. *Journal of Molecular Biology*. **425**(16), pp.2922–2939.

Haza, K.Z., Martin, H.L., Rao, A., Turner, A.L., Saunders, S.E., Petersen, B., Tiede, C., Tipping, K., Tang, A.A., Ajayi, M., Taylor, T., Harvey, M., Fishwick, K.M., Adams, T.L., Gaule, T.G., Trinh, C.H., Johnson, M., Breeze, A.L., Edwards, T.A., McPherson, M.J. and Tomlinson, D.C. 2021. RAS-inhibiting biologics identify and probe druggable pockets including an SII-α3 allosteric site. *Nature Communications*. **12**(1).

Hendriks, L.E.L. and Dingemans, A.M.C. 2017. Heat shock protein antagonists in early stage clinical trials for NSCLC. *Expert Opinion on Investigational Drugs*. **26**(5), pp.541–550.

Heske, C.M., Mendoza, A., Edessa, L.D., Baumgart, J.T., Lee, S., Trepel, J., Proia, D.A., Neckers, L. and Helman, L.J. 2016. STA-8666, a novel HSP90 inhibitor/SN-38 drug conjugate, causes complete tumor regression in preclinical mouse models of pediatric sarcoma. *Oncotarget*. **7**(40), pp.65540–65540.

Hinz, M. and Scheidereit, C. 2014. The IκB kinase complex in NF-κB regulation and beyond. *EMBO Reports*. **15**(1), pp.46–61.

Hóbor, F., Hegedüs, Z., Ibarra, A.A., Petrovicz, V.L., Bartlett, G.J., Sessions, R.B., Wilson, A.J. and Edwards, T.A. 2022. Understanding p300-transcription factor interactions using sequence variation and hybridization. *RSC Chemical Biology*.

Hopcraft, S.E., Pattenden, S.G., James, L.I., Frye, S., Dittmer, D.P. and Damania, B. 2018. Chromatin remodeling controls Kaposi's sarcoma-associated herpesvirus reactivation from latency. *PLoS Pathogens*. **14**(9).

Horibe, T., Kohno, M., Haramoto, M., Ohara, K. and Kawakami, K. 2011. Designed hybrid TPR peptide targeting Hsp90 as a novel anticancer agent. *Journal of Translational Medicine*.

Hoter, A., El-Sabban, M.E. and Naim, H.Y. 2018. The HSP90 family: Structure, regulation, function, and implications in health and disease. *International Journal of Molecular Sciences*. **19**(9).

Hua, L., Wang, D., Wang, K., Wang, Y., Gu, J., Zhang, Q., You, Q. and Wang, L. 2023. Design of Tracers in Fluorescence Polarization Assay for Extensive Application in Small Molecule Drug Discovery. *Journal of Medicinal Chemistry*.

Huang, X. 2003. Fluorescence polarization competition assay: The range of resolvable inhibitor potency is limited by the affinity of the fluorescent ligand. *Journal of Biomolecular Screening*. **8**(1), pp.34–38.

Hughes, J.P., Rees, S.S., Kalindjian, S.B. and Philpott, K.L. 2011. Principles of early drug discovery. *British Journal of Pharmacology*. **162**(6), pp.1239–1249.

Itzhaki, R.F., Golde, T.E., Heneka, M.T. and Readhead, B. 2020. Do infections have a role in the pathogenesis of Alzheimer disease? *Nature Reviews Neurology*. **16**(4), pp.193–197.

Kampinga, H.H. and Craig, E.A. 2010. The HSP70 chaperone machinery: J proteins as drivers of functional specificity. *Nature Reviews Molecular Cell Biology*. **11**(8), pp.579–592.

Karagöz, G.E. and Rüdiger, S.G.D. 2015. Hsp90 interaction with clients. *Trends in Biochemical Sciences*. **40**(2), pp.117–125.

Karass, M., Grossniklaus, E., Seoud, T., Jain, S. and Goldstein, D.A. 2017. Kaposi Sarcoma Inflammatory Cytokine Syndrome (KICS): A Rare but Potentially Treatable Condition. *The Oncologist*. **22**(5), pp.623–625.

Kiehstaller, S., Ottmann, C. and Hennig, S. 2020. MMP activation–associated aminopeptidase N reveals a bivalent 14-3-3 binding motif. *Journal of Biological Chemistry*. **295**(52), pp.18266–18275.

Kirsch, P., Jakob, V., Elgaher, W.A.M., Walt, C., Oberhausen, K., Schulz, T.F. and Empting, M. 2020. Discovery of Novel Latency-Associated Nuclear Antigen Inhibitors as Antiviral Agents against Kaposi's Sarcoma-Associated Herpesvirus. *ACS Chemical Biology*. **15**(2), pp.388–395.

Koren, O., Aviv, A., Kelbert, M.A., Rozner, E., Lihtman, L., Halfin, E. and Turgeman, Y. 2021. Primary effusion lymphoma in a patient with a good outcome on steroid alone treatment. *Clinical Case Reports*. **9**(4), pp.2305–2309.

Krishnan, H.H., Sharma-Walia, N., Streblow, D.N., Naranatt, P.P. and Chandran, B. 2006. Focal Adhesion Kinase Is Critical for Entry of Kaposi's Sarcoma-Associated Herpesvirus into Target Cells. *Journal of Virology*. **80**(3), pp.1167–1180.

Kumar, B. and Chandran, B. 2016. KSHV entry and trafficking in target cells—Hijacking of cell signal pathways,actin and membrane dynamics. *Viruses*. **8**(11).

Kumar, S., Basu, M. and Ghosh, M.K. 2022. Chaperone-assisted E3 ligase CHIP: A double agent in cancer. *Genes and Diseases*. **9**(6), pp.1521–1555.

Kyani, A., Tamura, S., Yang, S., Shergalis, A., Samanta, S., Kuang, Y., Ljungman, M. and Neamati, N. 2018. Discovery and Mechanistic Elucidation of a Class of Protein Disulfide Isomerase Inhibitors for the Treatment of Glioblastoma. *ChemMedChem*. **13**(2), pp.164–177.

Lang, B.J., Guerrero, M.E., Prince, T.L., Okusha, Y., Bonorino, C. and Calderwood, S.K. 2021. The functions and regulation of heat shock proteins; key orchestrators of proteostasis and the heat shock response. *Archives of Toxicology*. **95**(6), pp.1943–1970.

Lea, W.A. and Simeonov, A. 2011. Fluorescence polarization assays in small molecule screening. *Expert Opinion on Drug Discovery*. **6**(1), pp.17–32.

Lee, H., Torres, J., Truong, L., Chaudhuri, R., Mittal, A. and Johnson, M.E. 2012. Reducing agents affect inhibitory activities of compounds: Results from multiple drug targets. *Analytical Biochemistry*. **423**(1), pp.46–53.

Lenci, E. and Trabocchi, A. 2020. Peptidomimetic toolbox for drug discovery. *Chemical Society Reviews*. **49**(11), pp.3262–3277.

Li, J., Soroka, J. and Buchner, J. 2012. The Hsp90 chaperone machinery: Conformational dynamics and regulation by co-chaperones. *Biochimica et Biophysica Acta - Molecular Cell Research*. **1823**(3), pp.624–635.

Li, Z.N. and Luo, Y. 2023. HSP90 inhibitors and cancer: Prospects for use in targeted therapies (Review). *Oncology Reports*. **49**(1).

Lieberman, P.M. 2013. Keeping it quiet: Chromatin control of gammaherpesvirus latency. *Nature Reviews Microbiology*. **11**(12), pp.863–875.

Lin, B.Y., Makhov, A.M., Griffith, J.D., Broker, T.R. and Chow, L.T. 2002. Chaperone Proteins Abrogate Inhibition of the Human Papillomavirus (HPV) E1 Replicative Helicase by the HPV E2 Protein. *Molecular and Cellular Biology*. **22**(18), pp.6592–6604.

Liu, J.-S., Kuo, S.-R., Makhov, A.M., Cyr, D.M., Griffith, J.D., Broker, T.R. and Chow, L.T. 1998. *Human Hsp70 and Hsp40 Chaperone Proteins Facilitate Human Papillomavirus-11 E1 Protein Binding to the Origin and Stimulate Cell-free DNA Replication** [Online]. Available from: http://www.jbc.org.

Longshaw, V.M., Dirr, H.W., Blatch, G.L. and Lassle, M. 2005. The in Vitro Phosphorylation of the Co-Chaperone mSTI1 by Cell Cycle Kinases Substantiates a Predicted Casein Kinase II-p34cdc2-NLS (CcN) Motif. *Biological Chemistry*. **381**(11), pp.1133–1138.

Loynachan, C., Unsworth, H., Donoghue, K., Sonabend, R., Lamour-Julien, S., Rodriguez A, Meier, C., Serazin, E., Gooch, J., Aggarwal, P., Steene, A., Jayatunga, M., Nayak, S. and Randall, W. 2023. *Unlocking the potential of AI in Drug Discovery Current status, barriers and future opportunities*.

Lu, H., Zhou, Q., He, J., Jiang, Z., Peng, C., Tong, R. and Shi, J. 2020. Recent advances in the development of protein–protein interactions modulators: mechanisms and clinical trials. *Signal Transduction and Targeted Therapy*. **5**(1).

Macario, A.J.L. 1995. *Heat-shock proteins and molecular chaperones: implications for pathogenesis, diagnostics, and therapeutics*. Springer-Verlag.

Majerciak, V. and Zheng, Z.M. 2015. KSHV ORF57, a protein of many faces. *Viruses*. **7**(2), pp.604–633.

Malik, M.A., Wani, M.Y., Al-Thabaiti, S.A. and Shiekh, R.A. 2014. Tetrazoles as carboxylic acid isosteres: Chemistry and biology. *Journal of Inclusion Phenomena and Macrocyclic Chemistry*. **78**(1–4), pp.15–37.

Manners, O., Murphy, J.C., Coleman, A., Hughes, D.J. and Whitehouse, A. 2018. Contribution of the KSHV and EBV lytic cycles to tumourigenesis. *Current Opinion in Virology*. **32**, pp.60–70.

Mayer, M.P. and Bukau, B. 2005a. Hsp70 chaperones: Cellular functions and molecular mechanism. *Cellular and Molecular Life Sciences*. **62**(6), pp.670–684.

Mayer, M.P. and Bukau, B. 2005b. Hsp70 chaperones: Cellular functions and molecular mechanism. *Cellular and Molecular Life Sciences*. **62**(6), pp.670–684.

Mcdonough, H. and Patterson, C. 2003. *CHIP: a link between the chaperone and proteasome systems*. Cell Stress Society International.

McGeoch, D.J. and Gatherer, D. 2005. Integrating Reptilian Herpesviruses into the Family Herpesviridae . *Journal of Virology.* **79**(2), pp.725–731.

Mendez, A.S., Vogt, C., Bohne, J. and Glaunsinger, B.A. 2018. Site specific target binding controls RNA cleavage efficiency by the Kaposi's sarcoma-associated herpesvirus endonuclease SOX. *Nucleic Acids Research.* **46**(22), pp.11968–11979.

van der Meulen, E., Anderton, M., Blumenthal, M.J. and Schäfer, G. 2021. Cellular receptors involved in kshv infection. *Viruses.* **13**(1).

Muller, M. and Glaunsinger, B.A. 2017. Nuclease escape elements protect messenger RNA against cleavage by multiple viral endonucleases. *PLoS Pathogens.* **13**(8).

Naimo, E., Zischke, J. and Schulz, T.F. 2021. Recent advances in developing treatments of kaposi's sarcoma herpesvirus-related diseases. *Viruses.* **13**(9).

Nakamura, H., Lu, M., Gwack, Y., Souvlis, J., Zeichner, S.L. and Jung, J.U. 2003. Global Changes in Kaposi's Sarcoma-Associated Virus Gene Expression Patterns following Expression of a Tetracycline-Inducible Rta Transactivator. *Journal of Virology.* **77**(7), pp.4205–4220.

Naniima, P., Naimo, E., Koch, S., Curth, U., Alkharsah, K.R., Ströh, L.J., Binz, A., Beneke, J.M., Vollmer, B., Böning, H., Borst, E.M., Desai, P., Bohne, J., Messerle, M., Bauerfeind, R., Legrand, P., Sodeik, B., Schulz, T.F. and Krey, T. 2021. Assembly of infectious Kaposi's sarcoma-associated herpesvirus progeny requires formation of a pORF19 pentamer. *PLoS Biology.* **19**(11).

Narkhede, M., Arora, S. and Ujjani, C. 2018. Primary effusion lymphoma: Current perspectives. *OncoTargets and Therapy.* **11**, pp.3747–3754.

Nicolet, C.M. and Craig, E.A. 1989. *Isolation and Characterization of STIJ, a Stress-Inducible Gene from Saccharomyces cerevisiae.*

Nitzsche, B., Höpfner, M. and Biersack, B. 2023. Synthetic Small Molecule Modulators of Hsp70 and Hsp40 Chaperones as Promising Anticancer Agents. *International Journal of Molecular Sciences.* **24**(4).

Owen, D.J., Crump, C.M. and Graham, S.C. 2015. Tegument assembly and secondary envelopment of alphaherpesviruses. *Viruses.* **7**(9), pp.5084–5114.

Pearl, L.H. 2016. Review: The HSP90 molecular chaperone - An enigmatic ATPase. *Biopolymers.* **105**(8), pp.594–607.

Pimienta, G., Herbert, K.M. and Regan, L. 2011. A compound that inhibits the HOP-Hsp90 complex formation and has unique killing effects in breast cancer cell lines. *Molecular Pharmaceutics.* **8**(6), pp.2252–2261.

Pinchinat, S., Cebrián-Cuenca, A.M., Bricout, H. and Johnson, R.W. 2013. Similar herpes zoster incidence across Europe: results from a systematic literature review. *British Medical Council Infectious Diseases.* **13**(170), pp.1471–2334.

Poizot-Martin, I., Brégigeon, S., Palich, R., Marcelin, A.G., Valantin, M.A., Solas, C., Veyri, M., Spano, J.P. and Makinson, A. 2022. Immune Reconstitution Inflammatory Syndrome Associated Kaposi Sarcoma. *Cancers.* **14**(4).

Prodromou, C. 2016. REVIEW ARTICLE mechanisms of Hsp90 regulation. *Biochemical Journal.* **473**(16), pp.2439–2452.

Purushothaman, P., Dabral, P., Gupta, N., Sarkar, R. and Verma, S.C. 2016. KSHV genome replication and maintenance. *Frontiers in Microbiology.* **7**(FEB).

Qin, J., Li, W., Gao, S.J. and Lu, C. 2017. KSHV microRNAs: Tricks of the Devil. *Trends in Microbiology.* **25**(8), pp.648–661.

Qin, Z., DeFee, M., Isaacs, J.S. and Parsons, C. 2010a. Extracellular Hsp90 serves as a co-factor for MAPK activation and latent viral gene expression during de novo infection by KSHV. *Virology.* **403**(1), pp.92–102.

Qin, Z., DeFee, M., Isaacs, J.S. and Parsons, C. 2010b. Extracellular Hsp90 serves as a co-factor for MAPK activation and latent viral gene expression during de novo infection by KSHV. *Virology.* **403**(1), pp.92–102.

Qingwei, Z., Andrew, S., Zhiren, X., Michael, J.F. and Victoria, S. 2011. NOVEL BENZENESULFONAMIDES AS CALCIUM CHANNEL BLOCKERS.

Quintana-Gallardo, L., Martín-Benito, J., Marcilla, M., Espadas, G., Sabidó, E. and Valpuesta, J.M. 2019. The cochaperone CHIP marks Hsp70- and Hsp90-bound substrates for degradation through a very flexible mechanism. *Scientific Reports*. **9**(1).

Ramaswami, R., Lurain, K., Polizzotto, M.N., Ekwede, I., Waldon, K., Steinberg, S.M., Mangusan, R., Widell, A., Rupert, A., George, J., Gonçalves, P.H., Marshall, V.A., Whitby, D., Wang, H.W., Pittaluga, S., Jaffe, E.S., Little, R.F., Uldrick, T.S. and Yarchoan, R. 2021. Characteristics and outcomes of KSHV-associated multicentric Castleman disease with or without other KSHV diseases. *Blood Advances*. **5**(6), pp.1660–1670.

Ran, X. and Gestwicki, J.E. 2018. Inhibitors of protein–protein interactions (PPIs): an analysis of scaffold choices and buried surface area. *Current Opinion in Chemical Biology*. **44**, pp.75–86.

Ravalin, M., Theofilas, P., Basu, K., Opoku-Nsiah, K.A., Assimon, V.A., Medina-Cleghorn, D., Chen, Y.F., Bohn, M.F., Arkin, M., Grinberg, L.T., Craik, C.S. and Gestwicki, J.E. 2019. Specificity for latent C termini links the E3 ubiquitin ligase CHIP to caspases. *Nature Chemical Biology*. **15**(8), pp.786–794.

Reyes-del Valle, J., Chavez-Salinas, S., Medina, F. and del Angel, R.M. 2005. Heat Shock Protein 90 and Heat Shock Protein 70 Are Components of Dengue Virus Receptor Complex in Human Cells. *Journal of Virology*.

Röhl, A., Wengler, D., Madl, T., Lagleder, S., Tippel, F., Herrmann, M., Hendrix, J., Richter, K., Hack, G., Schmid, A.B., Kessler, H., Lamb, D.C. and Buchner, J. 2015. Hsp90 regulates the dynamics of its cochaperone Sti1 and the transfer of Hsp70 between modules. *Nature Communications*. **6**.

Rohner, E., Wyss, N., Trelle, S., Mbulaiteye, S.M., Egger, M., Novak, U., Zwahlen, M. and Bohlius, J. 2014. HHV-8 seroprevalence: A global view. *Systematic Reviews*. **3**(1).

Rosenzweig, R., Nillegoda, N.B., Mayer, M.P. and Bukau, B. 2019. The Hsp70 chaperone network. *Nature Reviews Molecular Cell Biology*. **20**(11), pp.665–680.

Rozen, R., Sathish, N., Li, Y. and Yuan, Y. 2008. Virion-Wide Protein Interactions of Kaposi's Sarcoma-Associated Herpesvirus. *Journal of Virology*. **82**(10), pp.4742–4750.

Russo, J.J., Bohenzky, R.A., Chien, M., Chen, J., Yan, M., Maddalena, D., Preston Parry, J., Peruzzi, D., Edelman, I.S., Chang, Y. and Moore, P.S. 1996. Nucleotide sequence of the Kaposi sarcoma-associated herpesvirus (HHV8). *Proc. Natl. Acad. Sci. USA*. **93**, pp.14862–14867.

Saibil, H. 2013. Chaperone machines for protein folding, unfolding and disaggregation. *Nature Reviews Molecular Cell Biology*. **14**(10), pp.630–642.

dos Santos, J.L. 2015. Pan-Assay Interference Compounds (PAINS): Warning Signs in Biochemical-Pharmacological Evaluations. *Biochemistry & Pharmacology: Open Access*. **04**(02).

Sathish, N., Zhu, F.X., Golub, E.E., Liang, Q. and Yuan, Y. 2011. Mechanisms of autoinhibition of IRF-7 and a probable model for inactivation of IRF-7 by Kaposi's Sarcoma-associated herpesvirus protein ORF45. *Journal of Biological Chemistry*. **286**(1), pp.746–756.

Sathish, N., Zhu, F.X. and Yuan, Y. 2009. Kaposi's sarcoma-associated herpesvirus ORF45 Interacts with kinesin-2 transporting viral capsid-tegument complexes along microtubules. *PLoS Pathogens*. **5**(3).

Sausen, D.G., Reed, K.M., Bhutta, M.S., Gallo, E.S. and Borenstein, R. 2021. Evasion of the host immune response by betaherpesviruses. *International Journal of Molecular Sciences*. **22**(14).

Scheufler, C., Brinker, A., Bourenkov, G., Pegoraro, S., Moroder, L., Bartunik, H., Hartl, F.U. and Moarefi, I. 2000. Structure of TPR domain-peptide complexes: Critical elements in the assembly of the Hsp70-Hsp90 multichaperone machine. *Cell*. **101**(2), pp.199–210.

Schmid, A.B., Lagleder, S., Gräwert, M.A., Röhl, A., Hagn, F., Wandinger, S.K., Cox, M.B., Demmer, O., Richter, K., Groll, M., Kessler, H. and Buchner, J. 2012. The architecture of functional modules in the Hsp90 co-chaperone Sti1/Hop. *EMBO Journal*. **31**(6), pp.1506–1517.

Schmid, M., Speiseder, T., Dobner, T. and Gonzalez, R.A. 2014. DNA Virus Replication Compartments. *Journal of Virology*. **88**(3), pp.1404–1420.

Schneider, J.W. and Dittmer, D.P. 2017. Diagnosis and Treatment of Kaposi Sarcoma. *American Journal of Clinical Dermatology*. **18**(4), pp.529–539.

Sharma, V., Mobeen, F. and Prakash, T. 2016. Comparative Genomics of Herpesviridae Family to Look for Potential Signatures of Human Infecting Strains. *International Journal of Genomics*. **2016**.

Sharma-Walia, N., Krishnan, H.H., Naranatt, P.P., Zeng, L., Smith, M.S. and Chandran, B. 2005. ERK1/2 and MEK1/2 Induced by Kaposi's Sarcoma-Associated Herpesvirus (Human Herpesvirus 8) Early during Infection of Target Cells Are Essential for Expression of Viral Genes and for Establishment of Infection. *Journal of Virology*. **79**(16), pp.10308–10329.

Sharma-Walia, N., Naranatt, P.P., Krishnan, H.H., Zeng, L. and Chandran, B. 2004. Kaposi's Sarcoma-Associated Herpesvirus/Human Herpesvirus 8 Envelope Glycoprotein gB Induces the Integrin-Dependent Focal Adhesion Kinase-Src-Phosphatidylinositol 3-Kinase-Rho GTPase Signal Pathways and Cytoskeletal Rearrangements. *Journal of Virology*. **78**(8), pp.4207–4223.

Sherman, M.Y. and Gabai, V.L. 2015. Hsp70 in cancer: Back to the future. *Oncogene*. **34**(32), pp.4153–4161.

Singh, V.V., Dutta, D., Ansari, M.A., Dutta, S. and Chandran, B. 2014. Kaposi's Sarcoma-Associated Herpesvirus Induces the ATM and H2AX DNA Damage Response Early during De Novo Infection of Primary Endothelial Cells, Which Play Roles in Latency Establishment . *Journal of Virology*. **88**(5), pp.2821–2834.

Song, H.O., Lee, W., An, K., Lee, H. suk, Cho, J.H., Park, Z.Y. and Ahnn, J. 2009. C. elegans STI-1, the Homolog of Sti1/Hop, Is Involved in Aging and Stress Response. *Journal of Molecular Biology*. **390**(4), pp.604–617.

Stokes, J.M., Yang, K., Swanson, K., Jin, W., Cubillos-Ruiz, A., Donghia, N.M., MacNair, C.R., French, S., Carfrae, L.A., Bloom-Ackerman, Z., Tran, V.M., Chiappino-Pepe, A., Badran, A.H., Andrews, I.W., Chory, E.J., Church, G.M., Brown, E.D., Jaakkola, T.S., Barzilay, R. and Collins, J.J. 2020. A Deep Learning Approach to Antibiotic Discovery. *Cell*. **180**(4), pp.688-702.e13.

Sun, D., Gao, W., Hu, H. and Zhou, S. 2022. Why 90% of clinical drug development fails and how to improve it? *Acta Pharmaceutica Sinica B*. **12**(7), pp.3049–3062.

Taipale, M., Krykbaeva, I., Koeva, M., Kayatekin, C., Westover, K.D., Karras, G.I. and Lindquist, S. 2012. Quantitative analysis of Hsp90-client interactions reveals principles of substrate recognition. *Cell*. **150**(5), pp.987–1001.

Tittelmeier, J., Nachman, E. and Nussbaum-Krammer, C. 2020. Molecular Chaperones: A Double-Edged Sword in Neurodegenerative Diseases. *Frontiers in Aging Neuroscience*. **12**.

Trepel, J., Mollapour, M., Giaccone, G. and Neckers, L. 2010. Targeting the dynamic HSP90 complex in cancer. *Nature Reviews Cancer*. **10**(8), pp.537–549.

Trus, B.L., Heymann, J.B., Nealon, K., Cheng, N., Newcomb, W.W., Brown, J.C., Kedes, D.H. and Steven, A.C. 2001. Capsid Structure of Kaposi's Sarcoma-Associated Herpesvirus, a Gammaherpesvirus, Compared to Those of an Alphaherpesvirus, Herpes Simplex Virus Type 1, and a Betaherpesvirus, Cytomegalovirus. *Journal of Virology*. **75**(6), pp.2879–2890.

Uppal, T., Banerjee, S., Sun, Z., Verma, S.C. and Robertson, E.S. 2014. KSHV LANA—The Master Regulator of KSHV Latency. *Viruses*. **6**(12), pp.4691–4998.

Vaaltyn, M.C., Mateos-Jimenez, M., Müller, R., Mackay, C.L., Edkins, A.L., Clarke, D.J. and Veale, C.G.L. 2022. Native Mass Spectrometry-Guided Screening Identifies Hit Fragments for HOP-HSP90 PPI Inhibition**.

Vieira, J. and O'Hearn, P.M. 2004. Use of the red fluorescent protein as a marker of Kaposi's sarcoma-associated herpesvirus lytic gene expression. *Virology*. **325**(2), pp.225–240.

Wang, L., Gaigalas, A.K., Abbasi, F., Marti, G.E., Vogt, R.F. and Schwartz, A. 2002. *Quantitating Fluorescence Intensity From Fluorophores: Practical Use of MESF Values Volume 107 Number 4* [Online]. Available from: http://www.nist.gov/jres.

Wang Xin AND Zhu, N.A.N.D.L.W.A.N.D.Z.F.A.N.D.W.Y.A.N.D.Y.Y. 2015. Mono-ubiquitylated ORF45 Mediates Association of KSHV Particles with Internal Lipid Rafts for Viral Assembly and Egress. *PLOS Pathogens.* **11**(12), pp.1–26.

Wang, Z., Li, Y., Yang, X., Zhao, J., Cheng, Y. and Wang, J. 2020. Mechanism and Complex Roles of HSC70 in Viral Infections. *Frontiers in Microbiology.* **11**.

Wen, K.W. and Damania, B. 2010a. Hsp90 and Hsp40/Erdj3 are required for the expression and anti-apoptotic function of KSHV K1. *Oncogene.* **29**(24), pp.3532–3544.

Wen, K.W. and Damania, B. 2010b. Hsp90 and Hsp40/Erdj3 are required for the expression and anti-apoptotic function of KSHV K1. *Oncogene.* **29**(24), pp.3532–3544.

Whitley, D., Goldberg, S.P. and Jordan, W.D. 1999. Heat shock proteins: A review of the molecular chaperones. *Journal of Vascular Surgery.* **29**(4), pp.748–751.

Whitley R J 1996. Herpesviruses *In*: Baron S, ed. *Medical Microbiology.* Galveston (TX): University of Texas Medical Branch at Galveston.

Wouters, O.J., McKee, M. and Luyten, J. 2020. Estimated Research and Development Investment Needed to Bring a New Medicine to Market, 2009-2018. *JAMA - Journal of the American Medical Association.* **323**(9), pp.844–853.

Wu, J., Liu, T., Rios, Z., Mei, Q., Lin, X. and Cao, S. 2017. Heat Shock Proteins and Cancer. *Trends in Pharmacological Sciences.* **38**(3), pp.226–256.

Yamamoto, S., Subedi, G.P., Hanashima, S., Satoh, T., Otaka, M., Wakui, H., Sawada, K.I., Yokota, S.I., Yamaguchi, Y., Kubota, H. and Itoh, H. 2014. ATPase activity and ATP-dependent conformational change in the Co-chaperone HSP70/HSP90-organizing protein (HOP). *Journal of Biological Chemistry.* **289**(14), pp.9880–9886.

Yan, L., Majerciak, V., Zheng, Z.M. and Lan, K. 2019a. Towards Better Understanding of KSHV Life Cycle: from Transcription and Posttranscriptional Regulations to Pathogenesis. *Virologica Sinica.* **34**(2), pp.135–161.

Yan, L., Majerciak, V., Zheng, Z.M. and Lan, K. 2019b. Towards Better Understanding of KSHV Life Cycle: from Transcription and Posttranscriptional Regulations to Pathogenesis. *Virologica Sinica.* **34**(2), pp.135–161.

Yi, F. and Regan, L. 2008. A novel class of small molecule inhibitors of Hsp90. *ACS Chemical Biology.* **3**(10), pp.645–654.

Zhai, E., Liang, W., Lin, Y., Huang, L., He, X., Cai, S., Chen, J., Zhang, N., Li, J., Zhang, Q., He, Y., Zeng, Z., Chen, M., Xu, L. and Peng, S. 2018. HSP70/HSP90-Organizing Protein Contributes to Gastric Cancer Progression in an Autocrine Fashion and Predicts Poor Survival in Gastric Cancer. *Cellular Physiology and Biochemistry.* **47**(2), pp.879–892.

Zhang, J.H., Chung, T.D.Y. and Oldenburg, K.R. 1999. A simple statistical parameter for use in evaluation and validation of high throughput screening assays. *Journal of Biomolecular Screening.* **4**(2), pp.67–73.

Zhu, F.X., Chong, J.M., Wu, L. and Yuan, Y. 2005. Virion Proteins of Kaposi's Sarcoma-Associated Herpesvirus. *Journal of Virology.* **79**(2), pp.800–811.

Zhu, M.R., Du, D.H., Hu, J.C., Li, L.C., Liu, J.Q., Ding, H., Kong, X.Q., Jiang, H.L., Chen, K.X. and Luo, C. 2018. Development of a high-throughput fluorescence polarization assay for the discovery of EZH2-EED interaction inhibitors. *Acta Pharmacologica Sinica.* **39**(2), pp.302–310.

Zhu, Y.Z., Cao, M.M., Wang, W.B., Wang, W., Ren, H., Zhao, P. and Qi, Z.T. 2012. Association of heat-shock protein 70 with lipid rafts is required for japanese encephalitis virus infection in Huh7 cells. *Journal of General Virology.* **93**(1), pp.61–71.

Zoeteweij, J.P., Moses, A. V, Rinderknecht, A.S., Davis, D.A., Overwijk, W.W., Yarchoan, R., Orenstein, J.M. and Blauvelt, A. 2001. *Targeted inhibition of calcineurin signaling blocks calcium-dependent reactivation of Kaposi sarcoma-associated herpesvirus* [Online]. Available from: http://ashpublications.org/blood/article-pdf/97/8/2374/1672745/h8080102374.pdf.

Zuehlke, A.D., Moses, M.A. and Neckers, L. 2018. Heat shock protein 90: Its inhibition and function. *Philosophical Transactions of the Royal Society B: Biological Sciences*. **373**(1738).

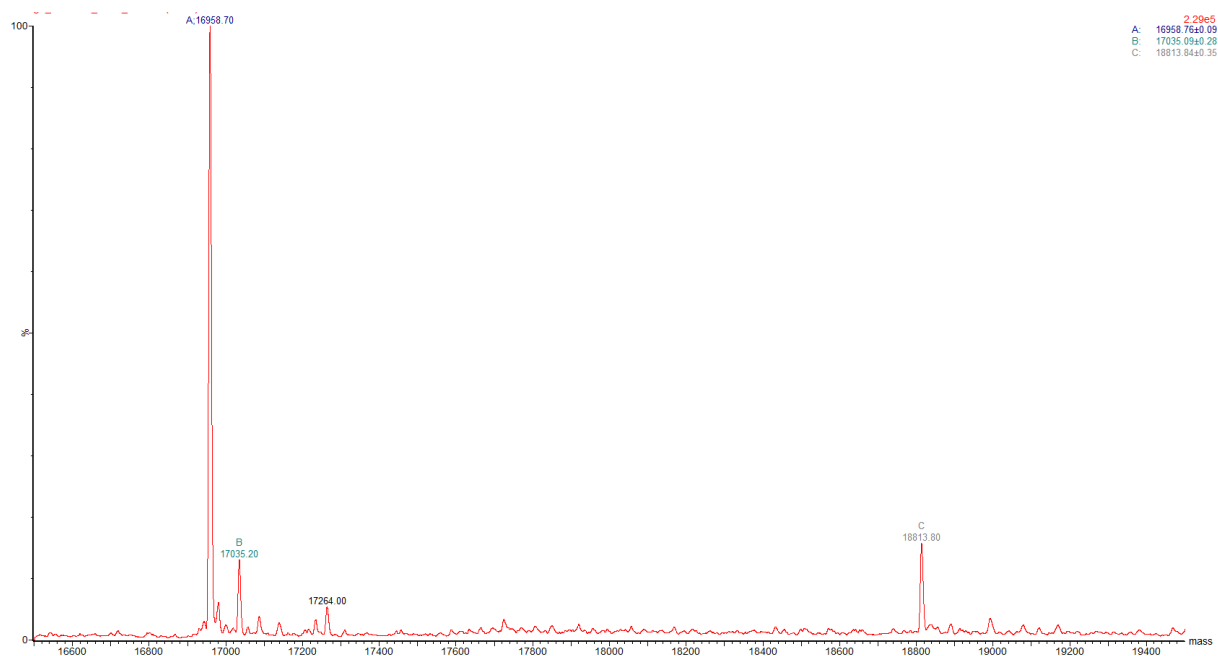# 8 Supplemental

8.1 Mass spectrometry of TPR2A excised band

Figure 68: Mass spectrometry of excised TPR2A coomasie gel band. Peak C corresponds to full length TPR2A domain with hexahistidine tag. Peak A and B corresponded to TPR2A domain with loss of hexahistidine tag.